INVESTIGATING THE LOCATION OF THE ~1620 C.E. WEST COAST EARTHQUAKE USING COSEISMIC LANDSLIDE MODELLING.

A thesis

submitted in partial fulfilment of the requirements for the degree

of

Master of Science in Hazard and Disaster Management

at the

University of Canterbury

By

Jason Clyde Briggs

UNIVERSITY OF CANTERBURY

2016

Multiple landslide deposits representing different events in the Hooker Valley, New Zealand, 2015 (Taken by the author).

“There is nothing like looking, if you want to find something. You certainly usually find something, if you look, but it is not always quite the something you were after.”

- J. R. R. Tolkien, Writer/Poet/Philologist/Professor

ABSTRACT

Palæoseismic indicators of large earthquakes within the Southern Alps of New Zealand are widespread and the methods by which they are obtained and interpreted vary greatly. The palæo-earthquake record of the Alpine Fault is a primary goal of many research programmes, so attribution of these indicators to a particular fault aids in understanding the past to better prepare for the future. An earthquake event around 1620 C.E., hitherto attributed to the Alpine Fault, does not appear to directly reflect these various forms of evidence; neither does it match the currently understood recurrence interval of Alpine Fault ruptures.

One primary result of large earthquakes is coseismic landsliding, which has the potential for damage and destruction of both the natural and built environments. Within the Southern Alps, topography and climatic factors exacerbate erosion rates following such events. In addition to the immediate effects, longer-term issues like river aggradation and avulsion can further hinder recovery. On the West Coast, substantial aggradation has been directly attributed to the ~1620 C.E. earthquake, and is considerably higher than modelled aggradation from an Alpine Fault event. Based on the incongruence between the palæoseismic indicators, inferred earthquake properties, and other models, a 7.6 M_W earthquake on a hypothetical fault within the western Southern Alps was investigated to see if it better matched these effects.

A Shakemap model was developed, producing distributed shaking intensities for this hypothetical earthquake. The results were incorporated into a fuzzy logic based coseismic landslide susceptibility model and, using Monte Carlo analysis, landslide volumes, denudation depths, and aggradation depths in some order 5, and all order 6 and higher river catchments of the South Island were produced.

The results show that the smaller catchments in the western Southern Alps close to the hypothetical fault are significantly more impacted by coseismic landsliding associated with its rupture than in the case of an Alpine Fault earthquake. However, when the more northern and southern indicators of this event are compared, the hypothetical earthquake does not produce sufficiently intense impacts to match the ~1620 C.E. earthquake palæoseismic indicators. This implies that either a longer fault producing a larger, more geographically extensive earthquake or a secondary earthquake within the same timeframe is necessary.

ACKNOWLEDGEMENTS

Firstly, I would like to thank my Supervisor Professor Tim Davies. His assistance in developing a study proposal, procuring funding and displaying patience and advice when attempting to understand the intent of my sometimes hectic sentences has been outstanding. Overall his passion, knowledge and willingness to transfer that knowledge has been greatly appreciated. Thank you Tim.

Thanks must also go to Dr Tom Robinson for his help when, at times for me personally, the way ahead was unclear. As he essentially had no obligation to myself or my thesis, the effort spent to ensure that I coherently understood his methods was integral to completion of my thesis.

A big thank you to the EQC Capability Fund for their generous funding, which has made completing this thesis a little less arduous from a financial perspective.

Thanks to my colleagues in room 410, whom with multiple coffee/lunch breaks and tolerating my mental respite breaks, have helped keep me sane throughout. Especially Henry Winter who has borne the brunt of my whinging this year and kept me positive.

A special thanks to Alec Wild for motivating me to undertake postgraduate studies and his input on the coding aspects of my thesis.

A heartfelt thanks must go to my family: my mother Megan who has constantly provided so much to keep me in a positive and focused mind set throughout this endeavour, my father Rod with his timely reality checks and indirect funding and lastly my sister Kylie for her endless support, for whom I know post grad was her dream.

Thanks to my feline friends Claude and Hermes who were constantly being dragged to the computer to Skype and for tolerating my constant affection, albeit at a distant.

Finally, thank you for your last minute review Graeme Mustchin. The constructive criticism and analytical review has caught many things that had not previously been picked up.

To anyone else that I have missed, I wish to convey my thanks for your help, moral support and general input, as overall a multiple people have contributed in some way to the completion of this thesis.

CONTENTS

List of Tables

List of Figures

LIST OF ABBREVIATIONS AND CLARIFICATIONS

A.D. – Anno Domini (N.B. this has been used interchangeably with C.E. or Common Era. The usage within this thesis is based on the original context when discussing other researcher's work, i.e. if an author uses 1620 A.D. or A.D. 1620 this thesis will use the same within that context. Out of comparative context this thesis uses C.E. as default or inferred default.)

AUC - Area Under Curve – a method to measure the success of fuzzy methods in comparison to expected results

BP – Before Present

Ca. – circa – around or approximately at this time.

CDEM – Civil Defence and Emergency Management.

Cohort - a group of trees that simultaneously colonize a newly disturbed area (Wells et al., 1999).

DEM – Digital Elevation Model.

Disaster - a serious disruption of a community or a society involving widespread human, material, economic or environmental losses or impacts which exceed the ability of the affected community or society to cope using its own resources (ISDR, 2009).

ESRI - Environmental Systems Research Institute

Franz Inc. – A Franz Josef Glacier township local cooperation of businesses formed for the purpose of understanding and distributing natural hazard risk management information.

Fault Behavior:

- Bimodal– A fault exhibiting two forms of rupture behavior such that: "small to moderate magnitude earthquakes follow the Gutenberg-Richter (GR) inverse power-law relation" (Zielke & Arrowsmith, 2008). For example, a fault undergoes smaller partial ruptures and larger full ruptures as two forms of activity.
- Characteristic – earthquakes that follow an approximate Gaussian distribution around the maximum magnitude limited by fault geometry such that: "the

occurrence of earthquakes on individual faults and fault segments does not follow a log linear frequency-magnitude relationship of the form (log N = a - bM) described by Gutenberg and Richter [1954].” (Schwartz & Coppersmith, 1984).

GIS – Geographic Information Systems.

GNS – Geological and Nuclear Sciences Ltd.

GPS – Global Positioning System.

Hazard – a potential threat to humans and their welfare arising from a dangerous phenomenon or substance that may cause loss of life, injury, property damage, and other community losses or damage (ISDR 2009).

IML – Intensity Measure Level

IMT – Intensity Measure Type

IQR – InterQuartile Range

Kyr – a period of time representing 1000 years.

LSF – LandSlide Factor.

LiDAR – Light Detection and Ranging.

MCDEM – Ministry for Civil Defence and Emergency Management.

MM(I) – Modified Mercalli (Intensity) – a measure of earthquake impacts on the human environment. (N.B. this can be used with interchangeably with Arabic or Roman numerals. In this thesis these have been used in their original context when discussing other researcher’s work, i.e. if an author uses MM(I) IX, I have used the same instead of using MM(I) 9. Out of comparative context this thesis uses Arabic numerals.)

M_W – Moment Magnitude – a measure of the energy released during a fault plane rupture.

NIWA -National Institute of Water and Atmospheric Research

PGA – Peak Ground Acceleration – a measure of earthquake shaking intensity.

PGV – Peak Ground Velocity – a measure of earthquake shaking intensity.

Region – the use of region is context-specific. For example, when used in conjunction with entire South Island extents it would represent that entire region. Another example is its use in more local contexts, such as region being used to describe the immediate area surrounding a palæoseismic indicator site.

Risk – the combination of the probability of a hazardous event and its negative consequences (ISDR, 2009).

SAMBA – South Island Microearthquake Borehole Array.

SIGHT – South Island GeopHysical Transect.

SHA – Seismic Hazard Analysis

SRTM – Shuttle Radar Topography Mission (a Digital Elevation Model).

Stirling Fault Surface – a representation of a gridded surface where the trace and average dip are used to create a corrugated surface by translating the fault trace down dip, perpendicular to the average fault strike (Field et al., 2003).

USGS – United States Geological Survey.

Vs30 – a velocity model for seismic wave propagation in the top 30 metres of the ground.

Vulnerability – the characteristics and circumstances of a community, system or asset that make it susceptible to the damaging effects of a hazard (ISDR, 2009).

WDC – Westland District Council.

WCRC – West Coast Regional Council.

LIST OF APPENDICES

1 THESIS INTRODUCTION AND PRIMARY RESEARCH OBJECTIVES

1.1 Introduction

Large earthquakes and their cascading geomorphic consequences can be devastating to both the natural and built environments. Of these consequences, coseismic hazards such as the rapid mobilization of material during landsliding can potentially pose a threat greater than the initial earthquake shaking responsible. Landslides can cause extreme immediate damage and long term disruption to critical infrastructure networks and, in conjunction with other coseismic hazards, create a difficult disaster scenario for which to plan. Within the Southern Alps of New Zealand, topographic and environmental factors exacerbate landsliding, resulting in a region highly susceptible to coseismic landsliding and associated hazards.

The Southern Alps comprise the hanging wall of the Alpine Fault, the 470 km onshore section of the Australian-Pacific plate transform boundary, running the length of the South Island at the western edge of the Southern Alps (Sutherland et al., 2007). Within this active tectonic setting seismic activity is prolific due to the many known active faults of varying seismic potential. The plate-boundary Alpine Fault is

the largest of these and is capable of producing $M_W \geq 8.0$ earthquakes several times per millennium (Berryman et al, 2012a).

The Alpine Fault and its behaviour are relatively well understood. A large academic body of work describes its properties, rupture mechanisms, and recurrence intervals. However, of the ruptures attributed to the Alpine Fault within the last millennium, an event occurring at ~1620 C.E. appears a clear outlier of the inferred characteristic behaviour. Furthermore, the geomorphic evidence and palæoseismic indicators associated with this inferred earthquake do not align with the postulated earthquake properties.

This research investigates the hypothesis that the ~1620 C.E. event was not of Alpine Fault origin at the western rangefront but rather the result of an unknown fault rupture within the western Southern Alps. The work herein follows a deterministic approach to hazard modelling, generating coseismic landsliding estimates from a hypothetical fault rupture scenario. The regional landslide susceptibility and resultant sediment volumes, when compared with those determined by Robinson et al. (2016) for an Alpine fault rupture, will provide insight as to whether the ~1620 C.E. event was the result of a rupture of the Alpine Fault of an alternative fault. Additionally, the results generated may provide additional insight into the seismic and coseismic hazard potential within the Southern Alps, identifying areas of higher risk which could prove useful within a hazard management framework.

Although recently deterministic approaches to natural hazard modelling have been somewhat superseded by probabilistic approaches, instances still exist where a deterministic approach can produce relevant results. This is especially true when adequate details are available to formulate a realistic scenario. Although each approach has limitations, it is important to consider that any model is a highly simplified abstraction of complex real world processes. Relationships and simplifications will introduce uncertainties throughout the methods followed (Haneberg, 2000). This is the case when developing a hypothetical fault rupture, as fault parameters, rupture mechanisms, and to an extent location can be informed by previous research but introduce errors. Thus, the only remaining uncertain parameter for the scenario is the existence of the fault itself. Utilizing the current level of knowledge, the hypothetical fault's existence or non-existence remains unknown – which retains value as a hypothesis. In this case emphasis is placed on the regional

consequences of a large earthquake within the Southern Alps orogen; the location of seismogenesis is then of secondary importance.

Determining a comprehensive regional seismic hazard-scape requires knowledge of unknown faults and thus is not possible with the current level of knowledge. Therefore, it is necessary to consider geologic hazard scenarios from unknown sources; in particular, the research carried out by Cox et al. (2012) and Nicol et al. (2016). In their nation-wide active faulting model, Litchfield et al. (2014) describe the completeness of known faults within the central and central-northern Southern Alps as "medium", so it is certainly plausible that multiple unknown faults exist within these domains. The identification of hitherto unknown faults in the Southern Alps is further complicated by very high exhumation and denudation rates (Summerfield, 2014). In the Southern Alps, surface traces of active faulting can be removed by erosional processes between seismic episodes (Cox et al., 2012). Additional factors including poor access, dense forest and snow and ice cover mean that reliance on conventional geologic fault mapping techniques is insufficient. Thus, to determine the hazard potential of active faults within the Southern Alps, the provision of a realistic quantitative model could supplement the current understanding of coseismic landsliding within the region.

While the results of Robinson et al. (2016) demonstrated the potential coseismic landsliding of an Alpine Fault rupture scenario, alternative scenarios are useful not only for comparison but also to ensure more comprehensive disaster preparation. As the population adjacent to the Southern Alps is increasing, with heavy reliance of both population and industry on various critical infrastructure, it is imperative the understanding of potential coseismic landsliding within the region be improved.

1.2 Current state of research

This section will provide a brief summary of current research pertinent to this thesis. An in-depth review is provided in Chapter 2.

1.2.1 Active faulting in New Zealand

Knowledge of active faults in New Zealand, while constantly developing, is still far from complete. Recently, Cox et al. (2012) examined four previously unknown active

Faults within the central Southern Alps and estimated their probable moment magnitudes and recurrence intervals. As the region is highly susceptible to coseismic landsliding, these findings highlight a requirement to better understand the spatial density, activity, and hazard potential of faulting within the Southern Alps. Although an up-to-date model of active faulting within New Zealand exists (i.e. Langridge et al. 2016) a prior review by Litchfield et al. (2014) described the model as incomplete. The areas of interest to this thesis were described as at "medium" completeness, as the expected fault density is not currently fulfilled by the number of known faults. This point is further reinforced by Nicol et al. (2016), which with reference to the National Seismic Hazard Model of Stirling et al. (2012) and the known historical earthquake record of New Zealand, suggest that an additional ~140 active-fault earthquake sources capable of generating $M_W \geq 7$ earthquakes should exist nationally.

1.2.2 Coseismic landslide modelling and susceptibility

Estimation of regional coseismic landslide susceptibility has been a focus of research since the 1960s (e.g. Newmark, 1965; Clough & Chopra, 1966; Stewart et al., 2003; Robinson, 2014; Kritikos et al., 2015; Robinson et al., 2016). The earlier methods required both accurate spatial data and complete historic landslide inventories. These are not available in New Zealand. While attempts have been made to compile landslide information in the Southern Alps, notably Korup's (2005) mapped distribution of 778 landslides in southwest New Zealand, the inventory is still too limited to empirically map regional susceptibility or determine which of these landslides were of coseismic origin. To overcome these limitations, Kritikos et al. (2015) and Robinson et al. (2016) employed a mathematical set theory approach; commonly referred to as fuzzy logic. To model and map coseismic landslide susceptibility within the Southern Alps, two complete overseas coseismic landslide and ground motion inventories were incorporated, with a third independent inventory used to test it. These pieces of research provide a method, based on variable membership contributions of certain factors, to accurately map susceptibility in a repeatable manner. Using deterministic values of historic or hypothetical earthquake events, this method provides the capability to further the understanding of coseismic landsliding within the Southern Alps; with the potential for application in other locations or contexts.

1.2.3 Palæoseismic indicators and geomorphic evidence

Various forms of physical evidence, both on-fault and off-fault, have been attributed to a large West Coast earthquake circa 1620 C.E. These studies range from lichenometry, river terrace aggradation, river avulsion, dendrochronology, coastal dune progradation, lake sedimentation, and liquefaction and sand horizons (e.g. Berryman et al., 2012a, 2012b; Bull, 1996; Bull, 2008; Davies & Korup, 2007; Howarth et al., 2012, 2014, 2016; Wells & Goff, 2006, 2007; Yetton, 1998, 2000; Wells et al., 1999). However, the geomorphic evidence is inconsistent, partially due to the reliance on a range of dating techniques, suggesting that the geomorphic evidence could potentially have resulted from a non-Alpine Fault earthquake or a multi-earthquake scenario.

1.2.4 Segmentation and rupture behaviour of the Alpine Fault

The segmentation of the Alpine Fault is a key factor when considering its palæoseismic record and the implications this has on regions proximal to it. Fault segmentation can occur on a variety of scales and is believed to occur at topographic and structural discontinuities along a fault plane (Schwartz & Coppersmith, 1986). Different fault segments are presumed to represent lengths of a fault plane that rupture characteristically and similarly throughout successive rupture episodes (Schwartz & Coppersmith, 1986; Bull, 1996). In a New Zealand context, these factors were considered when assigning segmentation to the Alpine Fault. Currently, it is assumed the Alpine Fault comprises three discrete sections; the northern, central, and southern sections (Figure 1.1), which was implemented as a convenience for the coarse classification of the few most recent ruptures (Rhoades & Van Dissen, 2003). Of the three sections, the central and southern segments provide the best estimates for analysis of the previous Alpine Fault rupture behaviour, as the majority of research has been conducted pertaining to these segments. On these two sections the discrepancies between age determinations for the ~1620 C.E. event is a key driver in the hypothesis of this thesis. Off-fault palæoseismic indicators lateral to the southern segment display ~1620 C.E. activity, but none has yet been confirmed on-fault (Berryman et al., 2012a, 2012b). This event has been postulated as a central-northern segment earthquake (Yetton., 1998); however, the wide-spread geomorphic evidence of the earthquake does not appear to conclusively align with this proposal.

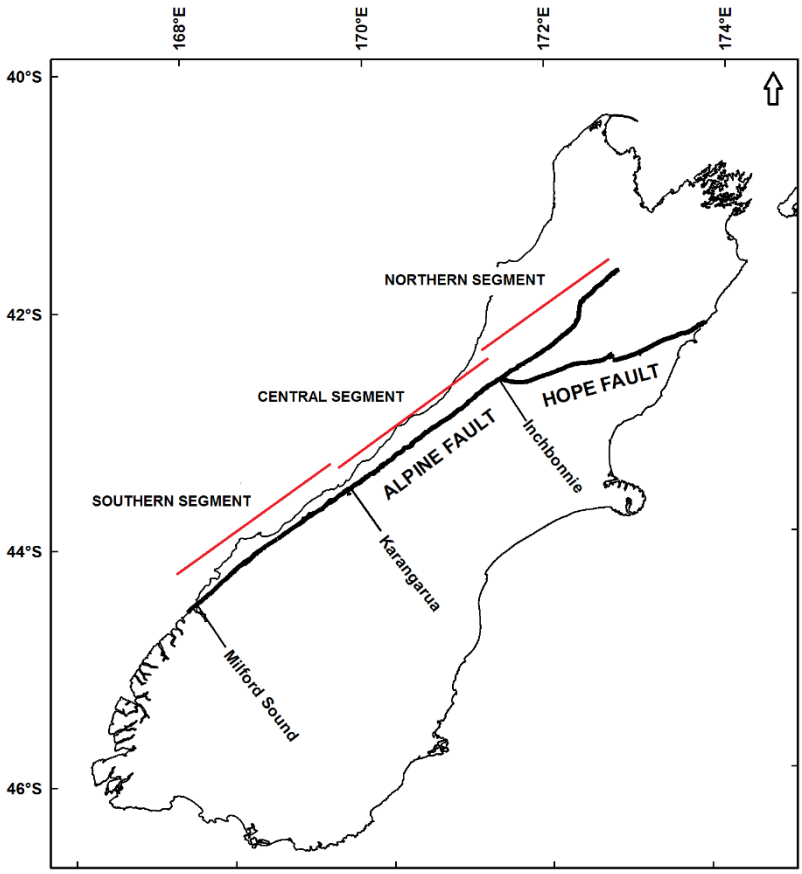

Figure 1.1: Segmentation of the Alpine Fault. After Rhoades and Van Dissen, 2003.

The research listed in **1.2.3** above also includes various attempts at dating other Alpine Fault events to better understand its rupture frequency and patterns. A common consensus is that the recurrence interval for the central section is approximately 300 years. To date, the Alpine Fault has been considered the dominant source for all palæoseismic evidence within its proximity unless otherwise proven. However, anomalies in the dating and location of geomorphic evidence have driven attempts to better understand its behaviour. Recent research incorporating LiDAR to measure dextral offsets of the central Alpine Fault by De Pascale et al. (2014) concluded that two possible scenarios could describe the Alpine Fault rupture history:

1) The Alpine Fault expresses bimodality, experiencing full-length ruptures every 270 ± 70 years and partial ruptures that result in smaller moment magnitude earthquakes with undefined frequency that do not result in significant fault offset.
2) The Alpine Fault ruptures characteristically, i.e. regularly with similar ~8.0 M_W events.

Evidence supporting bimodal behaviour is inconclusive for a number of reasons. Foremost it does not accurately represent expected slip-rate values when considering the plate-motion budget of the South Island. The Alpine Fault accumulates ~40 mm per year of potential dextral slip which exceeds the geodetic motion estimates of ~30 mm per year (DeMets et al. 1994; Wallace et al, 2007). This deficit could either be attributed to error propagation within the methods used to obtain it, or could be attributed to other hypotheses. These include the rotational plate motion suggested by Wallace et al. (2007) or unknown fault movement within the South Island. Secondly there is no indication in either the palæoseismicity or the historic earthquake record for bimodality. Therefore, as suggested by De Pascale et al. REPLY (2014), while plausible, the supporting evidence for bimodal behaviour is not strong. Thus the ~1620 C.E. event, smaller than other postulated Alpine Fault earthquakes, could have occurred on an alternative unknown fault within the Southern Alps; a hypothesis this thesis will explore.

1.3 Statement of the problem

Many unknown active faults may exist within the Southern Alps without identified surface expression. Their hazard potential is unknown but can be hypothetically estimated to better understand the potential coseismic risks they could pose. Moreover, ambiguities in palæoseismic indicators inferred to be related to the Alpine Fault, combined with the absence of ruptures since 1717 A.D., could imply that the ~1620 C.E. event was not a rupture of the Alpine Fault.

1.4 Significance of the study

To prove the accuracy and applicability of any modelling process, multiple iterations should be implemented. For this purpose, using the methods formulated by Kritikos et al. (2015) and further applied by Robinson et al. (2016) under different circumstances and comparing results provides quantifiable evidence to test the effectiveness of the modelling process. These comparisons could aid in understanding the hazard potential of unknown active faults within the central Southern Alps, as well as the magnitude of coseismic landsliding expected to result from a large ground-shaking event within the region; the implications of which could be used within a disaster management framework. Furthermore, the results obtained could

provide additional evidence to support various hypotheses regarding the geomorphic inconsistencies attributed to seismic behaviour within the region; predominantly surrounding the ~1620 C.E. earthquake event.

1.5 Primary research objectives

The primary aim of this research is to implement a coseismic landslide susceptibility model (with associated landslide volumes presented as denudation and aggradation depths) for a hypothetical fault rupture originating within the western Southern Alps. To this end the methods of Kritikos et al. (2015) and Robinson et al. (2016) will be employed (Figure 1.2). Understanding the coseismic hazard potential of this area could aid in refining emergency response planning and illustrate the need for additional research.

The following objectives will primarily be achieved or considered throughout the research:

Objective 1

Quantify coseismic landslide volumes likely to arise from the rupture of a hypothetical fault in the central northern Southern Alps capable of large M_W shaking.

Objective 2

Quantify anticipated denudation and aggradation resulting from Objective 1.

Objective 3

Determine whether or not the ~1620 C.E. earthquake occurred on the Alpine fault.

Objective 4

Analyse the above objective outcomes in comparison with previous research to determine inconsistencies and whether emergency response planning needs amendment or addendum.

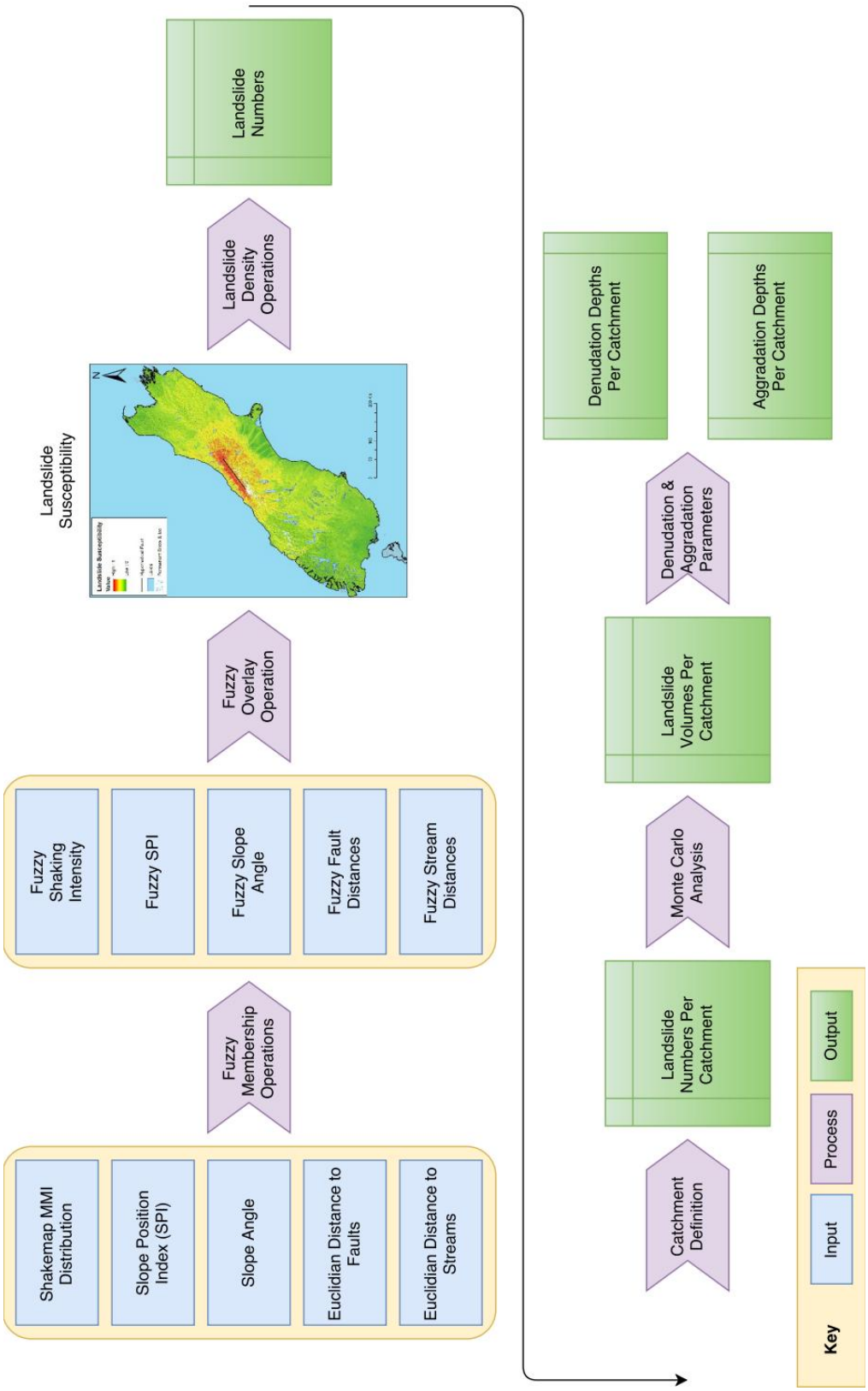

Figure 1.2: Flowchart of methods to be employed.

1.6 Thesis outline

- Chapter Two will consist of a literature review of the Alpine Fault, with its properties and previously inferred behaviour presented. Previous research and the methods therein will be scrutinized and ambiguities explored. Geomorphic evidence for a ~1620 C.E. event will be presented and previous regional coseismic landslide modelling and its implementation will then be examined.
- Chapter Three comprises two related sections:
    - Firstly, the modelling input parameters are defined and the methods employed in ArcGIS and OpenSHA are described. Their application to the research objectives will be explored, and justifications for their application and the inclusion of input parameters used presented.
    - Secondly, the results of each stage of modelling will be provided with key findings summarized for later discussion.
- Chapter Four provides a discussion of the results and their relationhsip to the current gaps in knowledge. The similarities and differences will be explored and potential reasoning provided.
- Chapter Five provides a brief overview of hazard management on the West Coast predominantly focusing on the Alpine Fault. Previous disaster response research and scenarios will be discussed and the implications this thesis could have on them will be discussed.
- Chapter Six concludes the thesis and provides a summary of the research as an overall contribution to both geoscience and disaster planning. Areas of potential future work will be highlighted and recommendations provided on how these could be carried out.

2 DETERMINING FACTORS OF INFLUENCE FOR INPUT PARAMETERS OF A ~1620 C.E. WEST COAST EARTHQUAKE

2.1 Introduction

The purpose of this literature review is to determine the parameters and both seismic and coseismic potential of a hypothetical active fault within the northern central Southern Alps. This review will investigate the large West Coast earthquake around 1620 C.E. which is generally attributed to the Alpine Fault. To assess the plausibility of an alternative fault rupturing during this period, the behaviour of the Alpine Fault will be explored and previous research on the palæoseismic indicators and geomorphic evidence within the region will be analysed.

2.2 Underlying geologic structure of the Southern Alps and Alpine Fault

To begin interpreting regional fault properties, the basic underlying geologic structure of the Southern Alps must first be understood. The driving factors behind fault distribution and geometry can be deduced through analysis of structural studies of both the Southern Alps and other similar continental transform boundaries globally.

Geologically, the hypothetical fault is positioned within the Rakaia Terrane which is composed dominantly of Alpine Schists (more specifically Haast Schists) and contains a variation of schists and semischists with intermittent metamorphic mineral isograds delineating these variations (Cox et al., 2012; Cox and Sutherland, 2007; Cox and Findlay, 1995; Herman et al., 2009) The hypothetical fault's position, for the most part, runs parallel to one of these isograds where rock-type inconsistencies would promote faulting (Figure 2.1).

A large body of academic work exists related to the Alpine Fault's structure at depth (e.g. Davey et al., 2007; Koons et al., 2003; Little et al., 2002a, b; Norris & Cooper 2007; Norris & Toy, 2014; Stern et al., 2007; Van Avendonk et al., 2004). The resultant or adapted structural models therein provide a theoretical basis from which to hypothesise faulting properties within the Alpine Fault-proximal Southern Alps; namely the potential depth a hypothetical fault could reach in this area. Many of these models are the result of, or heavily influenced by the 1996 South Island Geophysical Transect (SIGHT) project, which employed seismic refractivity measurements along two transect lines to deduce the depth and continuity of the South Island's geologic structure (Figure 2.2).

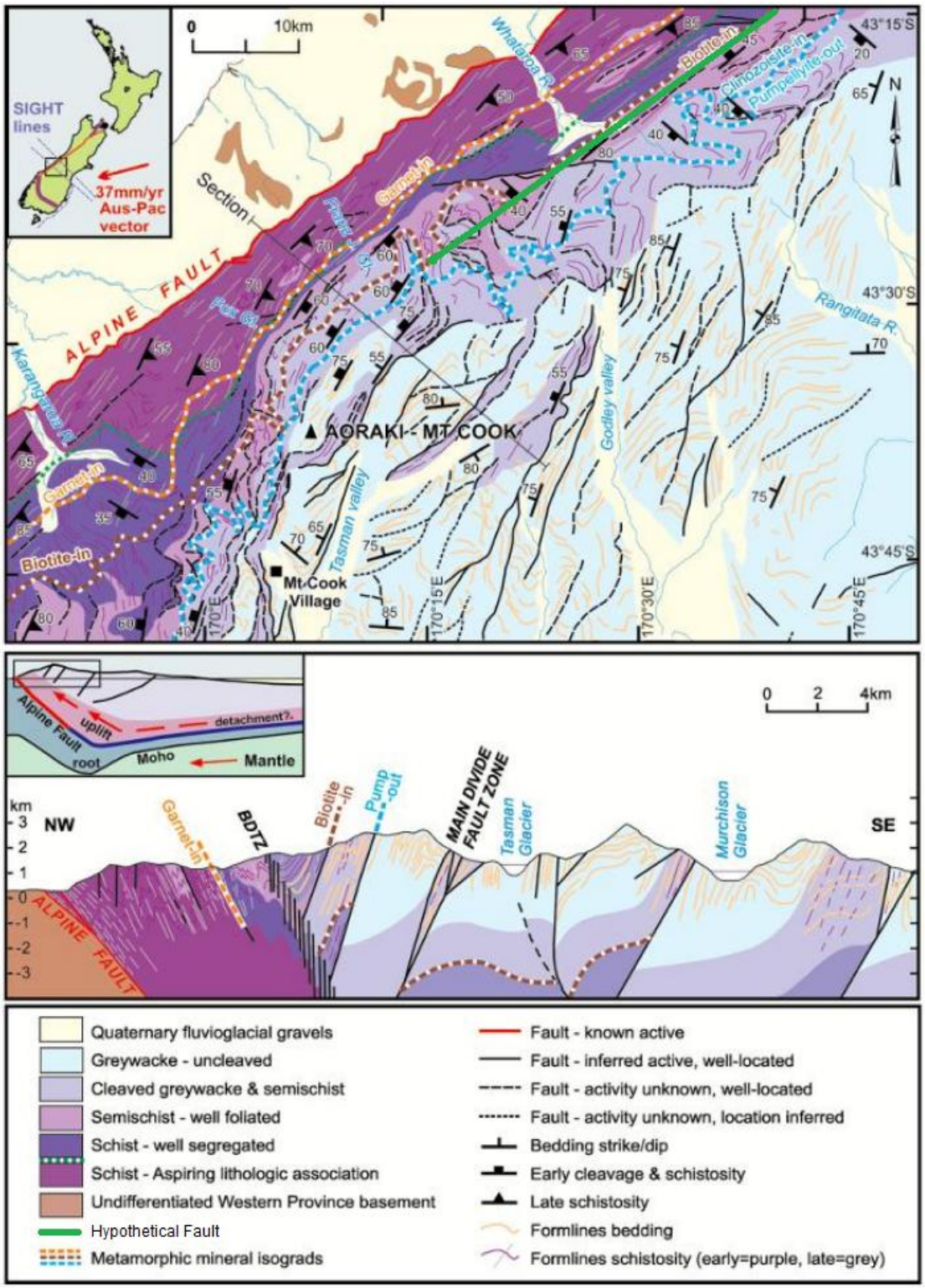

Figure 2.1: Map of central Southern Alps showing terrane transitions, generalised bedding orientations, and known faults with relation to the Alpine Fault and hypothetical fault (green), which extends northeast along strike for approximately 55 km. Adapted from Cox & Sutherland (2007).

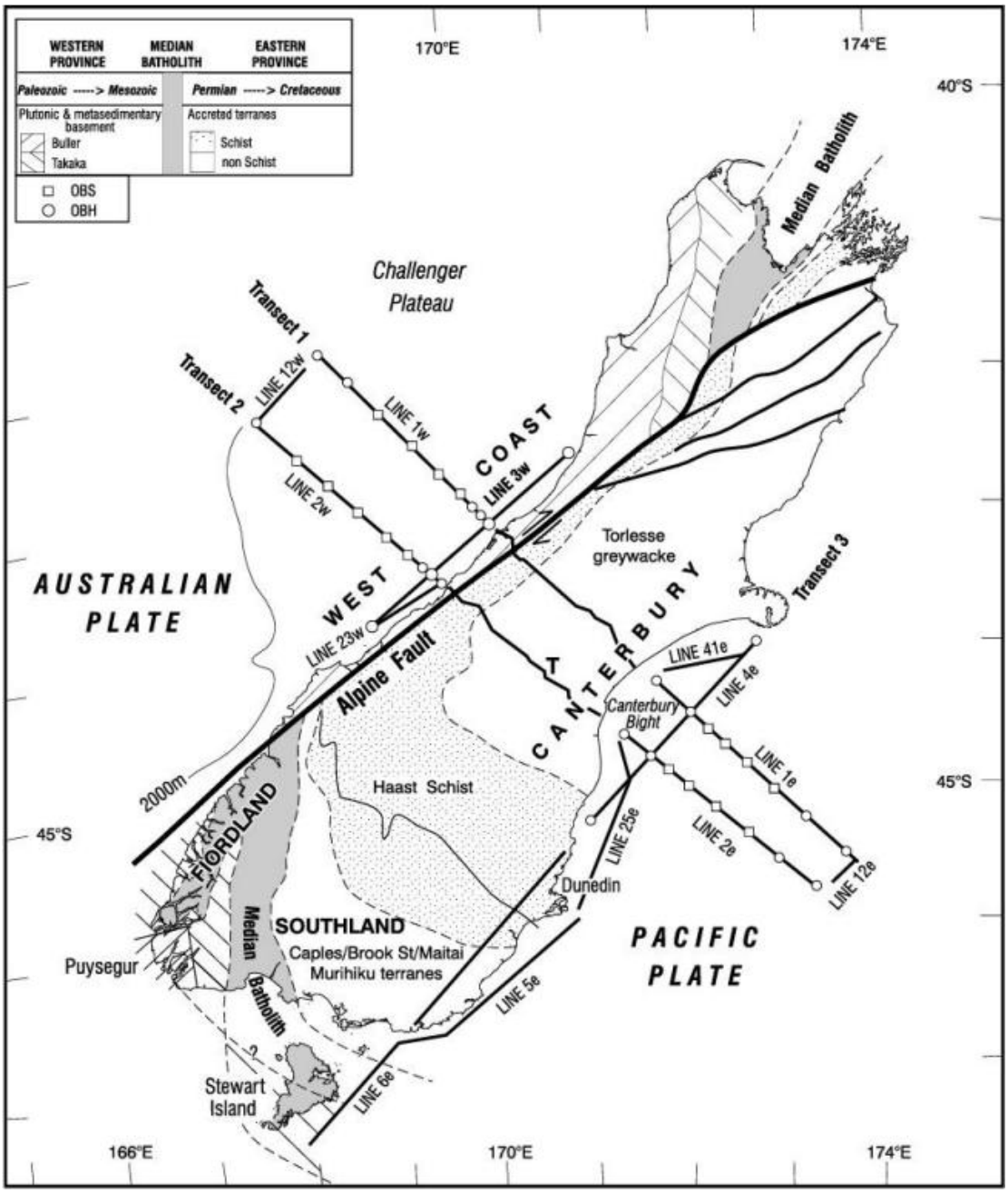

Figure 2.2: Location of SIGHT transect lines over the generalised geology of the South Island (Davey et al., 2007). Note the central position of transects relative to the Alpine Fault.

Refining work from Stern et al. (2007), Norris and Toy (2014) presented an interpretation of the Alpine Fault along the SIGHT 1 Transect profile (Figure 2.3).

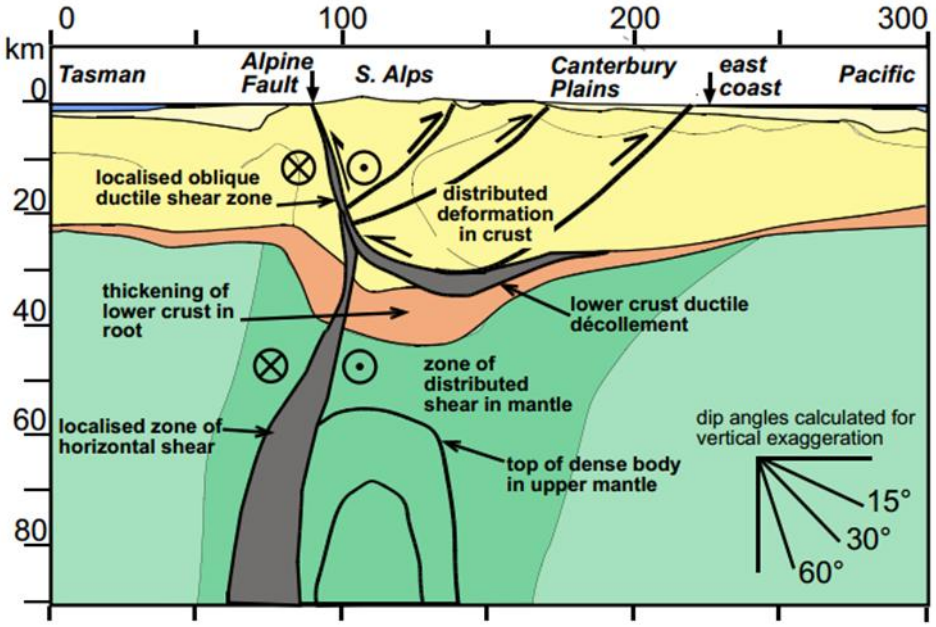

Figure 2.3: Interpretation of Alpine Fault structure at depth along the Sight 1 transect. Note outward deformation zone from the Alpine Fault to the Southern Alps (Norris and Toy 2014). Note vertical exaggeration.

Focusing on the crustal structure of this interpretation, the zone of outward deformation away from the Alpine Fault incorporates a crustal root extending from the Alpine Fault to the Southern Alps. This interpretation, among others provides a basis for potential fault depths in the vicinity of the Alpine Fault. It should also be noted that the extent of the distributed deformation may not be constant but rather a function of rheology and oblique collision along-strike (Upton et al., 2009). As the structural continuity along-strike of the Alpine Fault is unknown, the location of a hypothetical fault could be assumed within this zone of distributed deformation.

As this thesis has a hypothetical basis, plate boundary proximal fault systems from multiple locations should be considered; namely the Alpine Fault, San Andreas Fault system, and North Anatolian Fault. A recent review paper comparing these continental transforms and their proximal zones by Norris and Toy (2014) demonstrated various similarities that could influence the parameters of unknown faulting within the Southern Alps.

Factors of relevance to this study are:

- Both the San Andreas Fault and Alpine Fault have broad zones of distributed shear (>100 km wide) where other large faults could and do exist (Norris & Toy, 2014).
- All three transform zones accommodate at least 50% of interplate motion which correlates with other studies specifically focused on the Alpine Fault's plate motion budget (Norris & Toy, 2014).
- The viscous detachment zone (shown in Figure 2.3 as the lower crust ductile décollement) to the east of the Alpine Fault is linked to multiple convergent reverse faults in Southern Alps (Norris & Toy, 2014).

Utilizing this information, it is possible to begin allocating parameters influenced by the Alpine Fault to the hypothetical fault Shakemap model.

2.3 Faulting within the Southern Alps

2.3.1 Fault Categories

For the purpose of this research, faults within the Southern Alps faults are categorized as either active faults, inactive faults, or unknown faults:

- **Active faults** are faults that are known to have been active (i.e. have ruptured the ground surface) within the last 125,000 years, or are faults displaying a currently visible surface expression (Langridge et al. 2016).
- Conversely, **inactive faults** are faults that are known to have not ruptured within the last 125,000 years and have no visible surface expression.
- Finally, **unknown faults** are considered faults that have no known parameters aside from rough geographic position inferred from fault distribution research, such that their presence in a region is purely hypothetical. Although this may not seem a sound basis on which to conduct research, it is well accepted that the current level of knowledge regarding fault distribution within New Zealand - and especially the Southern Alps - is incomplete (Litchfield et al., 2014, Nicol et al., 2016). Therefore, unknown faults could be considered active or inactive. However, if an unknown hypothetical fault were to be

active, the hazard it poses to the natural and built environment can be determined and its potential modelled.

2.3.2 Regional Kinematics, fault distribution, and fault parameters

Of further consideration when determining realistic parameters for a hypothetical fault, the properties of known faults within the Southern Alps and their kinematics and governing tectonic regime are considered.

2.3.2.1 Regional kinematics and fault distribution

New Zealand is divided into 15 tectonic domains, which at the time of publication, included 635 individual fault zones (Litchfield et al., 2014). The 15 tectonic domains are primarily delineated by grouping fault zones with similar geometries and kinematics within a geographic region (Berryman & Beanland, 1991; Stirling et al., 2012; Wallace et al., 2007) (Figure 2.4). Although currently available research was used in defining the boundaries, clearly defining discrete boundaries with data of varying quality leaves potential for uncertainty; so one area, although displaying properties of a specific domain, could belong to another. Litchfield et al. (2014) attempted to overcome this shortfall by defining a hierarchical quality code to reduce uncertainty and minimise the issue.

This research focusses on the domains 8-9 and 11-12, comprising the transpressional plate boundary convergence between the oceanic Australian Plate and the continental Pacific Plate (Litchfield et al., 2014). **Figure 2.4** shows the kinematics of these domains (measured by cumulative net slip rates) and quantifies the relative motion of the eastern South Island. The tectonic domains also encompass zones with unknown slip rates, adding weight to the argument that unknown active faults are responsible for a portion of the unallocated plate motion deficit (Figure 2.5). Although these zones do contain known faults, rapid erosion and access issues impede the accurate measurement of slip rates, which presents the ability to investigate hypothetical fault activity within this region.

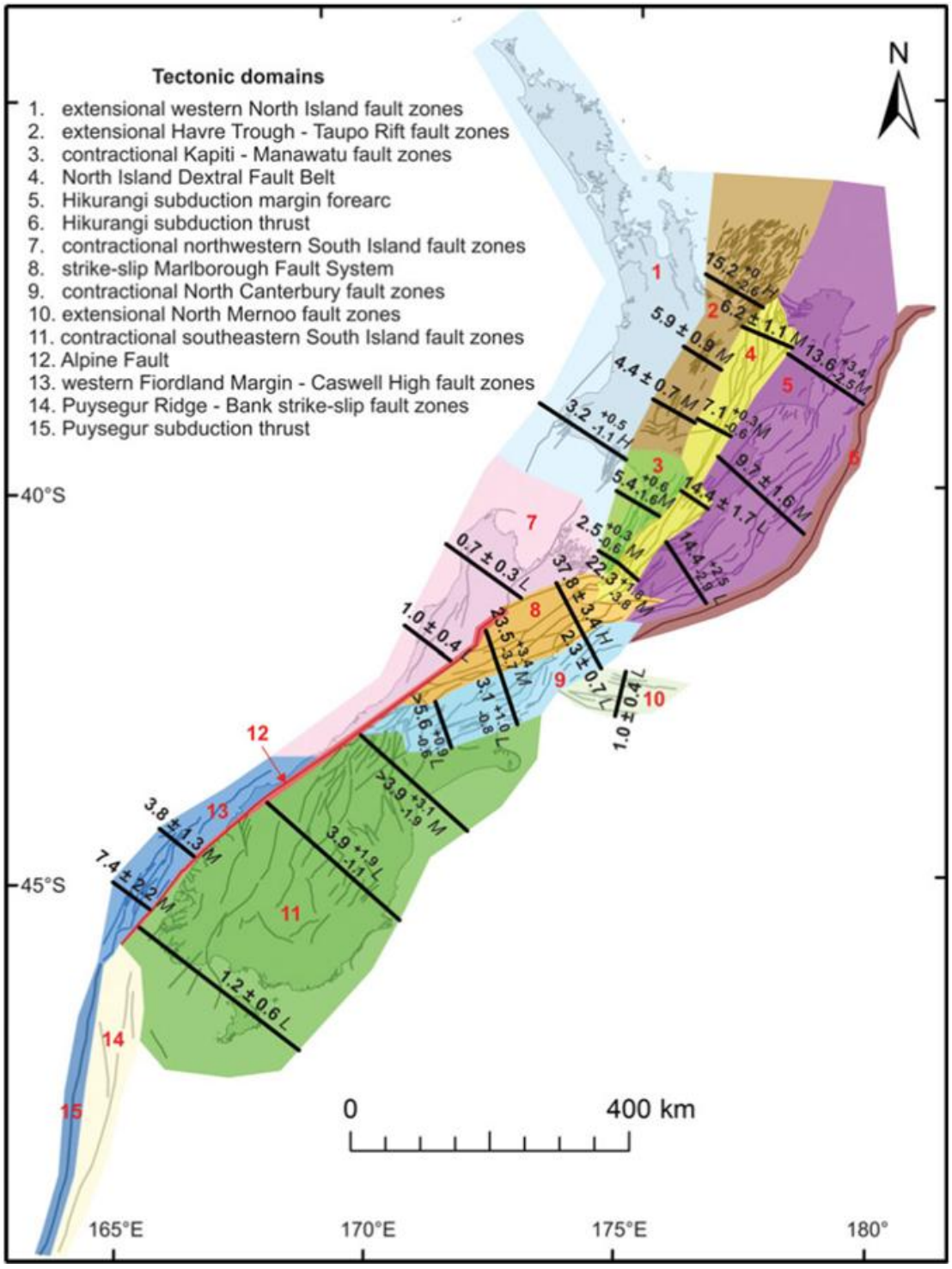

Figure 2.4: Major New Zealand tectonic zones grouped primarily by similar fault movement senses. Black lines represent cumulative slip rates (mm/yr.) and H, M, and L (High, Medium, and Low) represent inferred confidence in slip rates based on fault distribution completeness. The area of interest for this thesis is NW of zone 11, W of zone 9, S of zone 8, and the Alpine Fault (red line) (Litchfield et al., 2014).

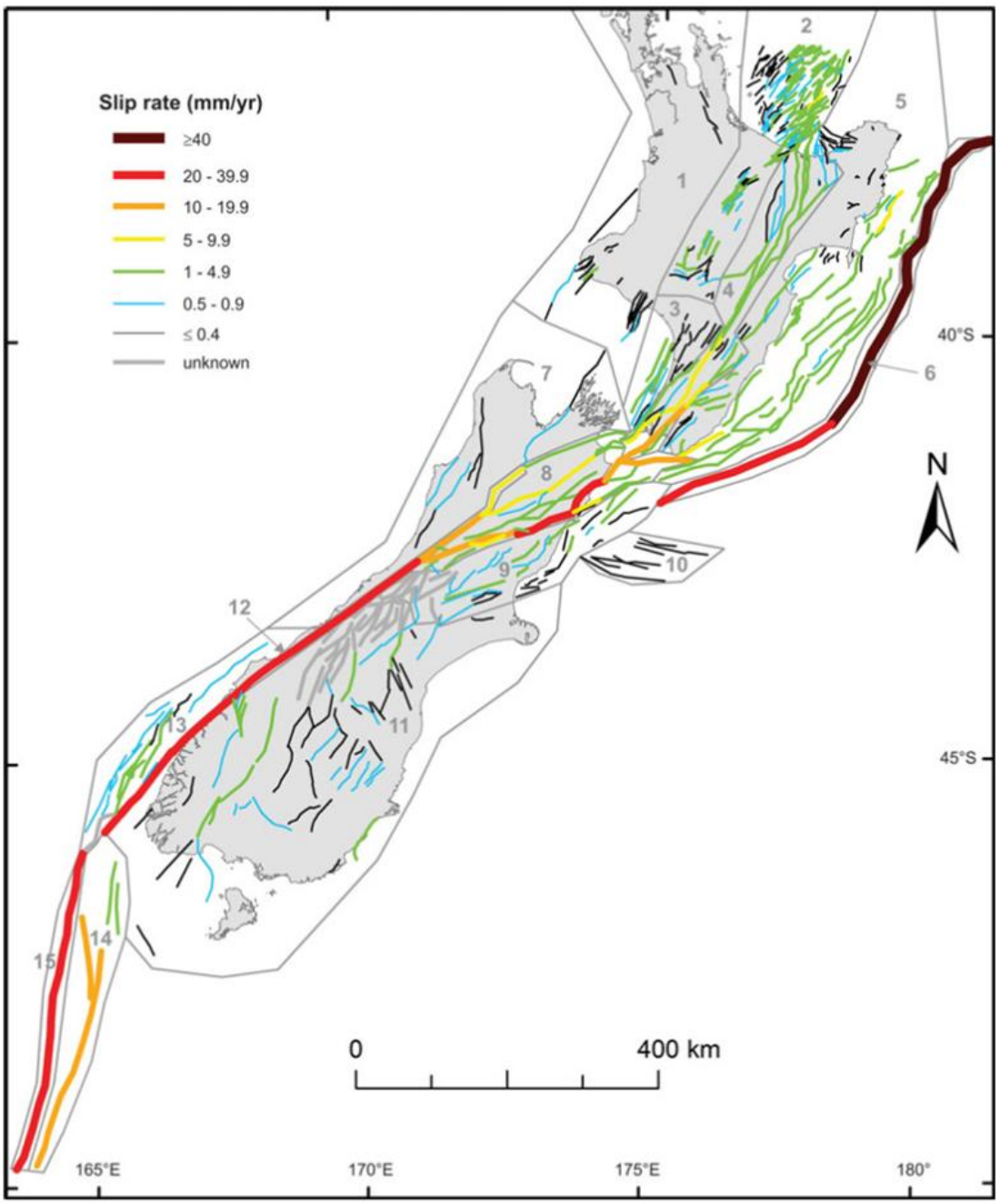

Figure 2.5: Map of New Zealand showing minimal or unknown slip rates within the Southern Alps and varied slip rates along the Alpine Fault and Marlborough Fault Zone junction (Litchfield et al., 2014).

It is the zone of convergence formed by these domains, where many unknown faults are believed to exist, which is integral to this research. Details of these zones relating to the position of the hypothetical fault are:

- Domain 8 - The westernmost zone bordering Domain 9 and 12 contains faults ranging from 18 to 145 km in length with cumulative slip rates of ~23.5 mm/yr. in a dominantly north-eastward direction transferring slip from the Alpine Fault to the Marlborough Fault System (Litchfield et al., 2014).
- Domain 9 - The domain is characterized by its contractional nature containing mixed fault types, with a majority of reverse faults interspersed with a smaller number of normal faults. Faults within the western section are transpressional with northwest-striking fault zones creating complex transfer structures between northeast-striking fault zones (Abercrombie et al., 2000; Cox et al., 2012; Litchfield et al., 2014; Robinson & McGinty, 2000). Fault zones of the western section have no assigned slip rates representing a lack of faulting knowledge within this zone (Litchfield et al., 2014).
- Domain 11 - Within this domain, the majority of fault zones strike north to northeast with additional faults striking northwest creating an orthogonal array (Litchfield et al., 2014). The north-western section, where this domain converges with the other key domains for this research, illustrates this orthogonal pattern. There is a gradual transition to a more northeast striking region trending toward the Marlborough Fault System.
- Domain 12 - The smallest domain, strictly dedicated to the Alpine fault and segmented into multiple sections. From Aoraki to the Marlborough Fault System, the dominantly dextral slip decreases as it is transferred to other faults (Langridge et al., 2010; Litchfield et al., 2014) It is within this zone of transfer that unknown slip rates could be heavily influenced by unknown faults.

2.3.2.2 Potentially active faults within the central Southern Alps

Incorporating supporting geologic evidence, Cox et al. (2012) described four recently discovered active faults within the central Southern Alps, indicating the potential for large unknown faults within the region. The faults, together with associated earthquake-shaking values ranging from 6.1-7.2 M_W can be considered representative

of the hazard potential of unknown faults within the region. Cox et al. (2012) constructed fault geometry and earthquake shaking calculations using the methods of Stirling et al. (2002), producing reliable and repeatable estimates applicable to determining input parameters for this thesis. The limitations outlined by Cox et al. (2012) are also applicable, where fault parameters in their entirety cannot be fully deduced due to uncontrollable factors. One such factor includes the ability to only map faults within exposed bedrock, when they might be continuous under alluvium-filled valleys and thus their hazard potential can be underestimated.

Having calculated seismicity-based recurrence intervals for 110 faults within the central Southern Alps, Cox et al. (2012) estimated an earthquake recurrence interval for $M_W > 6.3$ earthquakes of 4000-13000 years. This implies that, although large earthquake events within this region are not common, they are geologically frequent and the faults responsible are well within "active" faulting constraints, such that one could be responsible for the ~1620 C.E. event. Cox et al. (2012) suggest that average inter-seismic denudation could be up to two orders of magnitude greater than fault displacement during an event. This is a key area of interest within this thesis and aids in explaining why no evidence of displacement exists on the faults described by Cox et al. (2012). Furthermore, surface rupture evidence does not necessarily have to be present to justify a hypothetical fault location.

By examining similar factors within the domains described above in addition to the estimates and inferences presented by Cox et al. (2012) it is possible to allocate further estimated parameters to a hypothetical unknown fault. Combined with the other factors that influence or represent fault activity, a scientifically informed representation of an active fault can be hypothesized and subsequently have its hazard potential explored.

2.4 Plate motion budget and the justification for large unknown faults in the Southern Alps

Further related to kinematics within the region, many studies have contributed to estimating and understanding the distribution of the plate motion budget in the South Island; sometimes referred to as the slip-rate budget. The Alpine Fault accommodates approximately 50-80 percent of the plate motion budget of the South Island

(Langridge et al., 2010; Norris & Cooper, 2001; Sutherland et al, 2006). Norris and Cooper (2001) suggested that the remaining budget is accommodated by faults east of the Alpine Fault, adjacent to the central section of the Alpine Fault. However, ambiguity exists between geologic and seismologic data when determining where to apportion the remaining budget. Even when attributing the ~1620 C.E. event to the Alpine Fault, the remaining budget distributed among known faults does not represent the entire value (Beavan et al., 2002; Cox et al., 2012; DeMets et al., 1994, 2010; Wallace et al., 2007). Inherently the inclusion of additional unknown faults would reduce this value. Although hypothetical faults cannot be quantitatively used to substantiate reducing the deficit, determining their potential and modelling their outcomes could provide insight into the effects of unknown faults on the plate motion budget via rupture displacement potential.

Research of the plate motion budget include data across multiple disciplines and contexts, encompassing geologic slip rates (e.g. Norris & Cooper, 2001), seismological data (e.g. Langridge et al., 2014), and GPS data (e.g. Wallace et al., 2007). When summarizing the calculated deficit informed by these three methods, Wallace et al. (2007) theorized that the deficit could be balanced by the inclusion of a statistical model which incorporated the rotation of the tectonic blocks comprising the South Island. Furthermore, they mentioned the likelihood that the dextral and contractional components of known slip rates might be underestimated and that there could be undiscovered faults in the eastern foothills of the Southern Alps. Although this is likely, no comment is provided regarding the potential for undiscovered faults in the western Southern Alps. This appears to be an oversight, as faults have been discovered within the central Southern Alps (i.e. Cox et al., 2012) and the fault distribution within the Southern Alps is known to be incomplete (Lichfield et al., 2014).

More recent research provides an additional theory introducing implications for the allocation of the plate motion budget. Specifically seismological evidence, which could also have implications for the nature of the Alpine Fault's rupture periodicity. Utilizing the Southern Alps Microearthquake Borehole Array (SAMBA), Boese et al. (2012, 2014) presented a thorough review of microseismicity in the vicinity of the Alpine Fault over a 14-month period, capturing the seismicity of ~1800 small earthquakes. The relevant findings of Boese et al. (2012, 2014) showed four well-

constrained, distinct clusters of microseismicity within the central Southern Alps. These clusters surround a zone where minimal microseismicity no observed (macro)seismicity occured (Figure 2.6). This presents an opportunity to position a fault within this zone, where strain could potentially be accumulating to be released in a large rupture of an unknown fault. Furthermore, these data could be considered additional evidence against the bimodal rupture behavioural pattern of the Alpine Fault suggested by DePascale et al. (2014), as strain is continually released within the region so a longer interseismic period could logically be expected, even though the released energy would be minimal. Additionally, this would appear to conflict with multiple Alpine Fault rupture events within a period less than 300 years, (i.e. ~1460, ~1620 and 1717 A.D.) further supporting the hypothesis the ~1620 C.E. event could in fact be non-Alpine Fault derived.

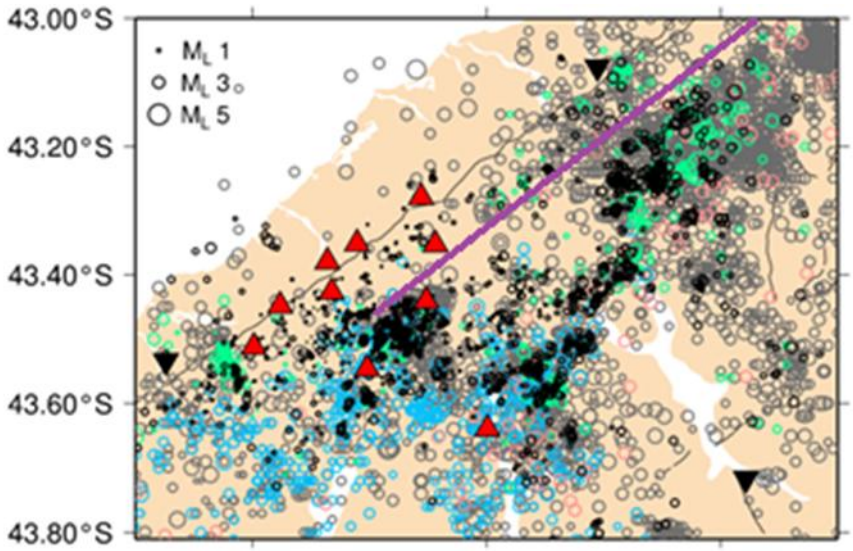

Figure 2.6: Recorded seismicity in the central Southern Alps since 1984 (Geonet = grey circles, Reyners, 1988 = blue circles, Leitner et al., 2001 = red circles, O'Keefe, 2008 = green circles), Red triangles showing monitoring stations and purple line representing the southern portion of hypothetical fault located within the zone of low seismic activity. Adapted from Boese et al., (2012).

2.5 Exhumation within the Southern Alps

The process of exhumation is believed to be a key factor influencing the susceptibility of the Southern Alps to both faulting and landsliding. In combination with intense climatic factors, the rapid rate of exhumation of various sections of the

Southern Alps is thought partially responsible for the mechanical behaviour of the region and the concentrated deformation at the plate boundary (Cox et al., 2012; Kamp et al., 1989; Koons, 1987, 1989, 1990, 1995; Koons et al., 2003; Norris and Cooper, 1997). Thus the young central section of the Southern Alps, with ages as low as 3-5 Ma and exhumation rates inferred at ~6-9 mm/yr., has resulted in oversteepened topography constantly affected by intense weathering, which overlies a complex system of faulting (Little et al., 2005). Consequently, the resulting landslide susceptibility due to seismicity, rock damage, and the gravitational potential of the topography demonstrates the effect exhumation has upon the Southern Alps. It also affects the availability of material for denudation.

2.6 Seismic and coseismic hazards within the Southern Alps

Earthquakes result in the release of massive amounts of energy which radiate from the rupture as ground shaking. This energy is transferred throughout the surrounding area generally decreasing in intensity with distance travelled (Sibson, 1989). The energy released can have catastrophic effects on the natural and built environments, both directly and indirectly. These effects are interrelated and can last for varying time frames, ranging from seconds to decades, with aftershock sequences hindering recovery attempts for unknown periods of time (Figure 2.7).

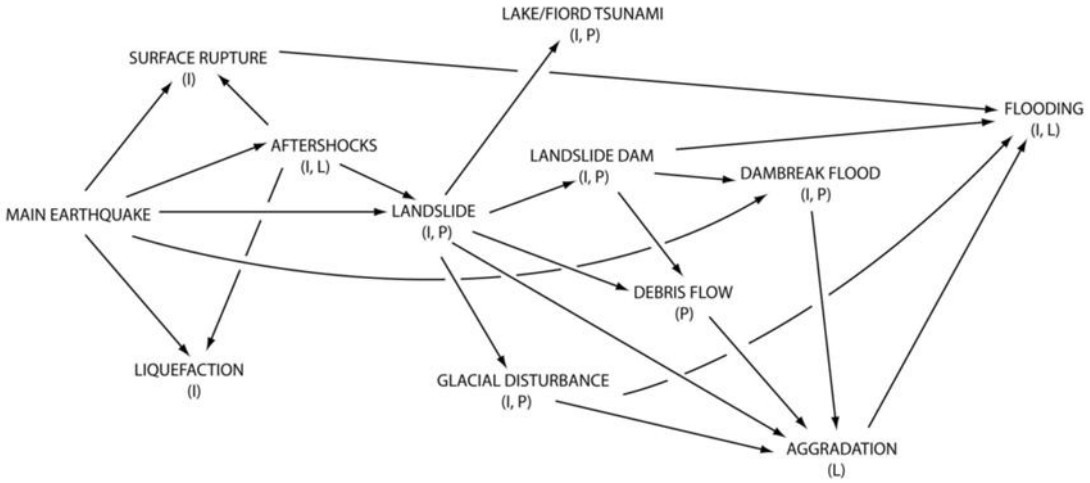

Figure 2.7: Seismic and coseismic hazard flow diagram showing potential geomorphic consequences resulting from earthquake (I = immediate; seconds to days, P = prolonged; weeks to years, L = long-term; years to decades) (Robinson & Davies, 2013).

2.6.1 Landslide Hazard

The United States Geological Survey (USGS) describe landslides as a "wide variety of processes that result in the downward and outward movement of slope-forming materials including rock, soil, artificial fill, or a combination of these" (USGS, 2004). The various types of landslides therefore have a classification system to differentiate the material and the motion it undergoes. The most widely accepted of these classification systems is that of Varnes (1978), updated by Hungr et al. (2014), which reviews and classifies a complete range of slope movement processes and the predominant materials (Figure 2.8).

Type of movement	Rock	Soil
Fall	1. *Rock/ice* fall[a]	2. *Boulder/debris/silt* fall[a]
Topple	3. Rock block topple[a]	5. *Gravel/sand/silt* topple[a]
	4. Rock flexural topple	
Slide	6. Rock rotational slide	11. *Clay/silt* rotational slide
	7. Rock planar slide[a]	12. *Clay/silt* planar slide
	8. Rock wedge slide[a]	13. *Gravel/sand/debris* slide[a]
	9. Rock compound slide	14. *Clay/silt* compound slide
	10. Rock irregular slide[a]	
Spread	15. Rock slope spread	16. *Sand/silt* liquefaction spread[a]
		17. Sensitive clay spread[a]
Flow	18. *Rock/ice* avalanche[a]	19. *Sand/silt/debris* dry flow
		20. *Sand/silt/debris* flowslide[a]
		21. Sensitive clay flowslide[a]
		22. Debris flow[a]
		23. Mud flow[a]
		24. Debris flood
		25. Debris avalanche[a]
		26. Earthflow
		27. Peat flow
Slope deformation	28. Mountain slope deformation	30. Soil slope deformation
	29. Rock slope deformation	31. Soil creep
		32. Solifluction

Figure 2.8: Hungr et al.'s (2014) updated version of Varnes' (1978) classification of slope movements. The words in italics are places holders; only one is used.

As observed in **Figure 2.7** and of key importance to this thesis, landslides are a central hazard amongst those originating from an earthquake. Landslides themselves are directly responsible for five further hazards originating from their occurrence with additional indirect hazards resulting in-turn from these. All landslides therefore have the potential to cause disaster at varying scales, with this potential growing with the magnitude and multitude of landslide instances. Large, deep-seated landslides ($>10^6$ m^3) are known to derive from the intense shaking of a large earthquake and can result in destruction, damage or the interruption of critical infrastructure (Whitehouse and Griffiths, 1983).

In a South Island context, the tectonic setting of the Southern Alps together with climatic factors and the oversteepening of hill slopes from rapid exhumation, combine to create a region highly susceptible to landslides. Other factors to consider regarding landslides and their impacts (not discussed in detail within this thesis as they are available elsewhere) include but are not limited to: run-out distance (see Hsü, 1975), site-specific geotechnical factors, and slope orientation to seismic wave propagation (Kritikos et al., 2015). An overview of the factors used within this thesis is provided in **Chapter 3**.

Historically, large earthquakes have been recorded as having caused widespread landsliding over very large areas in New Zealand. For example, the 1855 Wairarapa Earthquake of ~8.0 - 8.4 M_W is estimated to have triggered landslides over an area of 20,000 km^2 affecting areas up to 300 km distant from the epicentre (Darby & Beanland, 1992; Hicks & Campbell, 1998, Hancox et al., 1997). In addition, Robinson et al. (2016) estimated with 95% confidence that a mean estimate of ~50,000 landslides would occur within the South Island as a result of a full Alpine Fault rupture. However, following the ~80,000-100,000 landslides estimated during the Kaikoura Earthquake sequence of November 2016, this could now be considered conservative (Morton, 2016). These demonstrate well the potential of large earthquakes to cause widespread landsliding in mountainous environments when several influencing factors align. Hancox et al. (1997) show landslides becoming significant at earthquake shaking of MMI 6 or greater. Further to this, Yetton (2000) differentiated some site effects which could also exacerbate landsliding such as tertiary sandstone and mudstone experiencing slope failures on gentle to steep slopes of 10-40˚, or large rock avalanches occurring on high slopes steeper than 25-30˚

highly affected by topographic amplification. Therefore landslides can vary in size and can range from a small rock falling down a hill slope to colossal land displacements that comprise entire slopes such as the three giant landslides in Fiordland investigated by Hancox et al. (2013).

2.6.2 River Aggradation

Following the immediate response and recovery from earthquakes and landsliding, further strain can be placed on a region in the form of river aggradation. Caused by huge influxes of both aseismic and coseismic sediment to rivers and driven by climatic effects or landslide dam failures, aggradation results in the deposition of variable depths of sediment on floodplains, which can bury infrastructure and productive farmland. As modelled by Robinson et al. (2016), coseismic denudation resulting from a scenario M_W 8.0 Alpine Fault event providing sediment for aggradational processes could account for 10-70 years' worth of aseismic denudation within days, catastrophically altering river valleys, floodplains and alluvial fans.

Davies and Korup (2007) studied the effect of aggradation on alluvial fans, investigating several localities along the western rangefront of the Southern Alps. Trenching of fanheads and scale modelling indicated that the fan geomorphological features represented landslide-induced aggradation, demonstrating the drastically increased sediment supply to these river systems.

The trenching results of Davies and Korup (2007) provided evidence that the fanheads were formed by massive inputs of sediment at long time intervals. The soils responsible for the productive farmland formed between aggradation episodes and buried soils were found in alternating sequence with layers of coarse river gravel and other alluvium. Within one of these gravel units, wood fragments were retrieved and dated to 356 ± 33 years BP suggesting a date of emplacement between 1616 and 1682 A.D. The margin of error allows this aggradation episode to align with a ~1620 C.E. event.

2.7 Evidence for a large West Coast Earthquake approximately 1620 C.E.

In the geologic, seismologic, and geomorphic research determining prehistoric ruptures of the Alpine Fault, multiple inconsistencies arise with respect to a seismic shaking event occurring at ~1620 C.E. To shed light on these inconsistencies, the following section will review relevant previous research by dividing it into two sections: on-fault evidence and off-fault evidence.

2.7.1 On-fault evidence

2.7.1.1 Trenching of the northern and central Alpine Fault

Perhaps the most difficult research regarding a ~1620 C.E. Alpine Fault event to rebut is that conducted by Yetton (1998, 2000). Considered as established fact by those who have conducted research on Alpine Fault palæoseismicity since 2000, Yetton's research provided multiple insights into the previous activity on the Alpine Fault's trace at multiple locations. The rupture events determined were corroborated with other independent off-fault data sets creating a record almost beyond debate.

While Yetton's (2000) conclusions cannot be argued relative to the physical findings, the inferences and conclusions drawn can be reinterpreted. Of particular relevance to this thesis is Yetton's Crane Creek Event, evidenced at multiple locations along the fault trace. Yetton (2000) trenched across the Alpine Fault trace at multiple locations, radiocarbon dating vegetation specimens found in various soil units and ascertained that the Crane Creek Event corresponds directly to an earthquake occurring at approximately 1620 C.E. Of particular importance are three trenches interpreted by Yetton (2000) at Crane Creek, Coates Creek and Kokatahi (the Kokatahi 2 trench). The inferences arising from these three trenches provide key evidence of a ~1620 C.E. earthquake in the vicinity.

The Crane Creek trench is a small, hand dug trench, approximately 1 metre deep and perpendicular to a small furrow at the base of what was determined as the fault scarp. It is the key source of on-fault primary palæoseismic evidence of the ~1620 C.E. event, thus it requires thorough consideration herein. The trench face itself consists of very few layers and displays only one event horizon. Within a white sandy silt and

fine schist gravel layer two spatially close (~50 mm) samples were dated that align with a ~1620 C.E. event. Bounding this layer below is another layer comprising post glacial terrace gravels with no apparent base to it and above is a layer of peat and twigs. The data were interpreted to represent a fault scarp originating from surface ground rupture of an Alpine Fault earthquake which collapsed immediately post-earthquake into a furrow at the base of the scarp. The absence of other events within the trench, given the continuity of the post glacial terrace gravels and the thinness (~300 mm) of the dated layer, allows only minimal conclusions to be drawn directly. The absence of the most recent 1717 A.D. event (considered to be a full-length rupture) and the absence of events older than ~1620 C.E. also limits the inferences able to be drawn.

Approximately 6 km north of the Crane Creek trench, the Coates Creek trench is slightly more complicated while displaying similar palæoseismic indicators. Of particular interest is the presence of a thin (200-400 mm) layer of "loose blue grey silty sandy angular fine schist gravel". Yetton (2000) determined that this layer was of post-seismic aggradational origin. The angularity of the material clearly relates to a rapid-deposition sediment influx to the system and was likely provided by the aggradation of the Ahaura River fan in response to coseismic landsliding. Additionally, the radiocarbon dated samples from this unit relate to a ~1620 C.E. event. Further key properties of this trench are the presence of two fissures in coseismically deformed silt, subsequently infilled by the age-constrained sediment pulse. It is difficult to argue that these fissures are of non-Alpine Fault surface rupture origin, although the absence of a large scarp and a secondary fault trace less than 100 m distant may be relevant.

Approximately 70 km south along-strike of the Crane Creek trench, the Kokatahi 2 trench provides further, although less definitive, evidence of a ~1620 C.E. event. Yetton (2000) inferred that of the two apparent event horizons within the trench, the lower non-dated event was the Crane Creek Event. The trench itself is complex, containing multiple liquefaction features and variable unconformably bedded units. The smallest unit by two-dimensional surface area is a fault-bound soft brown peat layer which contained abundant twigs and young branches; although no samples were radiocarbon dated. Yetton (2000) inferred that this small layer represented the ~1620 C.E. event as the small stratum exhibited post-deposition modification by a

subsequent event (i.e. the 1717 A.D. event). While the trench provided evidence of a surface fault rupture, the proximity to the fault zone and the presence of peaty material, combined with the lack of dating reduces confidence in this inference, as it could have resulted from any proximal rupture prior to the 1717 A.D. event.

The radiocarbon dates that were obtained by Yetton (1998, 2000) were subsequently corroborated with tree cohort disturbances (discussed in more depth in the off-fault section). The inconsistencies and alternate interpretations provided below are for the most part separate from those conclusions focusing on physical evidence of the trench; either present or proximal.

- Crane Creek Trench – Northern Section (Figure 2.9)
    - The furrow described above could be pre-existing caused by an earlier event; the ~1490 event perhaps. There are no other layers in the trench representing a separate event, yet the depths of the layers and the timespan between this event and older events would indicate there should be, such that the material within the furrow could have been deposited during a different shaking event - not necessarily of the Alpine Fault.
    - The furrow may have acted as a small drainage channel incised at the scarp base for the catchment above to Crane Creek, which could have been infilled by sediment during the ~1620 C.E. shaking and subsequent sedimentation. Supporting this is the very evident erosion occurring at the bend in Crane Creek adjacent to the trench, although river undercutting and subsequent failure could also explain this. A flow channel would also help explain why there is no secondary peaty layer above the silty sandy schist gravel layer to represent another interseismic period, as flowing water would not allow the accumulation of such material. Additionally, dates of the fault gouge peat are far older than recent ruptures demonstrating that additional peat layers have not been amalgamated into it.
- Coates Creek Trench – Northern Section (Figure 2.10)
    - At Crane Creek and Haupiri River the fault is represented by a single trace, but there have been multiple rupture events, and no clear single event offsets can be recognized.

- Kokatahi 2 Trench – Central Section (Figure 2.11)
    - The fact that there are no dated samples from the layer, assumed to contain the material related to the Crane Creek Event, leaves interpretation open. Furthermore, there are two fault zones within this trench, yet the second fault zone contains no indication of vertical displacement.

There is no denying that a large earthquake occurred ca. 1620 C.E.; however, the fault trace evidence supporting this can be reinterpreted to suggest an alternate hypothesis for regional seismicity at this time. Also possible is the idea of multiple earthquakes within a small timeframe; perhaps involving the Alpine Fault. This has been previously recorded in the region when the Arthurs Pass Earthquake (M_W 7.1) and Murchison Earthquake (M_W 7.8) occurred within a four-month period in 1929 and has been further demonstrated in November 2016 with the Kaikoura Earthquake sequence, currently believed to be an activation of 4-6 fault planes, which resulted in two large earthquakes (McSaveney, 2014; Wright, 2016). Although it is not the intention of this thesis to devalue Yetton's findings, a fresh look at evidence to allow alternate investigations of regional coseismic geomorphology should be construed in a positive light and is a necessary step to justify this thesis' hypothesis.

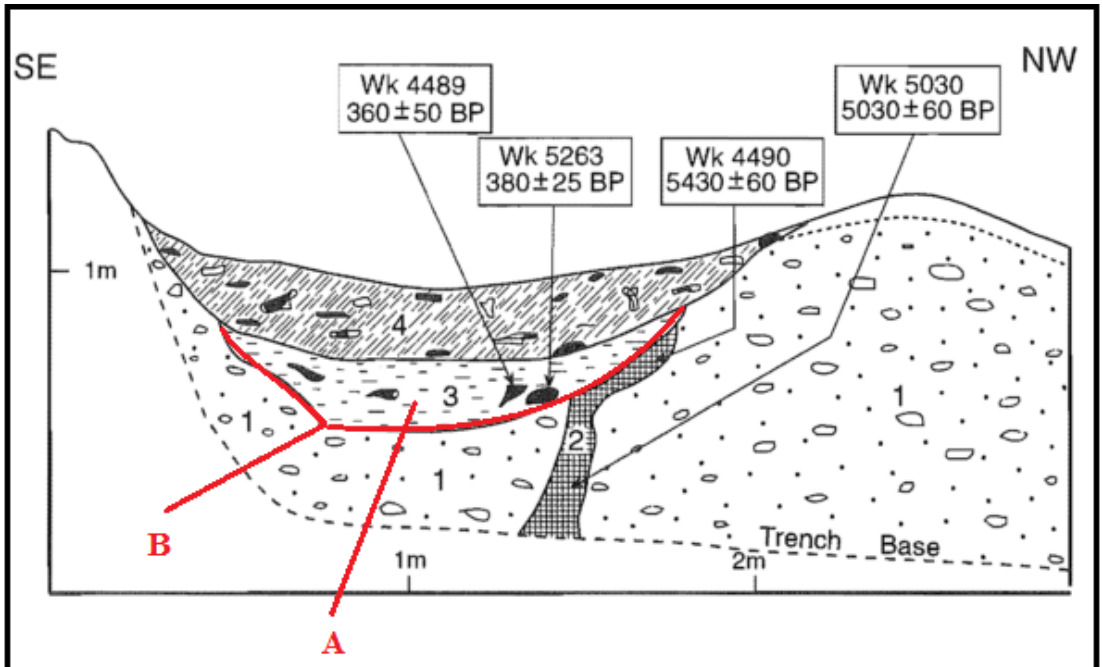

Horizon	Soil Description	Interpretation	Event Horizon
4	Soft brown peat and twigs	Forest litter since the last earthquake	
3	Firm white sandy silt and rare fine schist gravel and twigs	Coseismic scarp erosion sediment from last earthquake	← Most recent earthquake event
2	Hard dark brown clayey peat grading down into green silty clay with some peat	Old peat from numerous early events caught in fault plane and mixed with fault gouge	← Much earlier earthquake event
1	Light grey and white grey silty sandy schist gravel	Post glacial terrace gravels	

A)Only dated layer inferred as related to the scarp, although it is comprised of different sediments.

B) Base Layer of furrow comprised of terrace gravels and inferred as well vegetated pre-earthquake. Yet there exists no detritus suggesting this could have been a flow path infilled from denudation consequent from a distal earthquake.

Figure 2.9: Crane Creek trench face log. Annotations in red are related to brief descriptions at the base the of figure. Adapted from Yetton (2000).

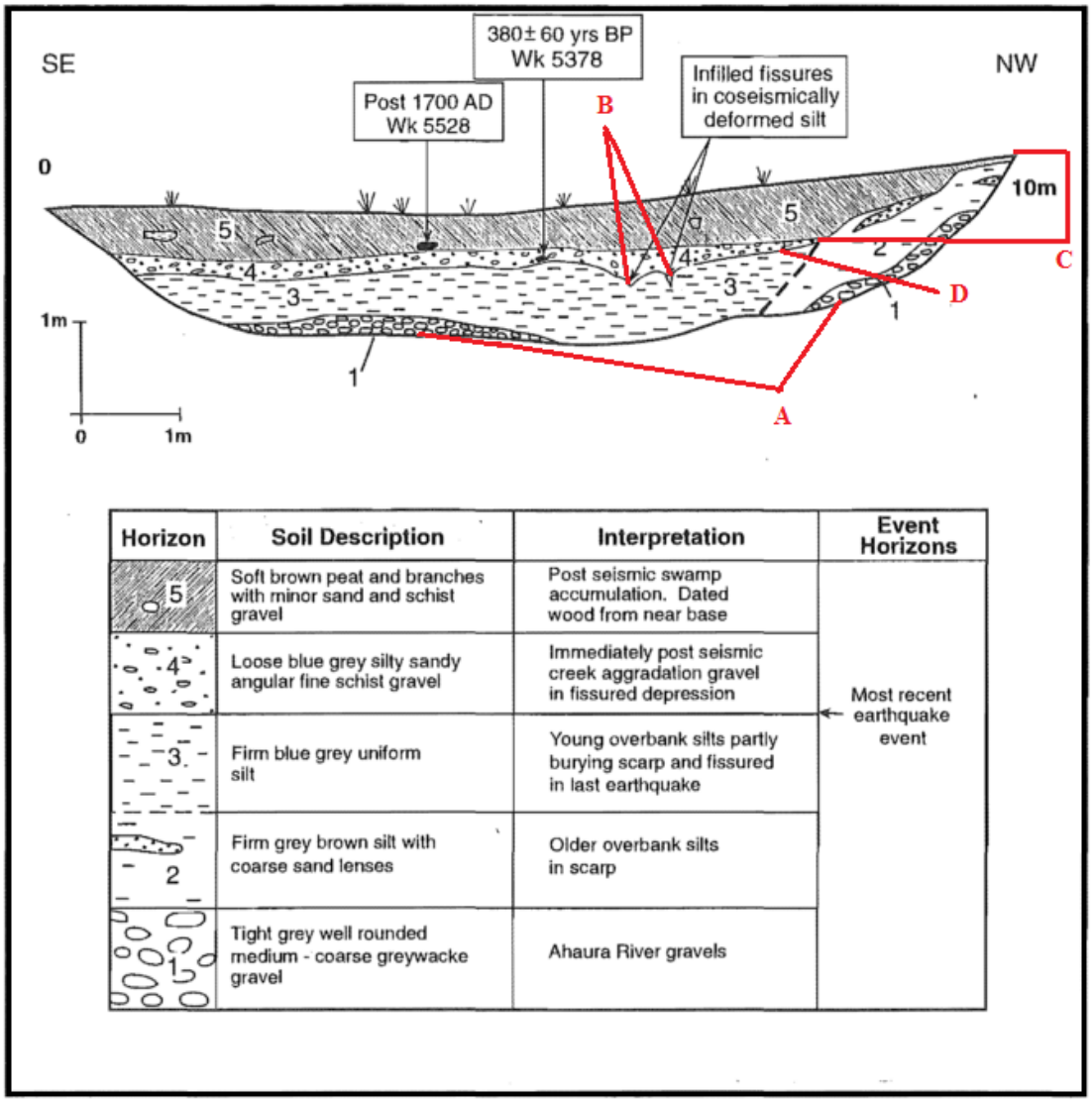

Horizon	Soil Description	Interpretation	Event Horizons
5	Soft brown peat and branches with minor sand and schist gravel	Post seismic swamp accumulation. Dated wood from near base	
4	Loose blue grey silty sandy angular fine schist gravel	Immediately post seismic creek aggradation gravel in fissured depression	Most recent earthquake event
3	Firm blue grey uniform silt	Young overbank silts partly burying scarp and fissured in last earthquake	
2	Firm grey brown silt with coarse sand lenses	Older overbank silts in scarp	
1	Tight grey well rounded medium - coarse greywacke gravel	Ahaura River gravels	

A) There is a clear vertical offset between these 2 units inferring rupture displacement at this location. Although there is no dated material within or directly adjacent to the units to suggest a time.	B) The fissures in the coseismically deformed siltcould be from any proximal seismic origin with no evidence to conclusively suggest a rupture at this location was responsible.
C) Height of scarp less than other location and could imply either more intense erosion at a location only ~2.5 Km from Crane Creek or a longer time period for which erosion to take place (i.e a 15th century earthquake).	D) No scarp colluvium present in the dated unit could infer that (C) may have been the case. Although post-seismic pertubations could be responsible.

Figure 2.10: Coates Creek trench face log. Annotations in red are related to brief descriptions at the base of the figure. Adapted from Yetton (2000).

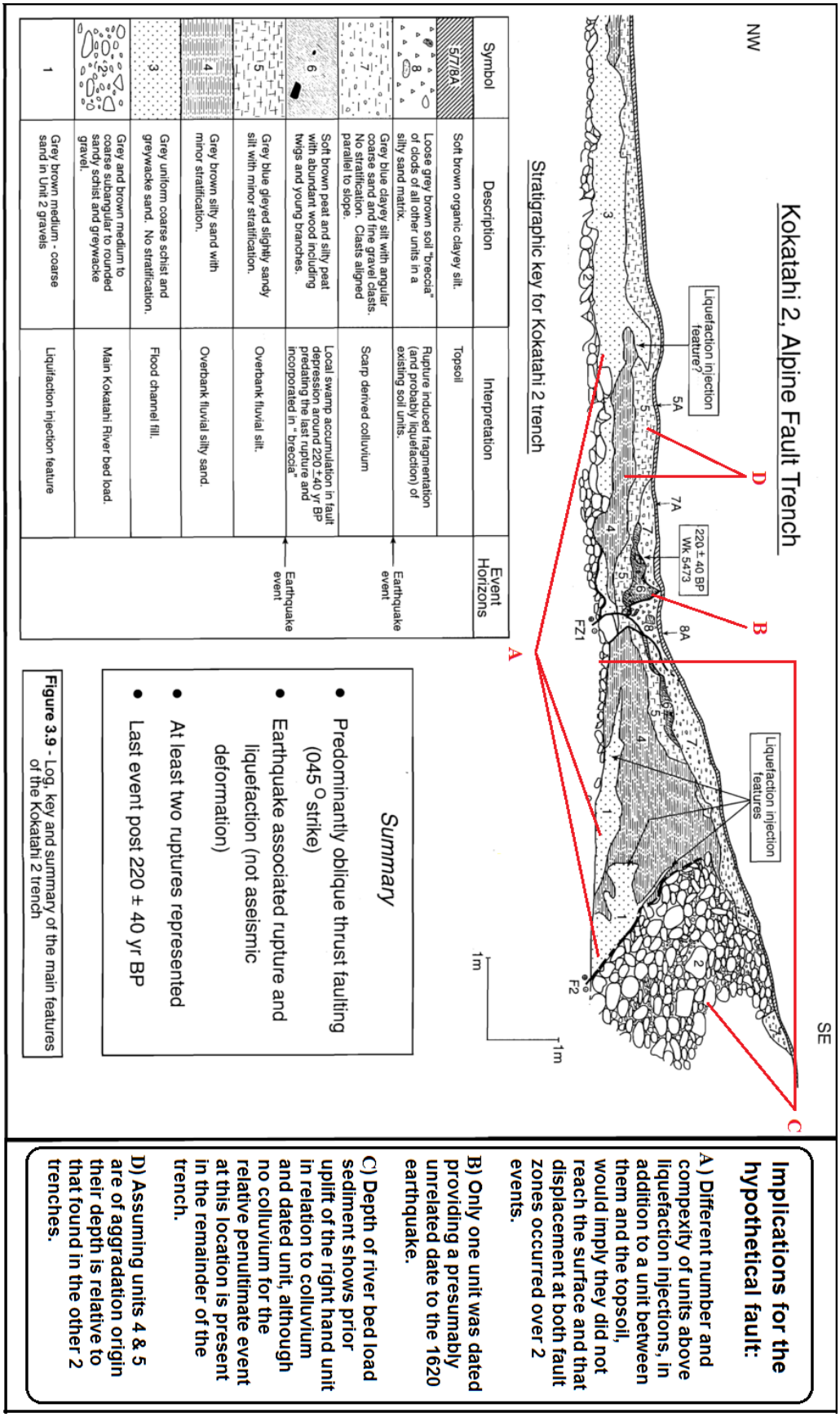

Figure 3.9 - Log, key and summary of the main features of the Kokatahi 2 trench

Figure 4.11: Kokatahi 2 trench face log. Annotations in red related to brief descriptions at base of figure. Adapted from Yetton (2000).

2.7.1.2 Trenching of the southern Alpine Fault

A recent on-fault study of the southern onshore section of the Alpine Fault by Berryman et al. (2012a) provides valuable insight into the frequency and by extension the distribution of large earthquake shaking events within the Southern Alps. The study analysed 22 alternating, sediment-derived peat-silt transitions. These were located in an exposed river terrace within an abandoned gorge perpendicular to the Alpine Fault trace. The river itself, Hokuri Creek, is a direct representation of the regular seismic activity to which it is exposed, having been gradually modified over time by aggradation and surface rupture.

Unfortunately Hokuri Creek was significantly altered at ~1000 C.E. leading to an inability to date the most recent events within the same dataset. Thus Berryman et al. (2012a) used dates obtained through trenching at a site 70 km north (Berryman et al., 2012b) to complete the 8000 year record and determined that the Alpine Fault displayed quasi-periodic behaviour. From these findings Berryman et al. (2012b) provided a revised average recurrence interval for this Alpine Fault section of 485 years, which possibly indicates the trench data are incomplete. If the ~1620 C.E. event, not present in the physical evidence discovered during these studies, was of non-Alpine Fault origin then the record would be more congruent with other recurrence interval estimates. Although the dates obtained do not directly reflect the northern segment of the Alpine Fault, they are still representative of the long term behaviour of the fault. For this purpose, the record's influence in determining accurate recurrence intervals and expected rupture patterns remains relevant to this thesis' hypothesis.

Of the ~1620 C.E. event and its landscape altering effects, Berryman et al. (2012b) simply state that earthquake shaking extends over a much larger area than surface fault rupture which while true, only provides weak support of an Alpine Fault derived earthquake at this time. Considering the MM shaking intensity required to cause the evidence attributed to the event (e.g. Howarth et al., 2012, 2014, 2016; Yetton, 2000) and the expected decrease of this value with distance from a northern rupture origin, it seems unlikely a northern Alpine Fault earthquake was responsible.

2.7.1.3 Dextral offsets of the central Alpine Fault

As new technologies become more widely available these methods are able to provide a different perspective in geomorphological analyses. In a recent demonstration of this, the utilization of LiDAR to penetrate dense vegetation cover revealed previously unrecognized dextral offsets along a portion of the central Alpine Fault (De Pascale & Langridge, 2012; De Pascale et al., 2014). Specifically, the research illustrated potential along-strike dextral movement of fault perpendicular features at Gaunt Creek. The processed LiDAR data were subsequently ground checked through varying forms of measurement, assessed for accuracy, although with large uncertainties, and included in results.

While suggesting the penultimate Alpine Fault event occurred at A.D. 1430 ± 65, and not attributing the ~1620 C.E. event as a central Alpine Fault rupture, De Pascale et al. (2014) provided an interpretation of dextral movement at Gaunt Creek over a timeframe of A.D. 1430 to current. A dextral offset of 6.5 ± 2 m was estimated for the penultimate event. However, it was noted that determining an offset smaller than this would not be possible with the methods employed and their cumulative uncertainties.

De Pascale et al. (2014) further suggested that the Alpine Fault experiences bimodal behaviour, while excluding the ~1620 C.E. event from the record at Gaunt Creek. This would be one of the key supporting factors for their argument. In contrast, other research does support the event in the Alpine Fault's record, inferring a smaller partial rupture of the northern section extending to the central section. Including the ~1620 C.E. event would seem logical to support bimodal behaviour, as Gaunt Creek is located within or proximal to the spatial extents of other research used to determine the rupture lengths of the ~1620 C.E. event (i.e. Howarth et al., 2012, 2014, 2016; Yetton, 2000). Justifying this conclusion, De Pascale et al. (2014) assessed the slip-rate deficit between mean slip-rates from their research and other geologic and geodetic research and, as other research has, found them inconsistent. Furthermore, it was suggested that these smaller ruptures were not seen in the seismicity and their geomorphic effects may be related to other faults.

While De Pascale et al.'s (2014) conclusions support this thesis' hypothesis, smaller magnitude events such as those suggested by De Pascale et al. (2014) would likely

not be capable of causing the widespread forest cohort disturbances reported in other research (e.g. Wells & Yetton, 2004). Within agreement is the exclusion of the shaking event from the Alpine Fault record around 1620 C.E. which does have potential to have been caused by a proximal, non-Alpine Fault earthquake or perhaps a combination multiple fault ruptures within a small timespan. Negating bimodal behaviour also aligns with the 8 Kyr. average recurrence intervals determined by Berryman et al (2012a), further supporting the logic that three events should not, statistically, occur within a timespan less than this average.

De Pascale et al.'s (2014) publication was heavily criticized by the academic community, having a notable lack of data to support conclusions and, when data were available, did not consider all factors that could have influenced the results (see De Pascale et al. REPLY, 2014).

2.7.2 Off-fault evidence

2.7.2.1 Regional lichenometric research

Employing lichenometric data, Bull (1996) determined previous Alpine Fault rupture dates to surprising levels of accuracy. The results were achieved through the measurement of 33,000 yellow rhizocarpons (herein lichen) at 85 locations within the Southern Alps. Using digital callipers and calibrating the resulting measurements using multiple probability distributions, accounting for regional climate and microclimate variations, Bull (1996) was able to date major regional rockfall events and relate them to their corresponding trigger event timings.

Bull's (1996) initial findings indicated that no event occurred on the central section of the Alpine Fault around ~1620 C.E. but rather that there was an event at ~1490 A.D. Through subsequent research and communication with other researchers, Bull (2008) later resolved this conundrum, attributing these findings to a large shaking event ~1620 C.E. Other shaking events represented in Bull's (1996) lichenometric data were also later attributed to the Alpine Fault by Bull (2008) at 1580 A.D., 1615 A.D. and 1715 A.D. and suggested that three Alpine Fault earthquake events occurred during a 135-year time span. While plausible, as these dates align with some other seismological research (i.e. Howarth et al., 2012, 2014, 2016), the absence of Alpine Fault activity during the last ~500 years at Hokuri Creek makes it seems highly

unlikely; as mean recurrence intervals were calculated at 329 ± 68 to 485 years (Berryman et al., 2012a, 2012b). Even when accounting for the Alpine Fault's segmentation, three large shaking events capable of regional landsliding on the central and northern segments should have representation elsewhere, thus could have been the result of error propagation or represent shaking events from more than one fault.

Issues with the conclusions of Bull's work include the fact that all shaking events were attributed to the Alpine Fault, especially as it only involves off-fault evidence and historic non-Alpine Fault earthquakes in the Southern Alps are known to have caused landsliding (Hancox et al., 1997; Yetton, 2000). Furthermore, events within a small temporal span were also all attributed to the Alpine Fault, even when Bull (1996) stated that the recurrence interval was estimated to be nearly twice the period (260 years) during which three events were attributed. As the data are spatially diverse with varying distances from the Alpine Fault, thus covering multiple shaking zones, these issues could surface in the data and be misinterpreted. A more plausible solution, if Bull's (2008) clustered temporal behaviour is truly representative of the data, would simply be clustered temporal seismic activity of multiple faults or an intense aftershock sequence resulting in large scale landsliding within the Southern Alps.

2.7.2.2 Regional coastal progradation and dune formation as evidence for historic events

Attributed to seismic activity of the Alpine Fault, the ~1620 C.E. event (referred to in text as A.D. 1615) resulted in regional progradation and dune formation along coastal South Westland (Wells & Goff, 2006; 2007). Formed through a combination of processes occurring in unison, including irregularly high sediment yields due to coseismic landsliding, regular intense storm events and longshore drift, the dunes appear to reflect large earthquake shaking events within the central Southern Alps, namely of the Alpine Fault (Wells & Goff, 2007).

Although not direct indicators of previous events themselves, the dunes were dated using dendrochronology on colonizing conifer trees, which have life expectancies of ~800 years and begin colonization from 5-50 years post-earthquake. Accounting for other studies (i.e. Howarth et al., 2014, 2014, 2016), the dating estimate of a large

earthquake based on episodic colonization at ~1620 C.E. fits the timeframe of the inferred partial rupture of the northern Alpine Fault. However, the data collected relating to this timeframe have been described by Wells and Goff (2007) as weak, with discontinuous or absent dune formation present at the two northernmost study sites. Whereas elsewhere the dunes' evidence relating to other known Alpine Fault ruptures is described as strong. The importance of these findings relative to this thesis is twofold. Firstly, weak evidence of disturbance implies a smaller disturbance coinciding with other conclusions regarding the ~1620 C.E. event. Secondly, the existence of strong evidence supporting Alpine Fault shaking coincides well with previously determined earthquake dates and corroborates conclusions from other bodies of research which have been developed through other means. Considering these two factors, it becomes apparent that a smaller partial rupture of the Alpine Fault could explain the situation. However, this opposes theories that the Alpine Fault ruptures characteristically and allows for the interpretation that this instance of episodic colonization and dune formation was the result of a non-Alpine Fault earthquake.

Further supporting these factors is the inclusion of climatic interference in the research. As this region is exposed to multiple large storm events per year, the fact that dunes form only as a result of large earthquakes emphasizes the quantity of sediment that coseismic landsliding can provide to river systems compared to aseismic landsliding. The impact a large coseismic sediment influx can have on the environment affects the interseismic sediment equilibrium, as here storm events are considered insignificant, background processes (Wells & Goff, 2007). Thus the impact a large earthquake has on the region is punctuated by dune formation and can be effectively employed as a dating method, even though the shaking origin may not necessarily be directly apparent.

2.7.2.3 Lacustrine palæoseismology proximal to the Alpine Fault

One of the most comprehensive recent bodies of research has been led by J. Howarth. Howarth et al.'s (2012, 2014, 2016) work on Alpine Fault proximal lake sediments has provided an approximately 1700-year record of seismic shaking within the Southern Alps; assumed to be representative of Alpine Fault activity. The research involved the coring of bedded hyperpycnal flow-derived turbidites and subaqueous

mass wasting deposits on lake floors. Entrained macrofossils in the cored layers were radiocarbon (^{14}C) dated, and with the inclusion of lithostratigraphy, magnetic susceptibility, and density, estimated calendric dates for regional intense shaking events were determined. The methods were conducted at three locations; Lake Paringa, Lake Mapourika and Lake Ellery, covering approximately 150 km of the central and southern section of the Alpine Fault. Consequently, Howarth et al. (2012) interpreted the megaturbitdite record and estimated that the penultimate event occurred at ca. A.D. 1570 conflicting with other studies by 20-50 years. Herein Howarth et al.'s (2012) A.D. ~1570 event will be synonymous with this thesis' ~1620 C.E. event and the terms will be considered to represent the same event unless otherwise stated.

Within the core sequences, two main types of sediments were determined to be directly related to earthquake shaking. Subaqueous mass wasting sediments are those that originate from the lake below water level and settle in the lake basins. Sediments derived from this form of mass wasting at Lakes Paringa and Mapourika were determined to relate to MM VI-VII shaking (Howarth et al., 2014). By contrast, post-seismic sediment fluxes, i.e. terrigenous sediment, were determined to relate to shaking of MM > IX. The sediments are further divided into sub-categories, of which Type 2 Rapidly Deposited Layers are pertinent to the ~1620 C.E. event (see Howarth et al., 2014, 2016 for full descriptions). Howarth et al. (2014) inferred that these suggested lake sedimentary records were able to distinguish between strong versus violent shaking at lake sites and that the use of lacustrine palæoseismology is therefore an adequate research technique within the region. Employing this logic, rupture extents of the Alpine Fault earthquakes were estimated for the penultimate event as a M_W 7.9 event rupturing 285 km of the Alpine Fault (Howarth et al., 2014).

Howarth et al. (2012) also determined that when averaged over the last ~1100 years, seismically derived deposits accounted for 27% of the total sediment flux from the lake's catchment. This aligns well with the findings of Wells and Goff (2007) regarding background denudation equilibrium and further supports the theory of intense post-seismic sediment pulses. Howarth et al. (2014) were able to determine that this fluctuation period lasted for approximately 50 years post shaking event, resulting in 300-400% higher sediment accumulation rates in the centre of lake basins.

With a dataset containing multiple lakes, Howarth et al. (2014, 2016) were able to explore shaking event synchronicity. Comparing calculated probability density functions for event timing, as well as physical evidence, it was determined that shaking event synchronicity could be confirmed at all three lakes. Although the probability density functions were not carried out for the ~1620 C.E. event, they were within error for five prehistoric events. Additionally, Type 2 Rapidly Deposited Layers were discussed as having deposition times of days to weeks, inferring the potential for lacustrine palæoseismology to accurately determine interseismic periods. This could possibly test the idea that multiple large events could be responsible for the geomorphic evidence attributed to the ~1620 C.E. event timeframe. However, this could also be due to the absence of available sediment for further denudation within a small timeframe, such that the capability of a shaking event to produce similar successive effects in the same area is not possible in such quick succession.

Finally, in the most recent publication (Howarth et al. 2016), similar results were obtained at Lake Ellery. However, some differences arose at this far southern lake in comparison with the more northern lakes. Most pertinent to this thesis, Howarth et al. (2016) noted the absence of intense (MM IX) shaking at all three lakes at A.D. ~1570. They concluded it was no longer prudent to attribute this event to the postulated northern Alpine Fault rupture, as the modelled shaking intensity present at Lake Ellery was lower than the lacustrine evidence would suggest and that the current palæoseismic data are insufficient. Furthermore, they suggested that the recorded shaking could have originated from a fault distal to the Alpine Fault.

2.7.2.4 Aggradation terraces as evidence supporting prehistoric earthquakes

The very nature of Yetton's off-fault evidence, although corroborated with on-fault evidence, makes attributing it to a non-Alpine fault earthquake much simpler. Contributing to the age of the Crane Creek Event, Yetton (2000) also investigated a small aggradation terrace 600 m downstream from the Crane Creek trench. Poorly imbricated and comprised of sand and coarse gravels, the terrace was of clear aggradational origin, as Yetton inferred. Within the deposit a radiocarbon age was obtained from a large beech tree of 390 ± 50 years. Additionally, the ages of other trees on the aggradation surface correspond to an event approximately 400 years ago.

These dates align with the ages obtained from the Crane Creek trench and thus a large sediment pulse and forest disturbance circa 1620 C.E.

2.7.2.5 Regional dendrochronology as evidence for large earthquakes

Further key indicators of large-scale shaking events within alpine regions are tree cohort aging and growth ring anomalies. For some time now the impacts of earthquakes have been employed when determining palæoseismicity and its impacts (Lawson, 1908; Fuller, 1912; Louderback, 1947; Gu, 1983). Further Southern Alps' landslide data related to these methods are the data assessed by Yetton (2000). The key strength of these data types are the reliable spatial distribution attainable, the abundance of indicators that can still be currently located and the ability to corroborate with other methods.

As described in Wells et al. (1999), the time taken by trees to establish a colony on an earthquake-disturbed surface can be accurately estimated. Given the proclivity of the Southern Alps to experience large earthquakes (> 6.5 M_W), forest cohort disturbances and their associated reestablishment periods are relatively common. The ability to date multiple trees within these cohorts allows the accurate age determination of a local earthquake shaking event. Furthermore, if a tree is not destroyed by ensuing geomorphic hazards, the disturbance of the earthquake will be detectable as anomalies in its growth rings. Consequently this method allows for potentially the most accurate dating method, as the tree rings can be dated to the nearest year with only minor inconsistencies.

Although the accuracy of the above two methods has allowed dating of multiple earthquake events, errors and uncertainties can arise. Foremost, cohort disturbances can relate to events of aseismic origin. Extreme weather and climatic events or periods can have large impacts on forest growth and mortality. Landsliding is also a key driver of cohort reestablishment by providing a new growth surface but can be of either seismic or aseismic origin. These factors and others create difficulty when attempting to determine the cause of a cohort disturbance. For this purpose corroborating evidence from multiple locations and evidence obtained through other methods is important.

The methods described above have been used on a number of occasions to estimate the recent palæoseismic record of the Alpine Fault (Wells et al., 2000; Wells &

Yetton, 2004; Yetton, 1998, 1999). One of the more comprehensive studies was compiled by Yetton (2000), including additional data from other sources (Wells et al., 1999; Adams, 1980). As part of the same research body as the on-fault evidence discussed above, Yetton compiled various data in order to estimate a calendric date and spatial extent for the Crane Creek Event. The resulting findings indicated a minimum Alpine Fault rupture length of 200 km, an estimated moment magnitude of $M_W > 7.8$ and an estimated calendric date of 1480-1645 A.D. However, using tree ring chronologies, what appears to be the most accurate date of 1620 A.D. ± 10 years was obtained.

The uncertainties inherent in Yetton's research were adequately covered in the corresponding publications. However, some of these require reiteration in the context of this thesis. Foremost, Yetton (2000) states that regional synchronicity alone does not demonstrate an earthquake origin, although the combination of the multiple data types can define palæoseismicity showing earthquakes did occur. This is a key conclusion and the fact that the earthquake origin is unknown allows the hypothesis in this thesis to be explored. Furthermore, Yetton (2000) employed Wells' expertise on dendrochronology to analyse the variation in North-South data. In doing so Wells was able to organise the regional data into 10-year age classes and suggested that the Crane Creek Event was a single earthquake. The possibility of a progressive series of smaller ruptures over a short time period was noted, although nothing was said about their possible origins. As the possibility of such a series of events could support this thesis, it is important to note that a timespan < 10 years would not be unexpected for a multi-earthquake scenario.

Subsequently Wells and Yetton (2004) carried out further research on the effectiveness of tree ring chronologies as a dating method within the Buller Region. They concluded that:

- earthquake events were the only context in which many assessed trees showed long-lasting growth changes,
- MMI 8-10 shaking was a requirement for growth impacts, although distinguishing between shaking intensities was not possible,
- no known factors about tree rings anomalies can distinguish between earthquakes and other disturbance events such as intense storm winds. Thus regional studies are necessary to attribute a shaking event to an earthquake.

For earthquake dating and the localization of shaking zones, tree ring chronology and forest cohort disturbance provides one of the better supportive methods. Such methods are of paramount importance to the ~1620 C.E. event; cohort disturbances and tree ring chronology have previously been employed and allow estimates of both shaking and spatial extent. By comparing these data with other sets, such as landslides, lake sediments and aggradation, estimates can be made of prehistoric earthquake dates and their associated shaking origins.

2.7.3 Summary of geologic and geomorphic evidence

Compiling an accurate palæoseismic record for the Alpine Fault is a difficult proposition. There are many factors that affect the outcomes different researchers have developed and determining the temporal context for one particular earthquake event further compounds the issue. The ~1620 C.E. earthquake being one such event exacerbates this situation, as interpreting the evidence in the above literature, stating with certainty whether it was of Alpine Fault origin or any other large fault within the affected vicinity is not possible.

2.8 Summary of available literature

Various studies contribute to the overall understanding of seismic and coseismic hazard activity within the Southern Alps. Unfortunately, as with all palæoseismic research, inferences and theories comprise the total available knowledge-base. With very little on-fault research, the investigation and reliance on off-fault research becomes necessary. Although the inherent weakness of off-fault evidence (i.e. uncertain seismic origin) is ever present, off-fault evidence allows the population of a dataset from which to evaluate palæoseismicity and its effects.

Certain key contributions described above have had more influence on this thesis than others. The works of Yetton, especially Yetton (2000), provided a solid foundation from which to begin parameterising a rupture and although this thesis contradicts some of the findings, consideration has been given to these aspects. Furthermore, Howarth et al.'s (2012, 2014, 2016) work on palæoseismicity using lacustrine sedimentology provided a large body of comparable research. This provided many inferences that required consideration as they acceptably opposed

older works with physical evidence. Wells and Goff (2007) provided important insights into the response of sediments to intense shaking and developed parallel dates when compared to other studies. Unfortunately, no other areas exist on the West Coast, particularly further north, where their methods could be applied to compare with central studies. Berryman et al.'s (2012a) research at Hokuri creek provided the most statistically populated interpretation of Alpine Fault rupture behaviour although the poor timing of river avulsion approximately 1000 years ago weakened the dataset's most recent inferences; having to determine date values from elsewhere. Additionally, the fact that this only covers the southern segment of the Alpine Fault's onshore trace somewhat lessens the research's application to this thesis' hypothesis. Robinson et al.'s (2016) method of associating geomorphic response (aggradation and denudation) with a specific fault location consequently had a large impact on this thesis, as quantifiable comparative data and an effective modelling method allow conclusions to be drawn which would otherwise not exist.

Relating to the research discussed in this chapter, there are clear discrepancies in dating of seismic and coseismic evidence and origins. Most research suggests dates of around 1620-1630 C.E. for the event this thesis is concerned with. A main outlier of this range is Howarth et al. (2012) and their data suggesting an event around A.D. 1570 which, although does not align with the values used within this thesis, does add to the multi-earthquake scenario hypothesis.

Some areas of current research could provide additional support to this thesis. Recent trenching of the Alpine Fault led by Dr Robert Langridge (GNS Science), expected to be published in 2017, could provide more details of palæoseismicity of the fault. Research by Dr Simon Lamb of Victoria University regarding the dextral movement of the plate boundary over time could also drastically affect the plate motion budget, potentially adjusting the values with which geodetic data are compared to and altering the proportion of non-Alpine Fault plate motion of the South Island.

Conclusively determining the origin of the ~1620 C.E. earthquake is a difficult task. Many hypotheses and theories exist, some more relevant and others more accurate. This thesis will provide quantitative estimates that can be compared with known indicators of coseismic landsliding, and even if proven untrue, disproving the existence of hitherto unknown large active faults within the Southern Alps is not possible through current methods.

3 COSEISMIC LANDSLIDING ESTIMATES FOR A HYPOTHETICAL FAULT RUPTURE IN THE SOUTHERN ALPS WITH ESTIMATED DENUDATION AND AGGRADATION DEPTHS IN MAJOR RIVER CATCHMENTS

3.1 Introduction

This chapter will provide an in-depth analysis of the methods employed in this thesis. There will be discussion of the validity and application of these methods, the tools used and the resulting data.

3.2 Determination and calculation of hypothetical fault earthquake parameters

Developing a realistic hypothetical fault rupture scenario within the central western range front of the Southern Alps requires the integration of various information sources. This includes the collation and analysis of active fault distribution and parameters within the area, the South Island's structure at depth and the palæoseismicity of the region. The justification for modelling such a fault, discussion of the parameters used and the interpretations behind them have been addressed in Chapter 2. A summary of the modelling values used is in **Table 3.1** below.

Table 3.1: Parameters used to develop the Shakemap in OpenSHA.

Data type	Input data	Reference
Intensity measure relationships		
Intensity measure type	MMI	
Tectonic region	Active shallow crust	
Component	Average horizontal	
Site data providers		
Vs30 (m s^{-1})	180.0 (default)	
Site data provider	Global Vs30	
Digital elevation model	SRTM30 version 2	
Region type	Active tectonic	
Earthquake rupture parameters		
Fault type	Reverse	Litchfield et al., (2014)
Fault surface type	Stirling's	Field et al. (2003)
Fault length	100 km	Stirling et al. (2002, 2013); Wells and Coppersmith (1994)
Rupture type	Finite source	
Magnitude	7.6 M_w	De Pascale et al. (2014); Howarth et al. (2012); Yetton (2000)
Rake	120˚	
Fault dip	70°	Litchfield et al., (2014)
Fault depth	7 km	Cox and Sutherland (2007); Norris and Toy (2014)
Fault tips	42.922S, 171.291E 43.442S, 170.287E	Boese et al. (2012); Cox and Barrell (2007); Langridge et al. (2016); Rattenbury and Jongens (2010); Nathan et al. (2002)

The first step utilized the open-source Seismic Hazard Analysis (SHA) tool OpenSHA, calculating the probability that an Intensity Measure Type (IMT) exceeds an Intensity Measure Level (IML) to develop a shakemap (Field et al., 2003). For this application MM intensity and a 50% threshold were used. The scenario developed was that of a 7.6 M_W earthquake originating from a 100 km fault derived from the seismic scaling relationships of Wells and Coppersmith (1994) and Stirling et al. (2002, 2013). The OpenSHA Shakemap plotted MMI spatially over the South Island. (Figure 3.1).

OpenSHA employs a rudimentary shear wave velocity model titled Vs30. Developed by Wald et al. (2004) and refined by Wald and Allen (2007), Vs30 estimates shear wave velocity using lithology and the topographic slope of the SRTM30 DEM as a proxy for seismic site conditions. Using these and other input parameters OpenSHA returns a value for average shear-velocity to 30 metres depth for use in further calculations. The resultant modelling for this thesis incorporates the Vs30 coefficient derived specifically for active tectonic regions known as Active Shallow Crust. Given its nature Vs30 also inherrently influences the expected duration of shaking.

A key limitation of the OpenSHA process is the inability to calculate topographic amplification (Buech et al., 2010). Considering the topographic properties that comprise approximately 60% of the area that experiences > MMI 5, it is evident this limitation could result in differences in the produced MMI distribution, as the construct of MMI has no scale between intensity levels and the Shakemap values do (e.g. MMI 8.5 and MMI 8.9 are both technically MMI 8). **Figure 3.1** displays a maximum MMI of 8; however multiple values were > 8.5 with a maximum of 8.91 and although still considered MMI 8 some values could plausibly increase to MMI 9 were topographic amplification incorporated. Thus, while adequate for initial investigation, other more accurate methods of intensity mapping would be preferred. Although this would certainly affect the final landslide susceptibility model and calculated denudation and aggradation values. Developing and implementing such a method would lead to drastically increased processing times and direct comparison with Robinson et al.'s (2016) research would no longer be possible, so is beyond the scope of this thesis.

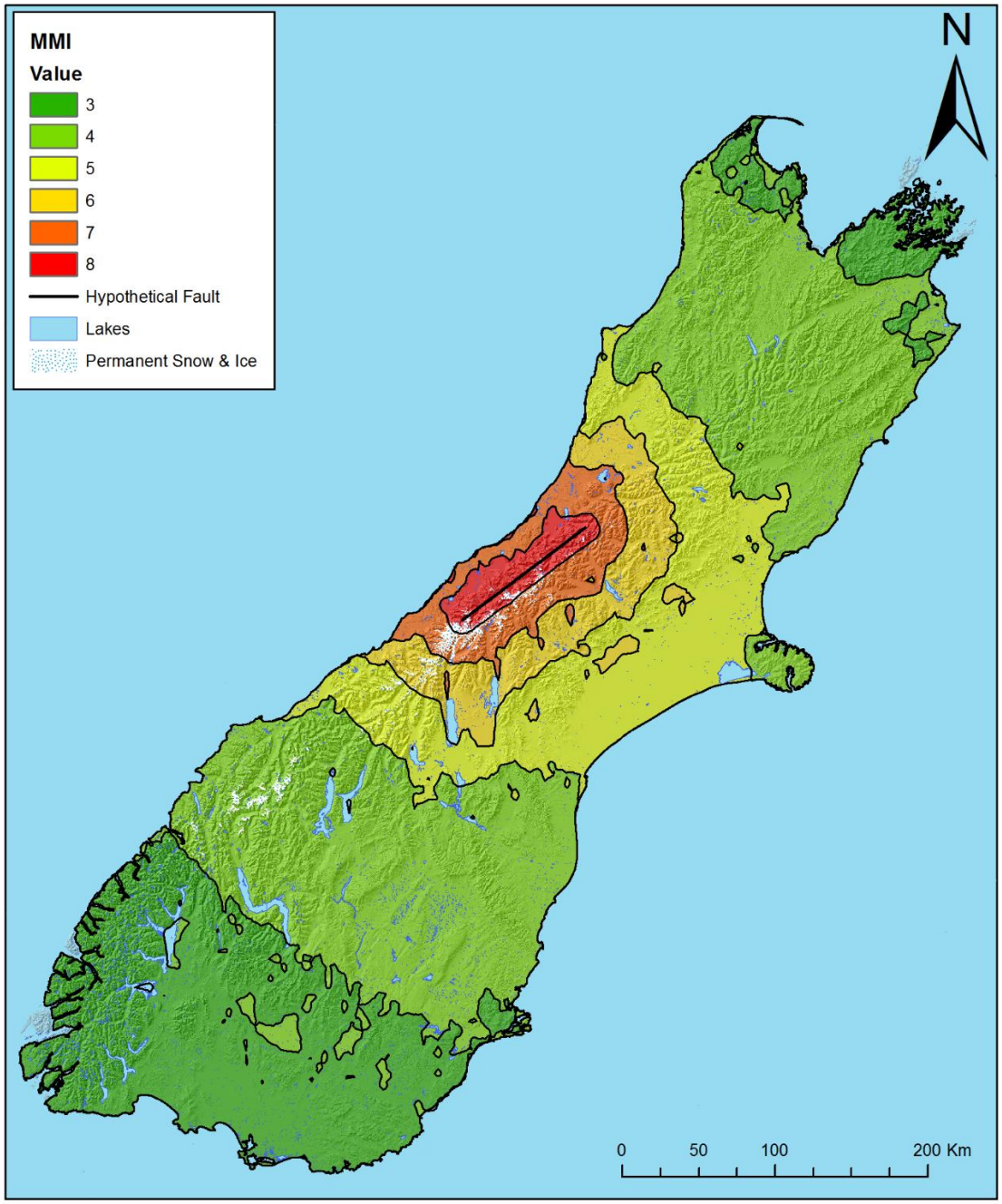

Figure 3.1: Shakemap data produced in OpenSHA overlying hillshade model of the South Island illustrating the MMI extents generated by the hypothetical fault-rupture scenario incorporated into further processing.

3.3 Landslide susceptibility

Determining landslide susceptibility is an extensive process. The isoseismals resulting from the initial step described above are subsequently transformed to suitable data for further manipulation in ArcGIS. The processes employed herein relate directly to those of Kritikos et al. (2015) and Robinson et al. (2016). This section will give a brief overview of those steps (Illustrated earlier in Figure 1.2) and relate them to the current hypothetical fault model and present the results.

For direct comparison with the results of Robinson et al.'s (2016) Alpine Fault event, the identical South Island DEM was used throughout processing. In-depth justification for this choice is provided in Robinson (2014) but in summary a 60x60 metre DEM contains sufficient spatial resolution in individual cells for accurate regional analysis (i.e. DEM averaged slope angle and other conditioning factors described below), while minimizing error propagation and moderating processing times. Although higher resolution DEMs are currently available and could have been employed in this study the processing times would be extensive and would create uncontrolled variability in processing and consequential results provided the prior sensitivity analyses.

Landslide susceptibility is produced through the application of fuzzy set theory (also known as fuzzy logic). This is implemented in ArcGIS by creating layers for MMI, slope position index, slope angle, distance to faults and distance to streams with the Fuzzy Membership tool and subsequently combining them with the Fuzzy Overlay tool. Fuzzy logic itself is a derivative of classical mathematical set theory, in which binary logic defines a membership between two elements such that membership equals either 0 or 1. In fuzzy logic this membership is based on the concept of partial membership such that the value can range between 0 and 1. This allows modelling of complex systems that often suffer from uncertainties, and inaccurate or limited data. Coseismic landsliding is such an application, where results can be produced without historic inventories for hypothetical events and/or an absence of in-depth lithologic data (Zadeh, 1965; Kritikos et al., 2015).

Although historic landslide inventories are no longer required to produce results for an event when utilizing this fuzzy logic approach, initially they were. To ensure accuracy and reliability Kritikos et al. (2015) and Robinson et al. (2016) utilized 5

historic landslide inventories comprising: the 1994 M_W 6.7 Northridge earthquake, the 2008 M_W 7.9 Wenchuan earthquake, the 1999 M_W 7.7 Chi-Chi earthquake, the 2003 M_W 7.2 Fiordland earthquake and the 2009 M_W 7.8 Fiordland earthquake. To be deemed successful each trial of the method had to achieve an Area Under Curve (AUC) > 0.7 ensuring results were above a reasonable chance of random success (Kritikos et al., 2015). The AUC is a decimal value between 0 and 1 showing the cumulative percent of landslides against the cumulative percent of overall landslide hazard. For example, the 2009 M_W 7.8 Fiordland earthquake achieved an AUC of 0.912 which corresponded ~90% of landslides occurring in the highest 20% of overall hazard values (Robinson et al., 2016).

Upon fulfilling the AUC criterion, conditioning factors were subsequently determined by the causative impact they imposed on the result. To develop fuzzy membership curves, frequency ratio distributions were created which enabled quantification of the factors on a 0 to 1 scale (Kritikos et al., 2015).

With the fuzzy membership layers created, the Fuzzy Overlay tool aggregated them creating the final hazard susceptibility layer. This step is carried out using a fuzzy operator which exists in ArcGIS. For their research Kritikos et al. (2015) and Robinson et al. (2016) employed the fuzzy Gamma operator to yield hazard maps showing the relative probability of landsliding from 0 to 1 for each pixel of the utilized DEM. This fuzzy Gamma value was altered corresponding with known landslide locations and other geomorphic features expected to be less or more susceptible to landsliding. It was determined that a value of 0.9 should be used. As this thesis encompasses the identical geographic extent of Robinson et al. (2016), 0.9 was also used when developing landslide susceptibility for the hypothetical fault rupture (Figure 3.2, 3.3A & B).

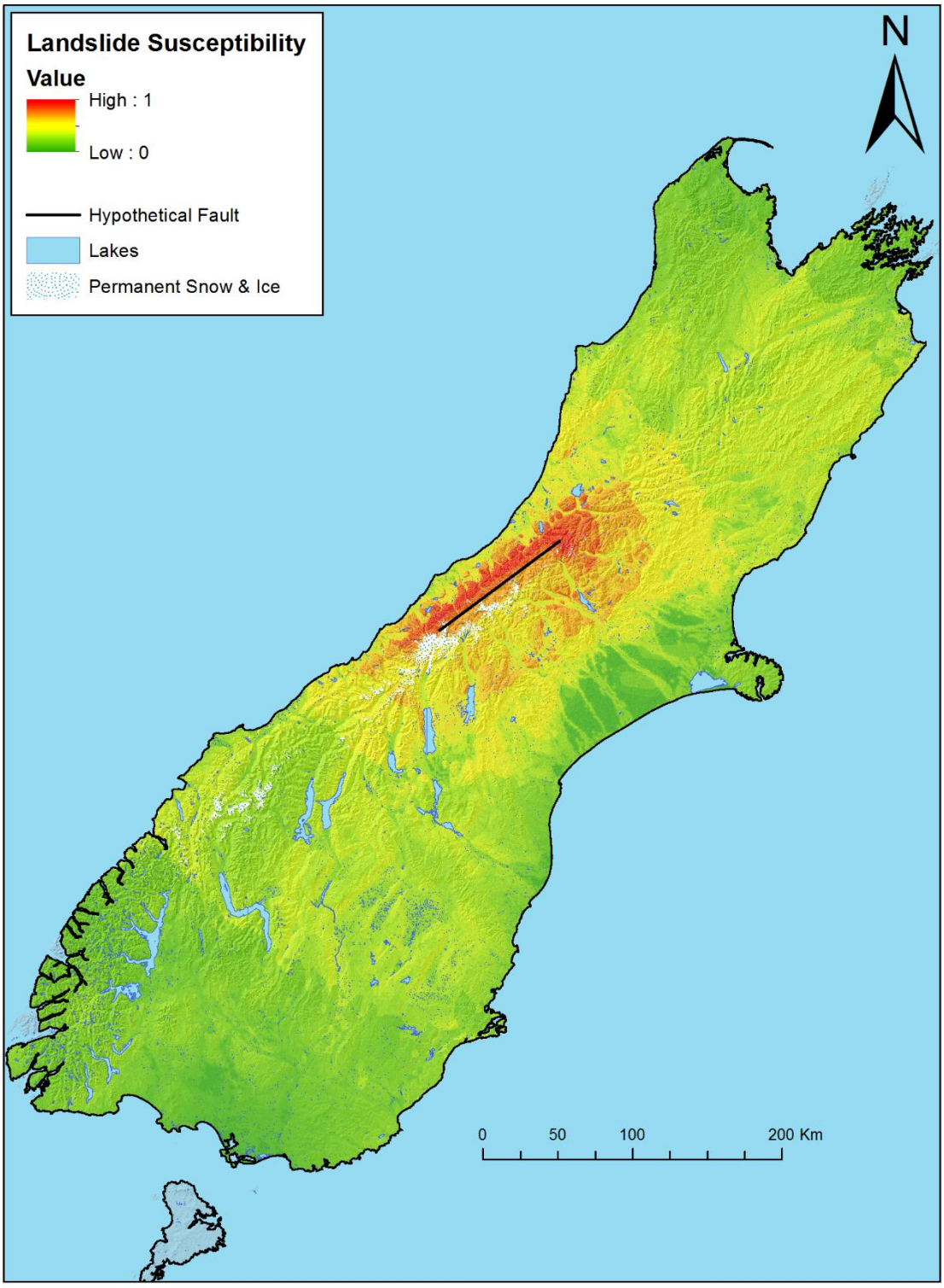

Figure 3.2: Hazard map showing landslide susceptibility values affecting the South Island mainland as a result of the hypothetical fault rupture scenario explored.

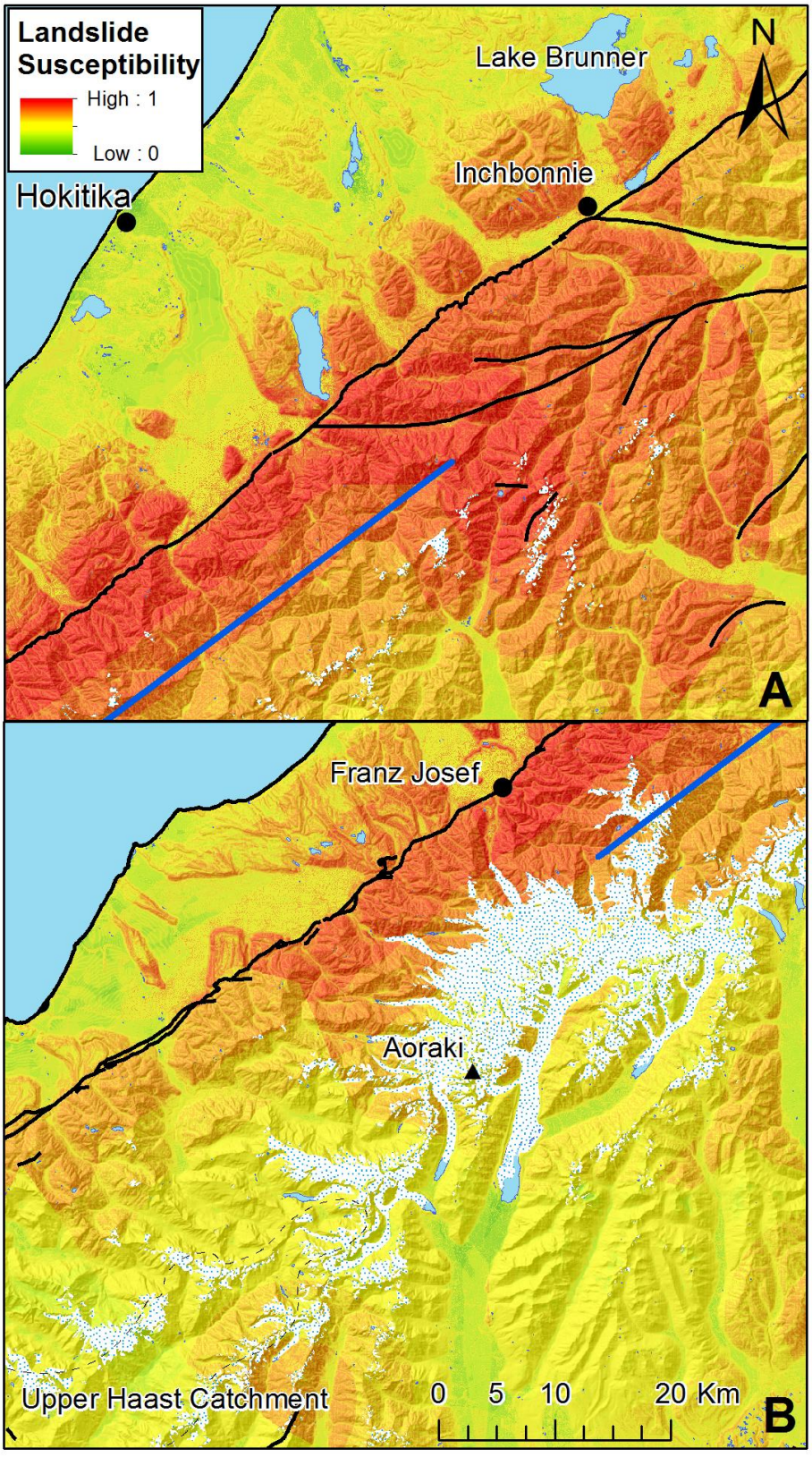

Figure 3.3A: northern intense shaking zone showing Alpine Fault – Marlborough Fault zone junction. Figure 3.3B: southern intense shaking zone and upper Haast catchment. Hypothetical fault is represented by blue line.

Figure 3.2 provides a general geographic perspective of the landslide susceptibility values generated by the hypothetical fault rupture. The extent of high susceptibility (≥0.5) is considerably less than that found by Robinson et al. (2016) for a full Alpine fault rupture, although considering a fault-rupture length of 100 km compared to 400 km, this was not unexpected. Notably, with the exception of one feature, the extreme susceptibility values (≥ 0.9) are focused solely in the region west of the hypothetical fault; affecting the western rangefront and other prominent glacially-derived and geomorphic features west of there. The Alpine Fault itself appears to have considerable constraining effects on susceptibility distribution, likely due to the abrupt change in topography encountered at the rangefront.

Also notable is the reduction of susceptibility values as distance increases from the tips of the fault. Although shaking intensity is expected to decrease as distance from rupture increases, accounting for additional factors when calculating susceptibility, this relationship does not seem significantly affected. Furthermore, the north-south distribution appears north biased. Where extreme values dissipate almost immediately beyond the southern fault tip, they continue ~18 km further from the northern fault tip (Figures 3.3A & B). When comparing the east-west distribution, susceptibility values remain relatively high in the east but appear truncated in the west and is possibly a result of Vs30 values affected by the lithographic and topographic differences of the predominantly low-lying coastal region.

Of further interest in **Figure 3.3A** is the hook shaped pattern of extreme susceptibility values originating from the northern fault tip. It appears to be significantly affected by the geometry of the Hura Fault which signifies the beginning of the Marlborough Fault Zone, and extends beyond the Hura Fault with a portion deflected tangentially south-eastward.

Figure 3.3B shows the upper Haast catchment extents for future reference. Of note here is the slight coverage of values approximately 0.7 in the northern extents, with a background average on the slopes of approximately 0.4-0.5. While it appears the hypothetical scenario has little impact this far south, this region is on the cusp of MMI 5 and 6 shaking where there are very few known active faults. These factors would have definite effects when determining susceptibility values for the locale.

3.4 Landslide numbers and impact factors

The severity of a regional coseismic landsliding event is related to the volume and number of landslides estimated to occur, in addition to other factors. Interpreting **Figure 3.2** above, large areas of high landslide susceptibility would be expected to generate the most landslides. Thus, for the hypothetical fault scenario, total landslide numbers are produced. Binning the hazard susceptibility values into ten linear bins and calculating the area each covers, the extent of each hazard bin was defined and subsequently quantified (Appendix A). Using the five-historic earthquake dataset listed above, Kritikos et al. (2015) and Robinson et al. (2016) developed landslide densities values per hazard class which included a sample mean and two standard error values either side (Table 3.2). Multiplying the hazard bin areas with the landslide density values, calculating total landslide number estimates per-catchment was possible (Figure 3.4).

Table 3.2: Landslide densities per hazard bin, altered from Robinson et al. (2016) after Kritikos et al. (2015).

Landslide	Hazard Bin				
Density	$h < 0.1$	$0.1 \leq h < 0.2$	$0.2 \leq h < 0.3$	$0.3 \leq h < 0.4$	$0.4 \leq h < 0.5$
$\overline{x}$	0	0	0.002	0.01	0.046
$\overline{x} + \sigma_{\overline{x}}$	0	0	0.004	0.02	0.083
$\overline{x} + 2\sigma_{\overline{x}}$	0	0	0.006	0.03	0.121
$\overline{x} - \sigma_{\overline{x}}$	0	0	0	0.001	0.008
$\overline{x} - 2\sigma_{\overline{x}}$	0	0	0	0	0
Landslide	Hazard Bin				
Density	$0.5 \leq h < 0.6$	$0.6 \leq h < 0.7$	$0.7 \leq h < 0.8$	$0.8 \leq h < 0.9$	$h \geq 0.9$
$\overline{x}$	0.164	0.362	1.369	4.234	12.9
$\overline{x} + \sigma_{\overline{x}}$	0.272	0.517	1.917	6.052	18.103
$\overline{x} + 2\sigma_{\overline{x}}$	0.381	0.672	2.465	7.869	23.304
$\overline{x} - \sigma_{\overline{x}}$	0.056	0.208	0.822	2.416	5.202
$\overline{x} - 2\sigma_{\overline{x}}$	0	0.053	0.274	0.598	2.496

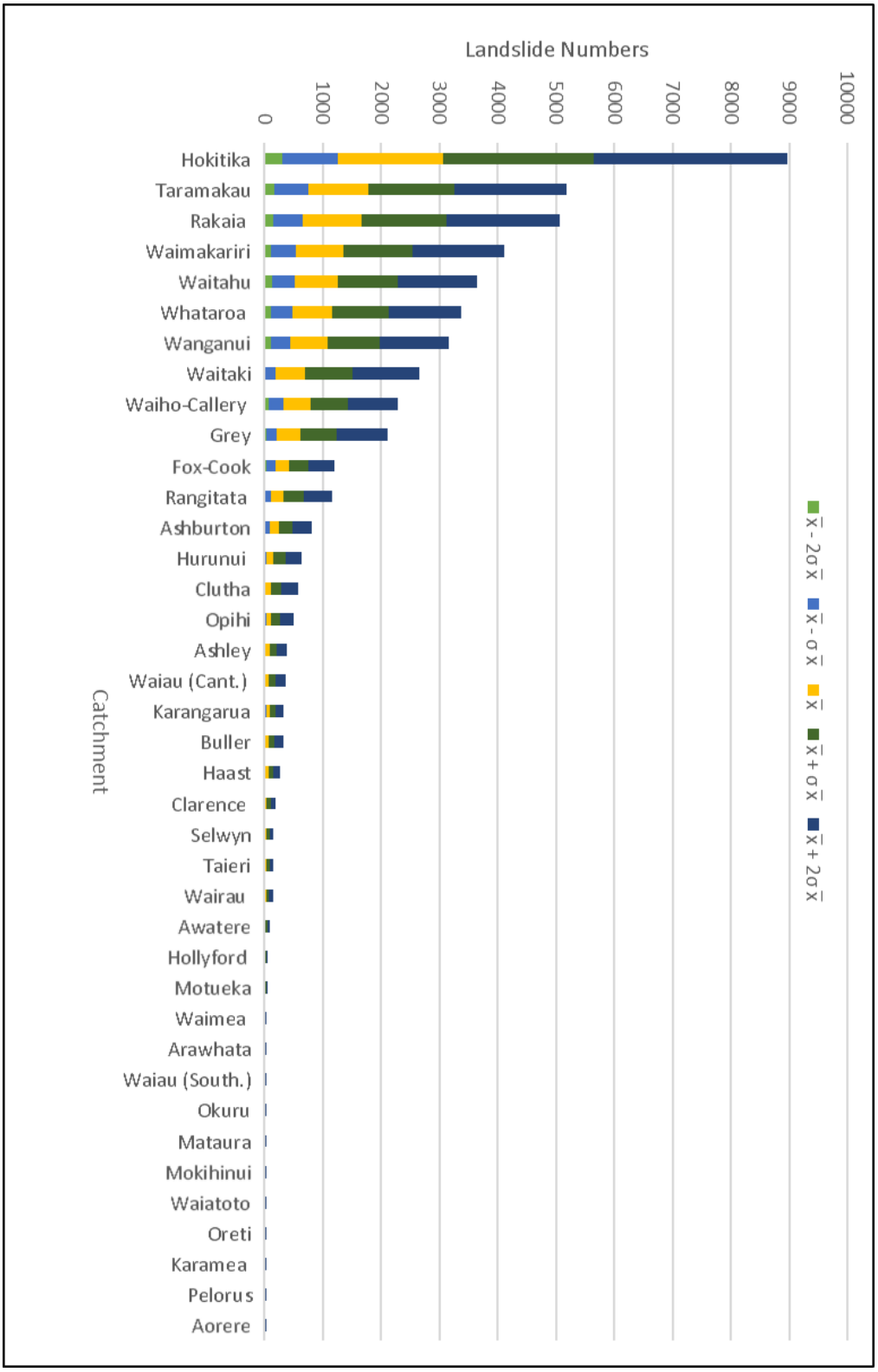

Figure 3.4: Landslide numbers for each catchment per sample mean and standard errors.

To begin analysing the impact coseismic landsliding poses to the environment, the effects on major river catchments can be used (Korup et al., 2004). Following Robinson et al. (2016), both denudation and aggradation resulting from coseismic landsliding are used for this purpose. Understanding these effects and their magnitude provides valuable insight when considering the ratio between coseismic and aseismic denudation, in addition to the potential impacts mass sediment input can have on rivers and their associated floodplains. The latter is of paramount importance within a West Coast context where extensive farming occurs on the fertile floodplains, making the industry highly susceptible to these effects as has been demonstrated historically (i.e. Davies et al., 2005).

As comparison to Robinson et al.'s (2016) research is a key outcome of this thesis, the results presented herein will utilize the same catchments. Under the National Institute for Water and Atmospheric Research's (NIWA) River Environment Classification system, 36 river catchments of order 6 or above exist in the South Island. Comparing quantifiable coseismic landsliding impacts on these catchments required a common scale, therefore Robinson et al. (2016) formulated a landslide impact factor (LSF) to establish a relative rate of landsliding such that:

$$\text{Landslide Impact Factor} = (NCi/NT)/(ACi/AT) \quad \textbf{(Eq. 3.1)}$$

where NCi is the number of landslides per individual catchment, NT is the total landslides, ACi is the area of an individual catchment, and AT is the total area of the South Island.

When interpreting **Equation 3.1**, any LSF value greater than 1 is considered above background landslide expectancy rates, such that the catchment experiences more landsliding than would be expected given its area. Robinson et al. (2016) determined an Alpine Fault earthquake would generate 16 catchments with a landslide impact factor above 1, to be subjected to further calculations. This thesis will provide results for these 16 catchments. Although these 16 catchments provide quantifiable insight to the impacts of an earthquake of the Alpine Fault, as previously stated the hypothetical scenario of this thesis appears to have a more focussed impact, covering a smaller region. Thus, to better display and analyse the results, the scenario in this thesis

incorporated additional catchments. To display valid results, external factors were considered when choosing these additional catchments. The Fox-Cook, Waitaha and Wanganui were chosen, given the exposure of both the tourism and agricultural sectors to events sourced in these catchments. Whereas only 10 of the 16 catchments of Robinson et al. (2016) achieved a landslide impact factor > 1 in this study, these additional 3 catchments, while of lesser order in the NIWA classification system exhibited drastically higher landslide impact factors (Figure 3.5, 3.6, 3.7).

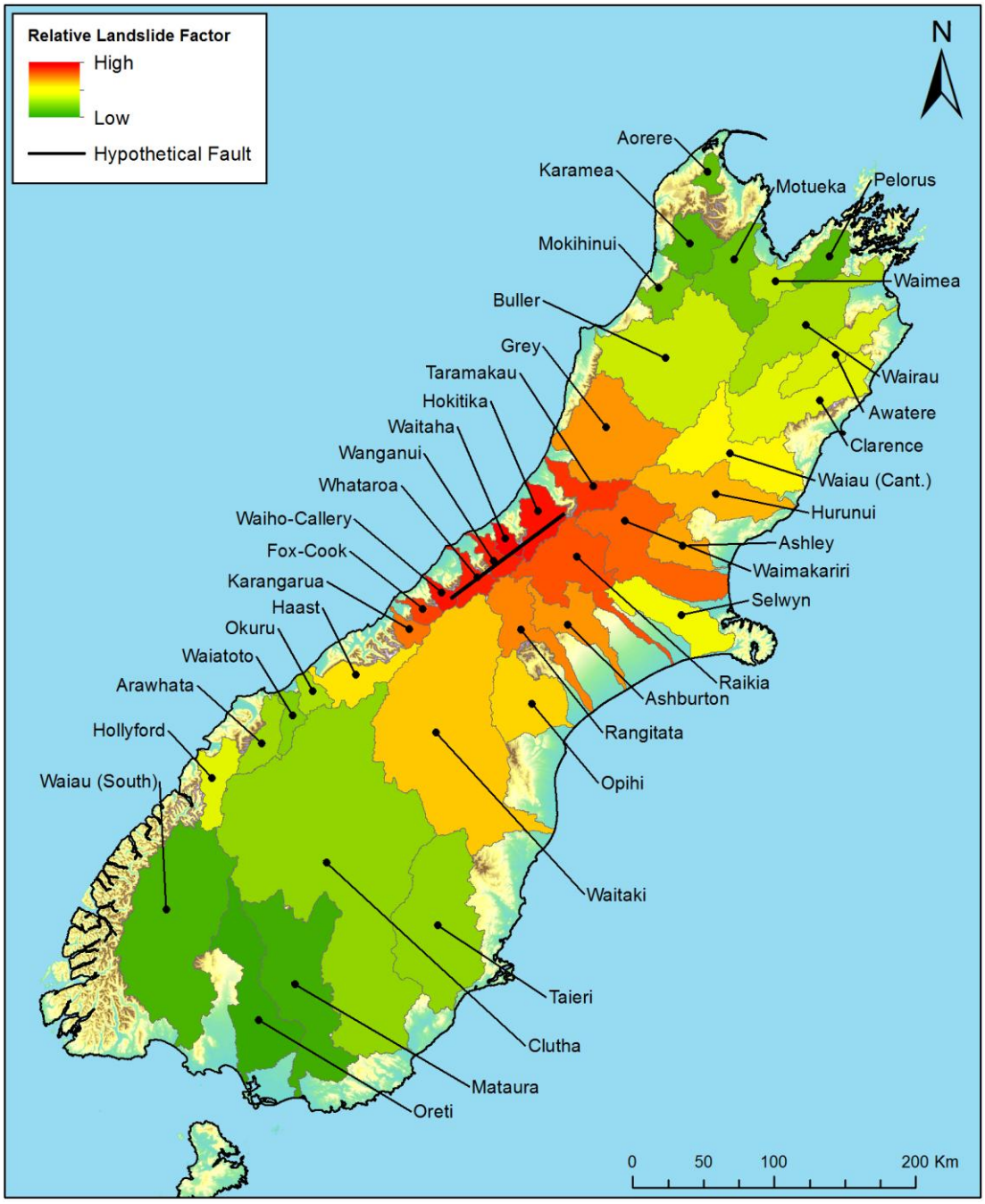

Figure 3.5: Visual representation of regional relative Landslide impact factors for all considered catchments

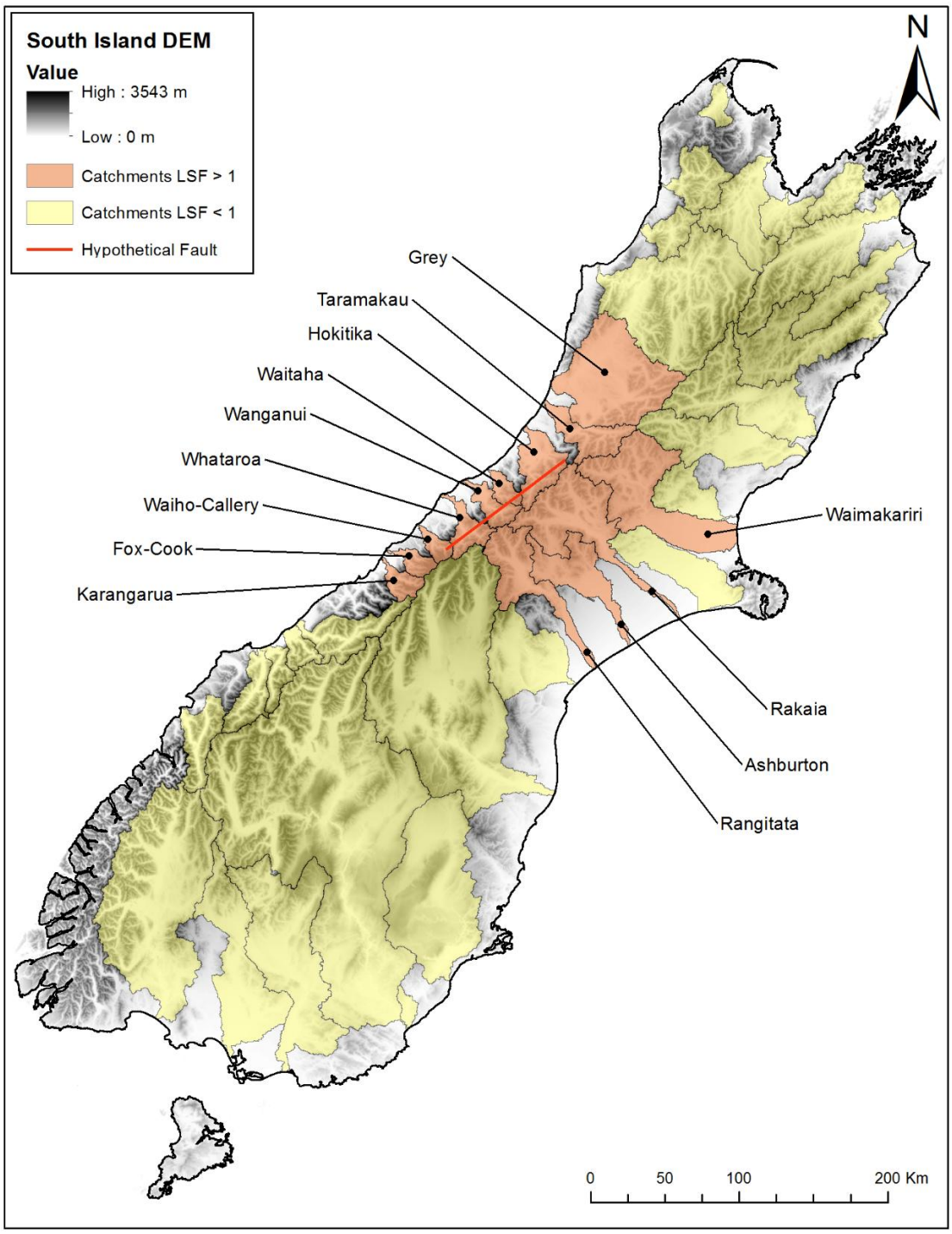

Figure 3.6:Location of catchments generating a Landslide Impact Factor greater than 1.

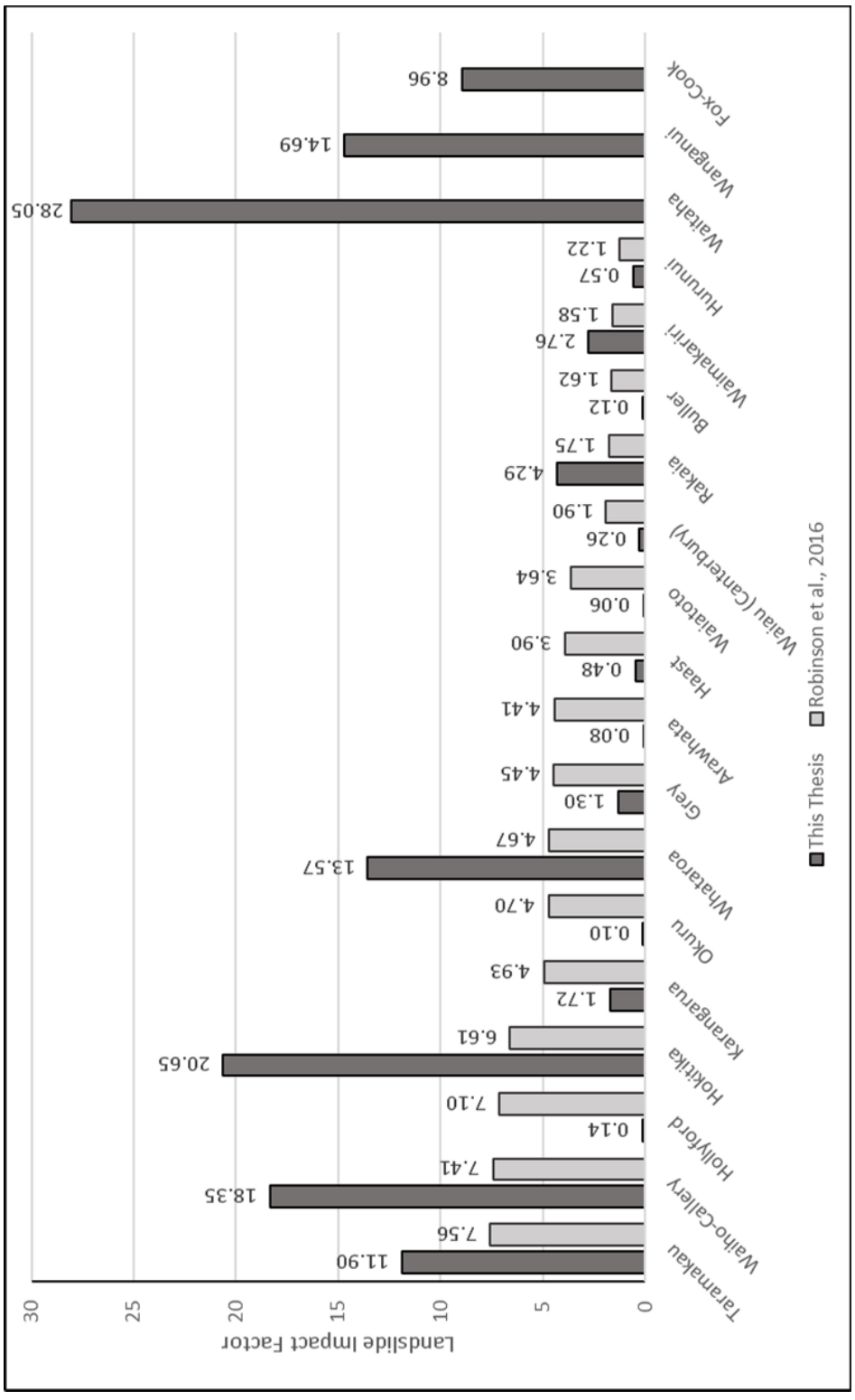

Figure 3.7: Landslide impact factors determined by this thesis and Robinson et al. (2016) for 19 and 16 catchments respectively.

3.5 Coseismic landsliding estimates

3.5.1 Individual landslide volumes

Due to the large number of potential values, calculating a range of individual landslide volumes requires Monte Carlo analysis be undertaken (Schreider, 2014). Repurposing the methods of Robinson et al. (2016), individual landslide volumes are calculated for the hypothetical fault scenario. A summary of this method is provided below and is followed by a description of **Equation 3.2**'s original form and its variables therein.

The method entails three key phases, each with a key component to determine. In phase-order these components are: *RAND, V'*, and *k* (Equation 3.2).

$$RAND = 1 - \int_{V'}^{10^9} kV^{-1.3}\,\mathrm{dV} \qquad \textbf{(Eq. 3.2)}$$

The first phase requires the determination of *RAND, RAND* being the solution to the integral of **Equation 3.2**, representing the probability that V is less than or equal to *V'* for each landslide. *RAND* is essentially a fraction of the area represented under the curve of **Equation 3.2** between an upper and lower limit if it were to be plotted. It is selected for each individual landslide by sampling from a uniform distribution.

In the second phase, employing an upper limit of 10^9 m^3 i.e. 1 km^3 as the maximum volume of the largest potential landslide, it is possible to solve for *V'* using the integral of *RAND* with respect to V. For an area under a curve to be integrated between two limits they must both be known, with the upper limit known and the lower limit represented by *V'*. With a *RAND* value selected *V'* can then be solved for from the Integral of *RAND* with respect to V. This phase produces a preliminary landslide volume in cubic metres.

The third phase deals with *k*. Whereas *RAND* varies, *k* is a coefficient and remains a constant value for each landslide set. Also determined by sampling a uniform distribution, the *k* value for each landslide set is used within **Equation 3.2**. The

absolute value of the product of k and *V′* provides the final resultant volume for an individual landslide.

Equation 3.2 and the variables therein derive from Brunetti et al. (2009), whereby 19 landslide datasets of different location and triggering mechanism displayed a cumulative probability density, where any given landslide displayed particular volume that followed a negative power law with a slope average component value (Robinson et al., 2016). The intersect value where this slope is equal to 1 represents the *k* value for that dataset. Although attainable with a historic landslide inventory, *k* can range greatly, varying over three orders of magnitude (Robinson et al., 2016). Thus a suggested conservative value of $0.001 \leq k \leq 0.1$ was used when sampling from a uniform distribution in this thesis. As for the upper landslide volume limit, 1 km^3 was used, as the maximum potential landslide volume is unknown and excluding an upper bound creates an unsolvable equation (i.e. ∞ km^3).

3.5.2 Total landslide volumes

With individual landslide volumes calculable and the study area divided into discrete areas, total landslide volumes could then be calculated. Monte Carlo analysis was used, incorporating total landslide numbers per catchment.

Directly using Robinson et al.'s (2016) methods, sampling from a uniform distribution, 10,000 *k* values ranging from 0.001 to 0.1 were determined, each unique to a single landslide set. Thus individual landslides were calculated, relating to the number of potential landslides estimated to occur within each catchment (Figure 3.4). This process was implemented five times per catchment to correspond with the sample mean and standard errors (i.e. the defined quantiles) utilized when obtaining landslide numbers. This resulted in 50,000 landslide sets per catchment providing varying volumes based on landslide numbers produced from density calculations. Each landslide set was subsequently summed providing a total volume for that set such that:

$$V_{LE} = \sum_{i=1}^{n} V'_i \qquad \textbf{(Eq. 3.3)}$$

where total landslide volume is *VLE*, *n* is the total number of landslides and *V′* is calculated for each individual landslide *i* using **Equation 3.2**.

Using 50,000 sets per catchment, a range of volumes are produced from which estimated landslide intensity was evaluated and compared with Robinson et al.'s (2016) Alpine Fault scenario (Figure 3.8, 3.9, & 3.10). The following box and whisker plots follow conventional practice representing quartile 1 (25%), median and quartile 3 (75%), left to right. The lower and upper whisker tips represent the furthest value either side of the box that is ≤ 1.5 times the interquartile range (IQR).

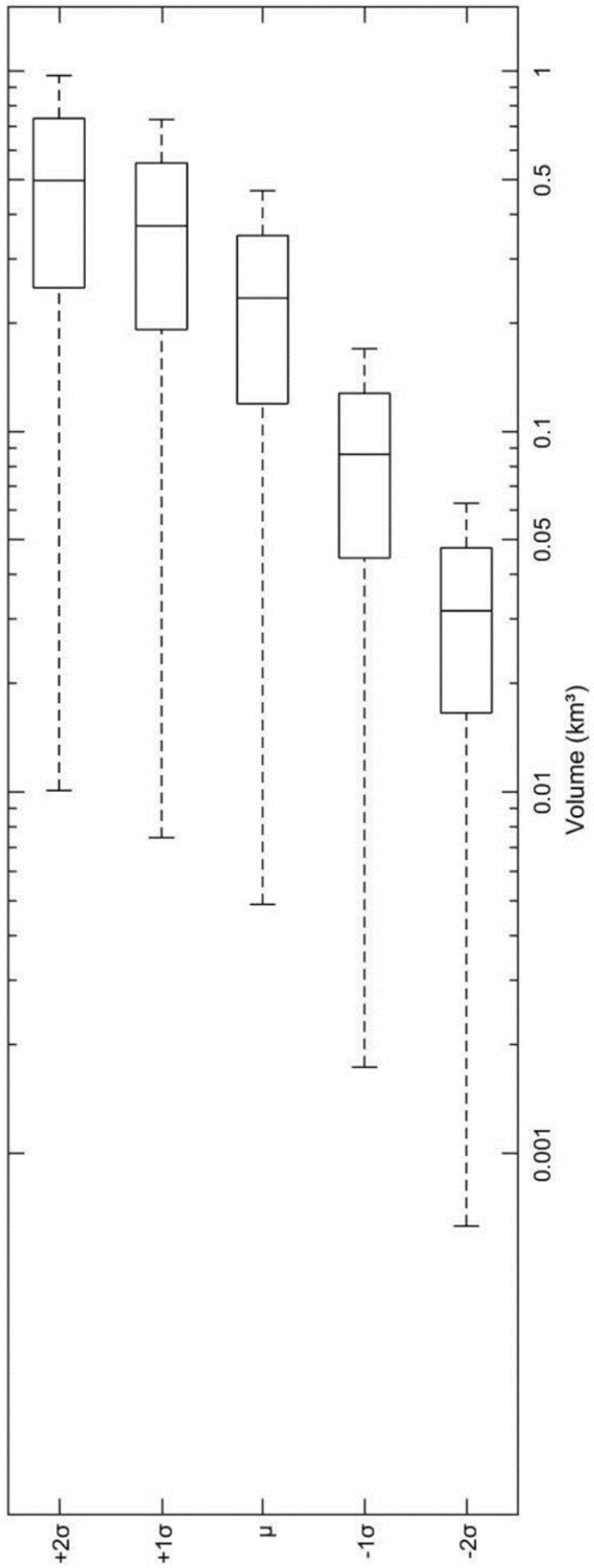

Figure 3.8: Modelling results for total landslide volumes resulting from a hypothetical fault earthquake using Monte Carlo analysis.

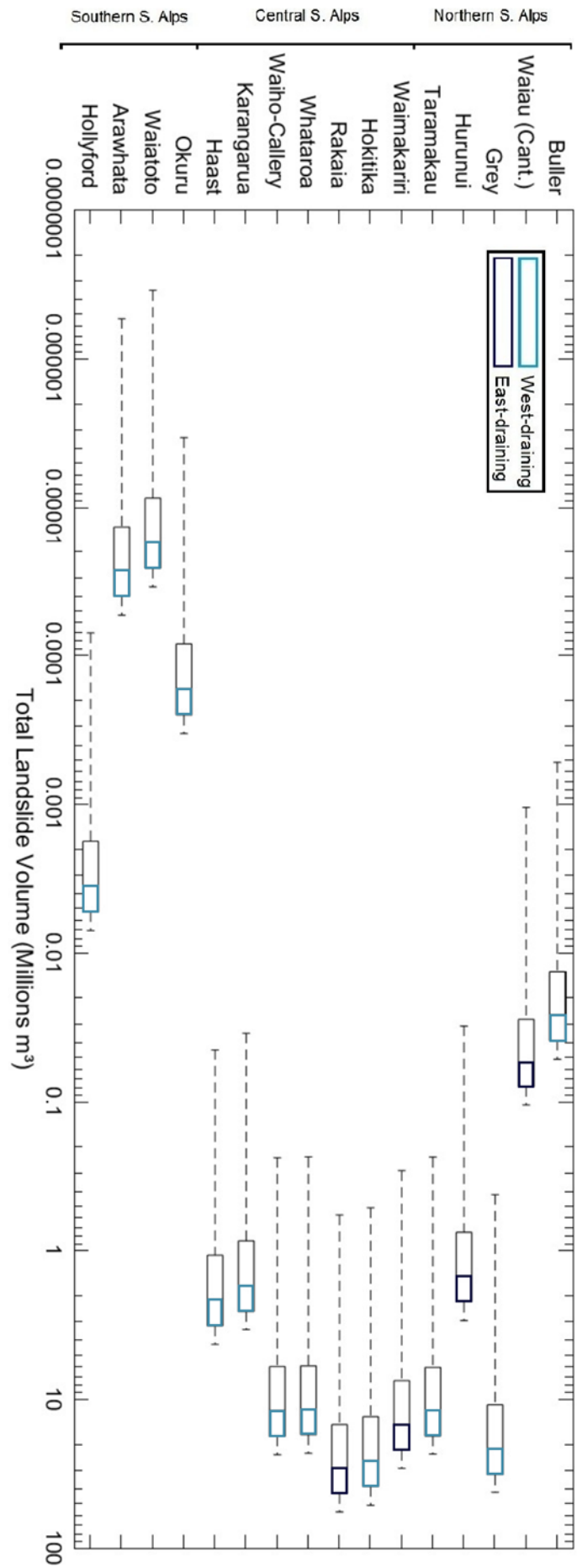

Figure 3.9: Total landslide volumes per catchment for the hypothetical fault earthquake using the 16 worst affected catchments from Robinson et al. (2016) for an Alpine Fault earthquake.

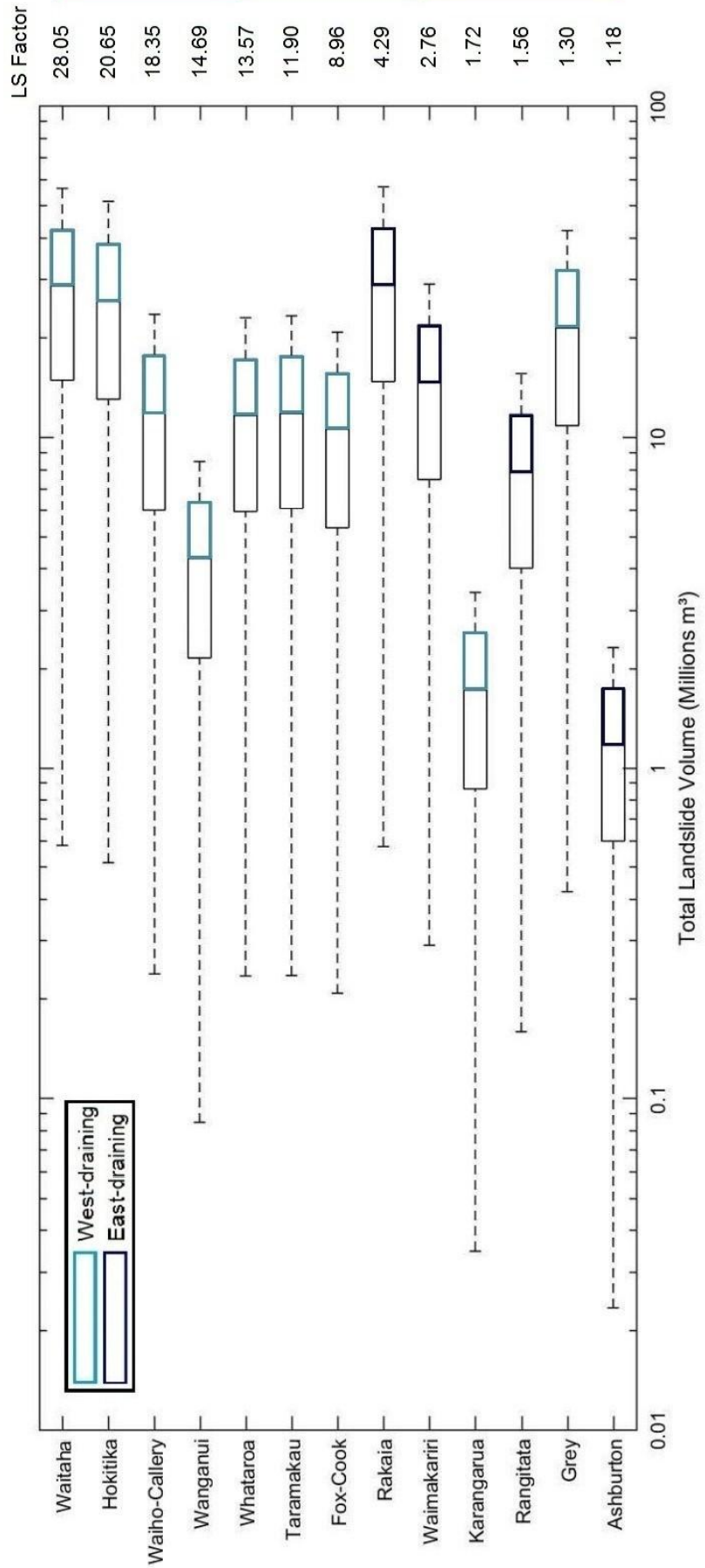

Figure 3.10: Total landslide volumes for the 10 worst affected catchments from the hypothetical fault earthquake, with the additional three catchments: Waitaha, Wanganui, and Fox-Cook included.

As seen in **Figure 3.8**, the five total landslide numbers for the hypothetical earthquake exhibit an expected increasing trend correlating with the increase in landslide numbers. Of specific note, the median of the mean volume distribution equates to 0.24. Given that the significantly larger spatial distribution of landslide susceptibility modelled by Robinson et al. (2016) for the Alpine Fault produced an equivalent value of 0.3, 0.24 seems a smaller difference than expected and demonstrates the impact potential of a large earthquake within the orogen (Table 3.3).

Table 3.3: Total landslide volumes (km^3) of mean median plot from this thesis (Figure 3.8) and Robinson et al. (2016).

	-2σ	-1σ	μ	+1σ	+2σ
This thesis	0.03	0.09	0.24	0.37	0.49
Robinson et al. (2016)	0.00	0.17	0.30	0.47	0.76
∑	0.03	0.08	0.06	0.10	0.27

Of further interest, the discrepancies at the opposing ends of the derived values exhibit an alternate trend to that anticipated. Where the -2σ value for Robinson et al. (2016) produced zero total landslide volume, this thesis' results produced 0.03 km^3. While minimal, the difference is curious as a smaller earthquake with less distributed landsliding potential would not be expected to produce a larger minimum value. This possibly derives from the Monte Carlo process where extreme values are less likely to occur, as the landslide density weighting values incorporated were identical, or could be the result of other variables between the two data sets. Whereas the minimum value did not follow the expected trend, the maximum value did. The +2σ values had a more significant difference, exhibiting a 54% difference when compared to the 27% difference at the median. Thus it is apparent when using this data alone that the maximum coseismic landsliding potential of an Alpine Fault earthquake is, as expected, significantly higher than that of a smaller non-Alpine Fault earthquake. However, the minimum of the latter could pose a larger hazard dependent on scenario.

The volume estimates per catchments as shown in **Figures 3.9** and **3.10**, allow interpretation of these results on a more refined scale. For comparison with Robinson

et al. (2016) the identical 16 catchments used in that study have been used in this thesis (Figure 3.9). Here the difference in susceptibility distribution is more apparent. As illustrated, the more northern and southern catchments that were heavily impacted by the Alpine Fault earthquake scenario are affected to a much lesser degree in the hypothetical fault scenario, experiencing erosion up to five magnitudes less. However, the results from the catchments where high susceptibility values overlap between the 16 catchments do not reflect those of Robinson et al. (2016). For example, while Robinson et al. (2016) stated most catchments displayed total volume interquartile ranges of 0.01-0.1 km³ (i.e. 10-100 million m³), the same catchments displayed no such correlation and further illustrates the differences between the two scenarios (i.e. Figure 3.11).

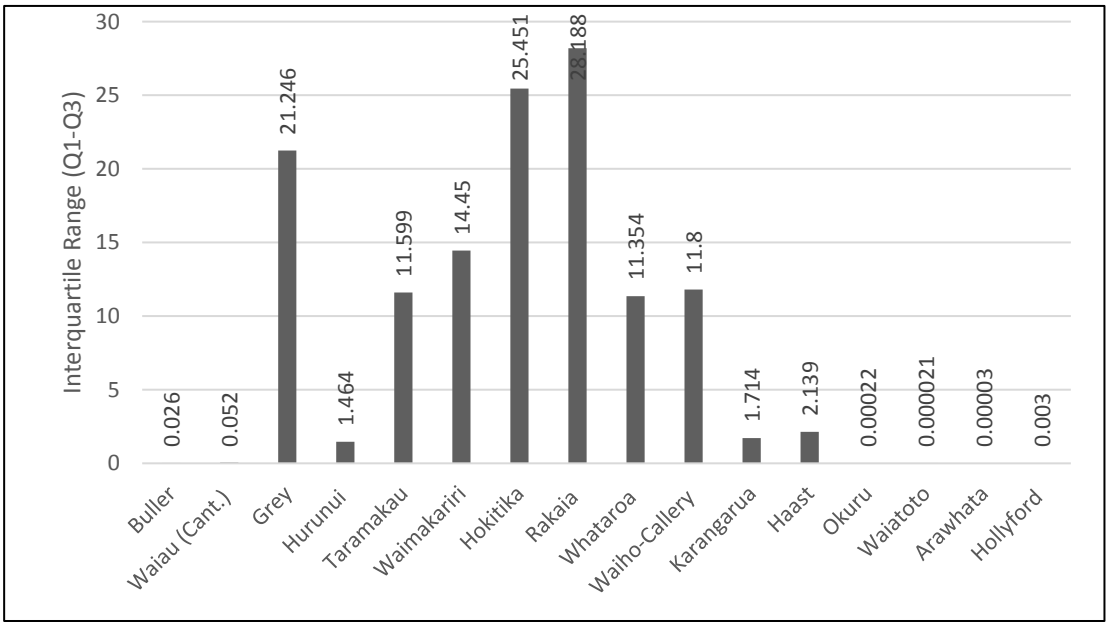

Figure 3.11: Interquartile ranges per catchment for the hypothetical fault earthquake using the 16 worst affected catchments from Robinson et al. (2016) for an Alpine Fault earthquake.

When considering the catchments that were significantly impacted during the hypothetical scenario, i.e. those that produced LSFs > 1, the considerable IQR differences are no longer as extreme (Figure 3.12). The west-draining catchments have mostly clustered IQRs whereas the east-draining catchments cover a larger IQR range, likely due to the much larger areas they cover. The much higher IQRs the additional 3 catchments exhibit are also apparent as the higher volumes they produce affect their range.

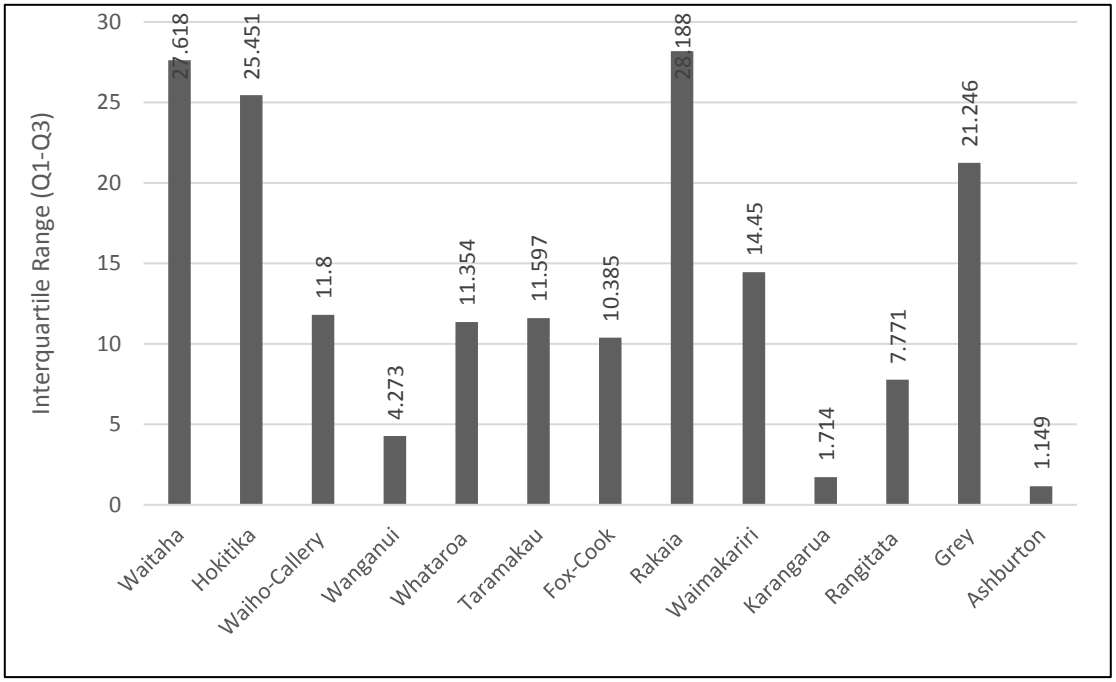

Figure 3.12: Interquartile ranges for 10 worst affected catchments ordered by LSF resulting from the hypothetical fault earthquake with the additional 3 catchments; Waitaha, Wanganui and Fox-Cook included.

3.5.3 Denudation results and discussion

To understand the effect of coseismic landsliding on the environment, the magnitude of the modelled denudation was determined. This provided the estimated available aggradation sediment values of each catchment for the five defined quantiles. Thus to calculate the catchment-specific denudation resulting from the hypothetical fault earthquake modelled, both the areas of individual catchments affected and landslide debris volumes were required. To this end the individual catchment areas had their respective areas of Holocene alluvial deposits subtracted (Figure 3.13). The corresponding landslide debris volumes were subsequently divided by the remaining area to attain an overall average denudation depth per catchment (Figure 3.14 & 3.15).

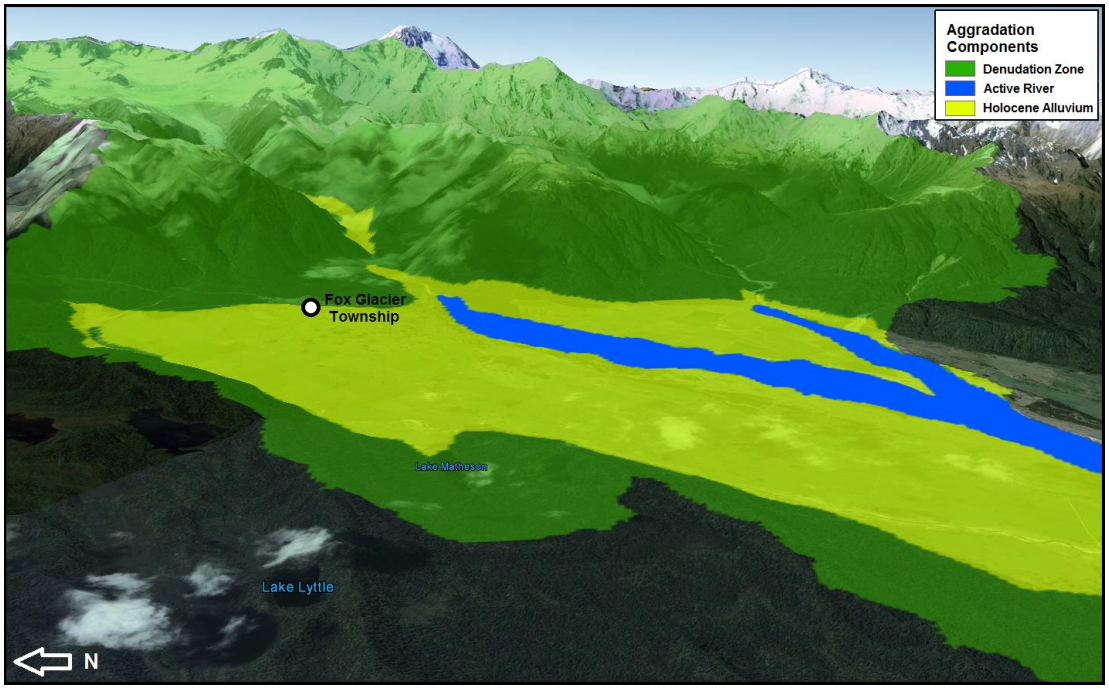

Figure 3.13: Three dimensional oblique view of the Fox-Cook Catchment showing the relative areas of active denudation and aggradation based on the method used.

Holocene alluvial deposit areas were removed from potential denudation areas for a variety of reasons. The most significant of these being that these are the areas where aggradation is expected to occur so logically denudation would not be present. Other factors derive from the physical properties, being flat, low-lying areas comprising of topographically constrained alluvial gravels. As a simple derivation of the volumes presented above, denudation follows much the same trends as the prior volumes, albeit now presented as averaged depth values in millimetres over a defined area.

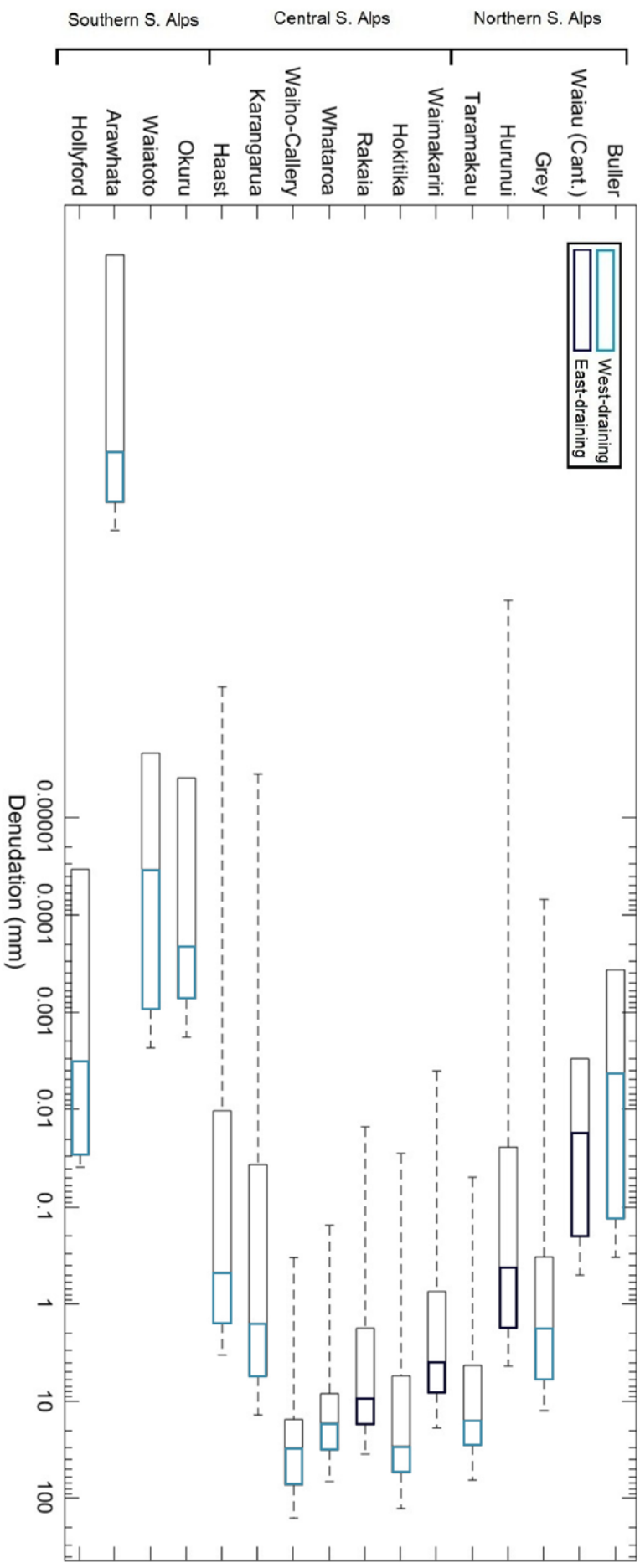

Figure 3.14: Denudation depths per catchment for the hypothetical earthquake using the 16 worst affected catchment from Robinson et al. (2016) for an Alpine Fault earthquake.

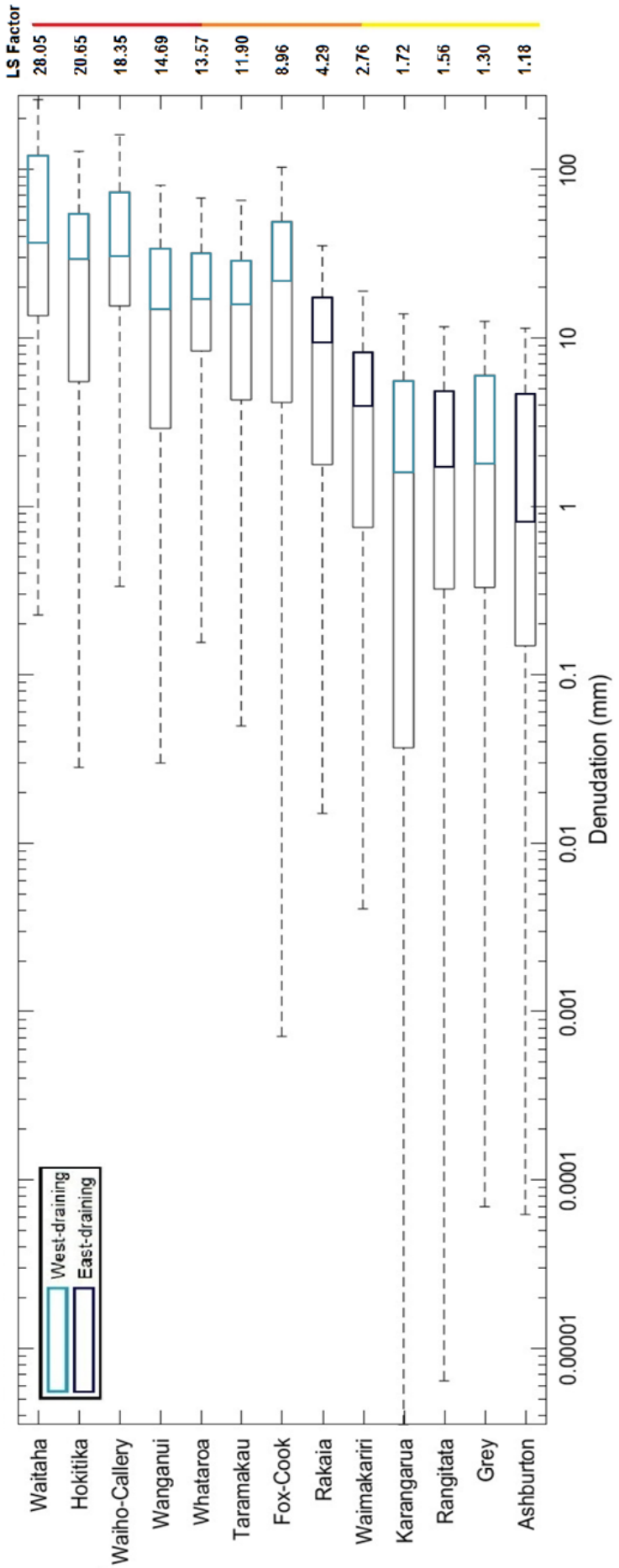

Figure 3.15: Denudation depths for the 10 worst affected catchments resulting from the hypothetical fault earthquake with the additional three catchments: Waitaha, Wanganui, and Fox-Cook included.

Of the original 16 catchments used for comparable values, the Taramakau, Hokitika, Whataroa and Waiho-Callery catchments experience the most denudation with median values above 10 mm and in the case of the Hokitika and Waiho-Callery, maximum values of ~130 mm and ~160 mm respectively; well above the background rates of 5.8 mm and 11.7 mm (Robinson et al., 2016). Notably in **Figure 3.14**, denudation values of catchments not directly proximal to the hypothetical fault are negligible, experiencing denudation magnitudes smaller than others. Although the risk from these catchments could be dismissed, it is pertinent to reinforce that these values are averages over entire catchment areas and that a small portion of this large area could experience the entirety of the landsliding for a catchment. With the inclusion of the additional three catchments, the maximum denudation value increases further with the Waitaha potentially experiencing up to 261 mm. The catchments also exhibit median values of 37 mm, 15 mm, and 22 mm for the Waitaha, Wanganui, and Fox-Cook respectively and emphasise the extreme short term erosion potential of these small West Coast catchments. Also of interest is the potential denudation experienced by the east-draining catchments included in **Figure 3.15**, with median values ranging between ~1-10 mm which, when considering the much larger average catchment areas, is an extreme amount.

3.5.4 Aggradation results and discussion

Obtaining aggradation depths follows much the same process as denudation (Figure 3.13). The only distinction between the two processes is a different area value being utilized during the division stage. The aggradation depth calculation distributes the landslide volume uniformly across the area of Holocene alluvium, producing depths reported in mm (Figures 3.16 & 3.17). As with denudation, the aggradation depths presented herein are also average values over their respective areas, although of note is that the areas are now significantly smaller. In aligning with Robinson (2014), a conservative estimate of 30% of total landslide volume is inferred to be involved in aggradation. This is based on the same reasoning, using estimates of aggradation sediments from prior research to determine the proportion naturally observed in local studies. Were this percentage to be increased so to would depths, drastically increasing hazard intensity.

In reality, the aggradation values obtained would not be spread evenly over the deposition areas. For the west-draining catchments much larger values would be expected at the rangefront, due to the heavily incised outlets before the floodplains creating a bottleneck effect. Depths would be expected to linearly decrease as distance from these features increased, spreading aggradational sediments over a wider area. These values begin to show the potential impacts of coseismic landsliding on sectors such as farming and transport, where large increases in the base ground level could bury pasture, roads and bridges among other features and infrastructure.

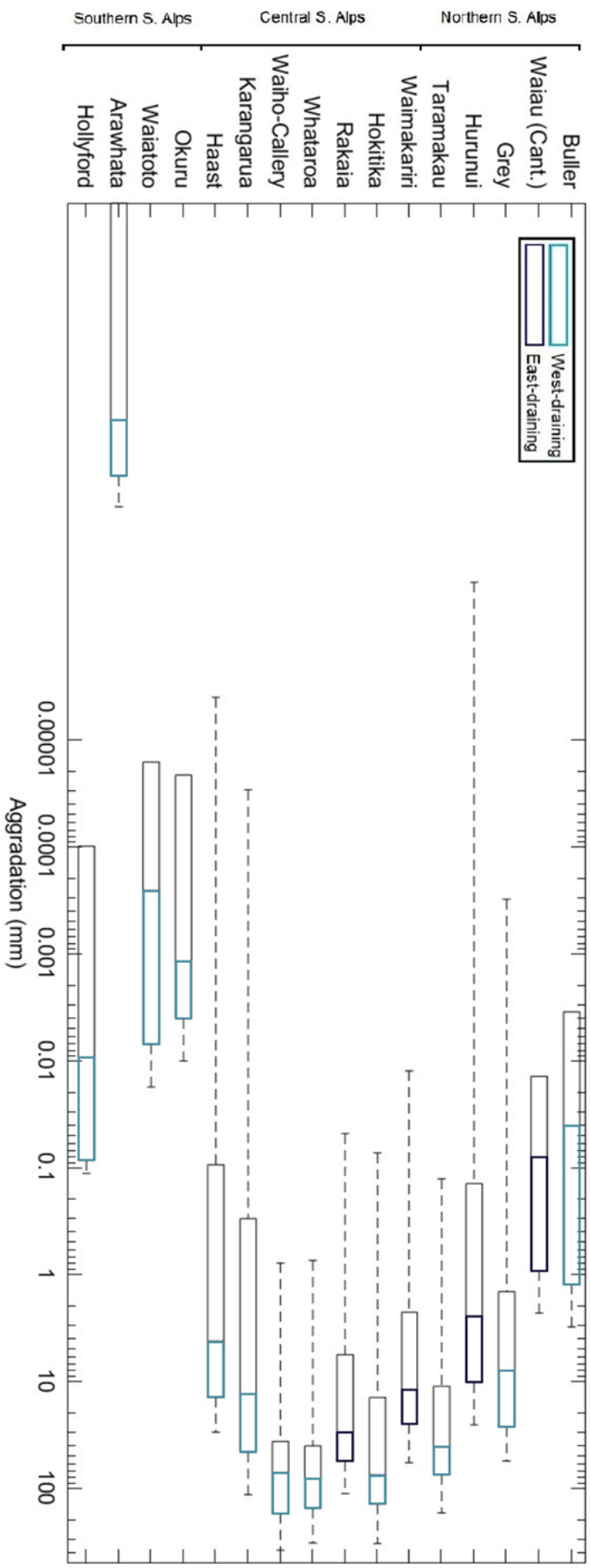

Figure 3.16: Aggradation depths per catchment for the hypothetical fault earthquake using the 16 worst affected catchments of Robinson et al. (2016) for an Alpine Fault earthquake.

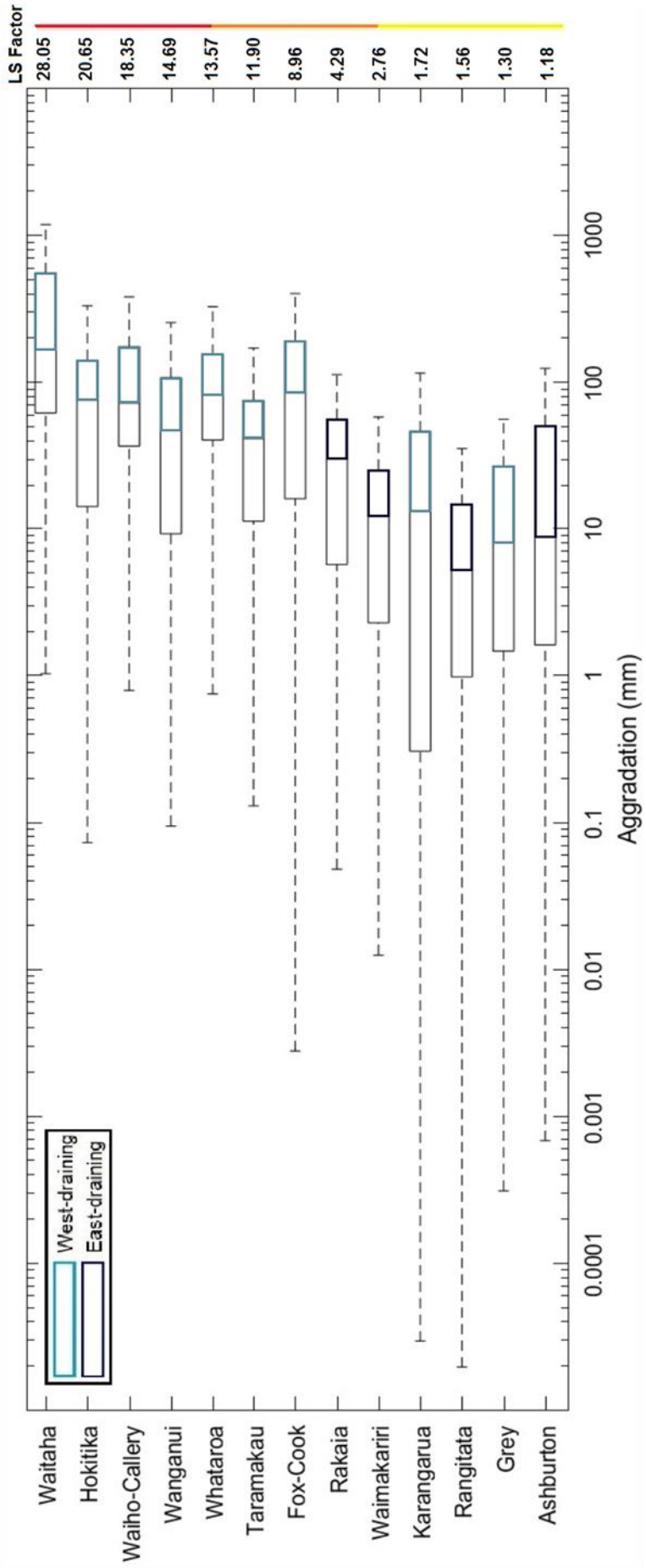

Figure 3.17: Aggradation depths for the 10 worst affected catchments resulting from the hypothetical fault earthquake with the additional three catchments: Waitaha, Wanganui, and Fox-Cook included.

As with denudation, the general data trends and catchment median clusters of the 13 most heavily affected catchments of this thesis remained relatively constant. The same can be stated for the original 16 used for comparison. This is due to the process used to obtain the area values, with depositional areas occupying on average approximately 13% of total catchment areas with a range of 5-20%. Thus aggradation values are the complementary value of denudation values relative to total volumes. Once again the smaller west-draining catchments display the most intense values, with the east-draining catchments at the lower end.

Using the 13-catchment dataset in **Figure 3.17**, median aggradation values range from 5 mm in the Rangitata catchment to 169 mm in the Waitaha following what appears to be a direct function of area and distance from fault rupture. The maximum values represented by the upper adjacent display some extreme results with an average depositional depth of 276 mm with a low in the Rangitata catchment of 37 mm and a high of in the Waitaha catchment of 1195 mm.

When compared to Robinson (2014), using identical catchments where available, the trend of fault rupture proximity to hazard intensity characterises the results. Where catchments are close to both Alpine Fault and hypothetical fault ruptures, the values are comparable. However, as the distance away from the hypothetical fault increases, these values decrease drastically. This is not the case with the Alpine Fault as given its ~400 km modelled rupture length it is still proximal to these catchments. Thus at distant locations the difference between depths achieved is considerably in favour of the Alpine Fault (Figure 3.18).

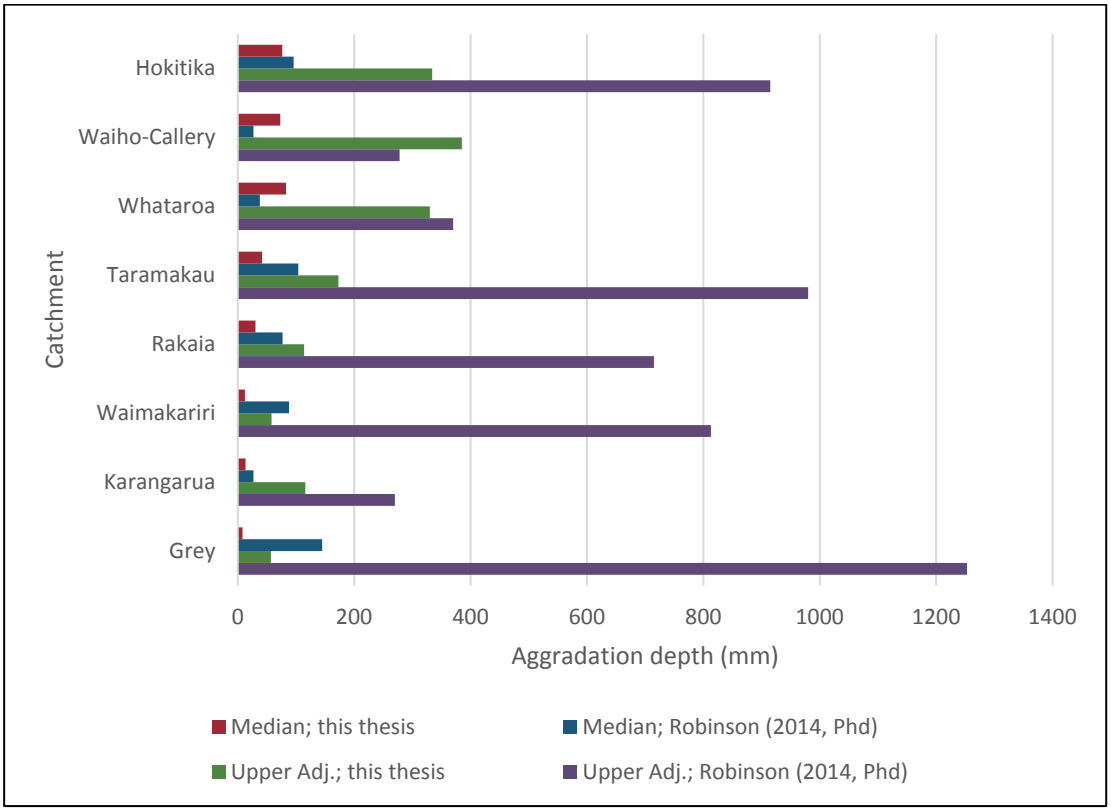

Figure 3.18: Comparable catchment aggradation depths between both this thesis and Robinson et al. (2016).

Unfortunately, the catchments from this thesis that achieved high depths were not included in Robinson's (2014) research, being less than Order 6. Nevertheless, as evidenced by the maximum achieved by the Waitaha, Wanganui, and Fox-Cook catchments, similar results could be expected to correlate with the similarities shown in the Waiho-Callery and Whataroa catchments in **Figure 3.15**.

3.6 Summary of results

All volumes, denudation depths and aggradation depths follow the same general trend. Namely, as distance from the hypothetical fault increases hazard intensity decreases. When considering Robinson et al.'s (2016) results, this was not unexpected and although those results had more intense values in other areas, both the length of rupture and earthquake magnitude would be responsible for these differences and the much smaller areas of distributed high intensity shaking.

The cessation of shaking intensity proximal to the Alpine Fault-MFZ junction also produced interesting results regarding the dispersion of landslide susceptibility

values, resulting in high values for the Taramakau and Waimakariri catchments. However, the transfer of rupture energy between these fault zones is not fully understood and so the susceptibility values produced in this region should be viewed with a certain amount of caution.

While more distant catchments were less affected in this thesis, the smaller central West Coast catchments experienced a significantly higher amount of denudation and aggradation from a smaller earthquake. The proximity of the hypothetical fault to the Alpine Fault and the apparent concentration of rupture energy in the triangular shaped wedge between the two faults appears to create a much more landslide-susceptible region within these catchments (Figure 3.19). This is further demonstrated by the additional order 5 catchments reviewed. These achieved values equivalent to the highest produced by the Alpine Fault scenario, with other catchments in this region included in both studies producing similar values.

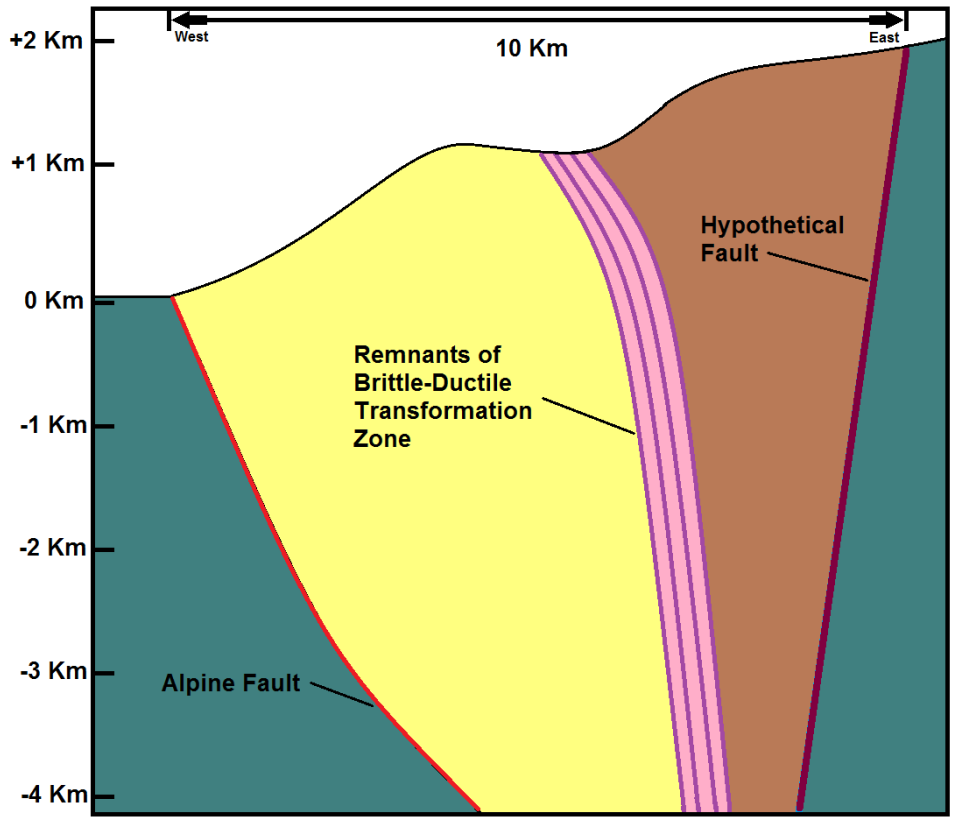

Figure 3.19: Triangular wedge formed by the Alpine Fault and Hypothetical fault where much of the seismic energy and therefore high landslide susceptibility values derive from. (Redrawn based on cross section of Cox and Sutherland (2007).

4 COMPARISON OF RESULTS WITH DATA AND INFERENCES FROM PREVIOUS RESEARCH

4.1 Introduction

The coseismic landsliding estimates from a hypothetical fault earthquake can now be related to previous research. The outcomes can then be used to answer the remaining primary research objectives of Chapter 1.

The seismic and coseismic modelling herein were designed to represent a realistically intense earthquake, whose consequences can be compared with those of an Alpine Fault event. Although the methods used have limitations, in a regional context the results produced are sufficiently accurate to be compared with other research around the South Island with respect to the ~1620 C.E. event. The conclusions could have implications for the established palæoseismic record of the Alpine Fault, as well as suggesting the presence of an additional seismogenic source in the Southern Alps and its associated hazard potential.

As established in the previous chapters, an alternative seismic origin of the ~1620 C.E. event has received little attention to date. Howarth et al. (2012, 2014, 2016) alone concluded that the Alpine Fault was not responsible for the effects of this event at their research locations. In passing, other researchers have noted the potential for multi-earthquake scenarios and the inability of off-fault data to conclusively attribute evidence to the Alpine Fault (e.g. De Pascale et al., 2014).

In the event that the consequences of the hypothetical fault rupture do not match the physical evidence for the ~1620 C.E. event, the hypothetical consequences nevertheless represent landslide intensity and zones of extensive aggradation on the West Coast for a large earthquake and therefore still provide relevant information.

The present chapter will discuss the literature reviewed in Chapter 2 in the light of the results presented in Chapter 3. This will be conducted for each individual study and follow the same progression as Chapter 2. A summary discussion will follow, consolidating and explaining the key outcomes.

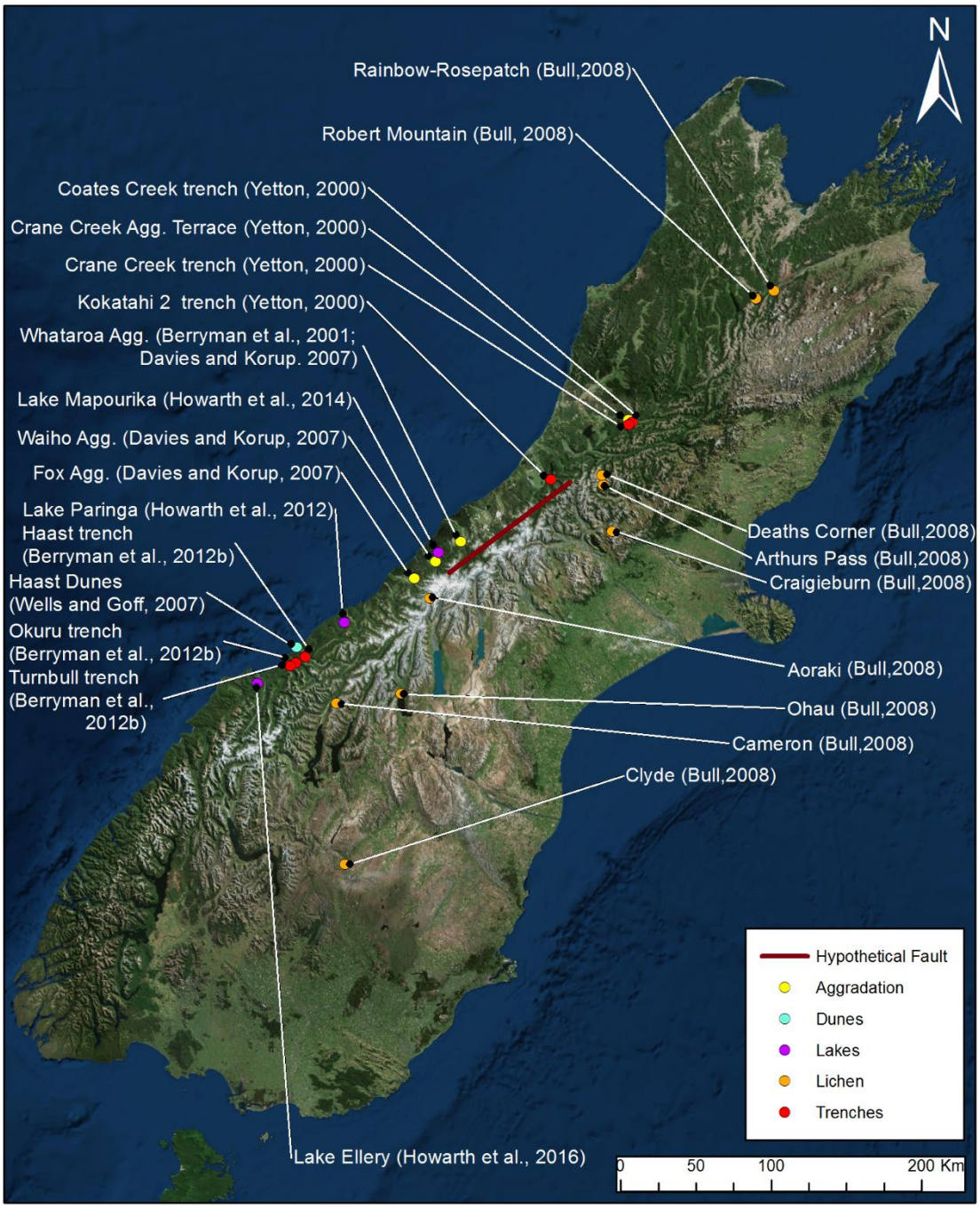

Figure 4.1: Location map showing the approximate spatial locations of palæoseismic indicators of the ~1620 C.E. event. Red indicates fault trenching sites. Purple indicates lacustrine sites. Orange indicates lichenometry sites. Yellow indicates aggradation trenching sites. Teal indicates coastal progradation dune formations.

4.2 Comparison and discussion of on-fault evidence

On-fault evidence of Alpine Fault rupture is scarce and relies heavily on a few publications and their conclusions. The methods used in these studies and their associated limitations have been discussed in Chapter 2, although it is important to once again note the limited spatial distribution of the studies and the limitations of the methods employed.

4.2.1 Northern Alpine Fault trenching – Crane Creek event

The research conducted by Yetton (2000) presents us with arguably the most spatially extensive in-depth study of on-fault trenching of the Alpine Fault's surface trace.

Using the hypothetical earthquake scenario, the Crane Creek locality experienced MMI VI shaking, with values for landslide susceptibility ranging from approximately 0.3-0.7. As part of the Grey catchment, Crane Creek was among the 13 catchments with an LSF higher than 1. Although the Grey catchment did produce a relatively low LSF value of 1.3, it remains above background rates but the catchment itself is not an ideal comparative medium for Crane Creek. As shown by the denudation and aggradation depths, a considerable amount of landsliding occurred within the catchment. The inadequacy of using regional results for site specific values does somewhat limit the inferences that can be made about a particular location. However, with this in mind, the median aggradation depth for the catchment of 8 mm and upper value of 57 mm, in addition to higher values expected at the rangefront, are comparable at order-of-magnitude scale to the ~200 mm of the sandy silt and schist gravels found in the Crane Creek trench dated to ~1620 A.D. It is important to note that this location is not in the main Crane Creek channel but rather situated at the base of a very minor tributary catchment, so comparison to the catchment-averaged denudation depths of 2 mm median and 12 mm upper value, rather than aggradation depths, may be of more relevance. Yetton (2000) concluded that this face layer, which differs in sediment composition to that of the scarp, was infilled by the scarp and post-seismic erosion sediment (Figure 4.2).

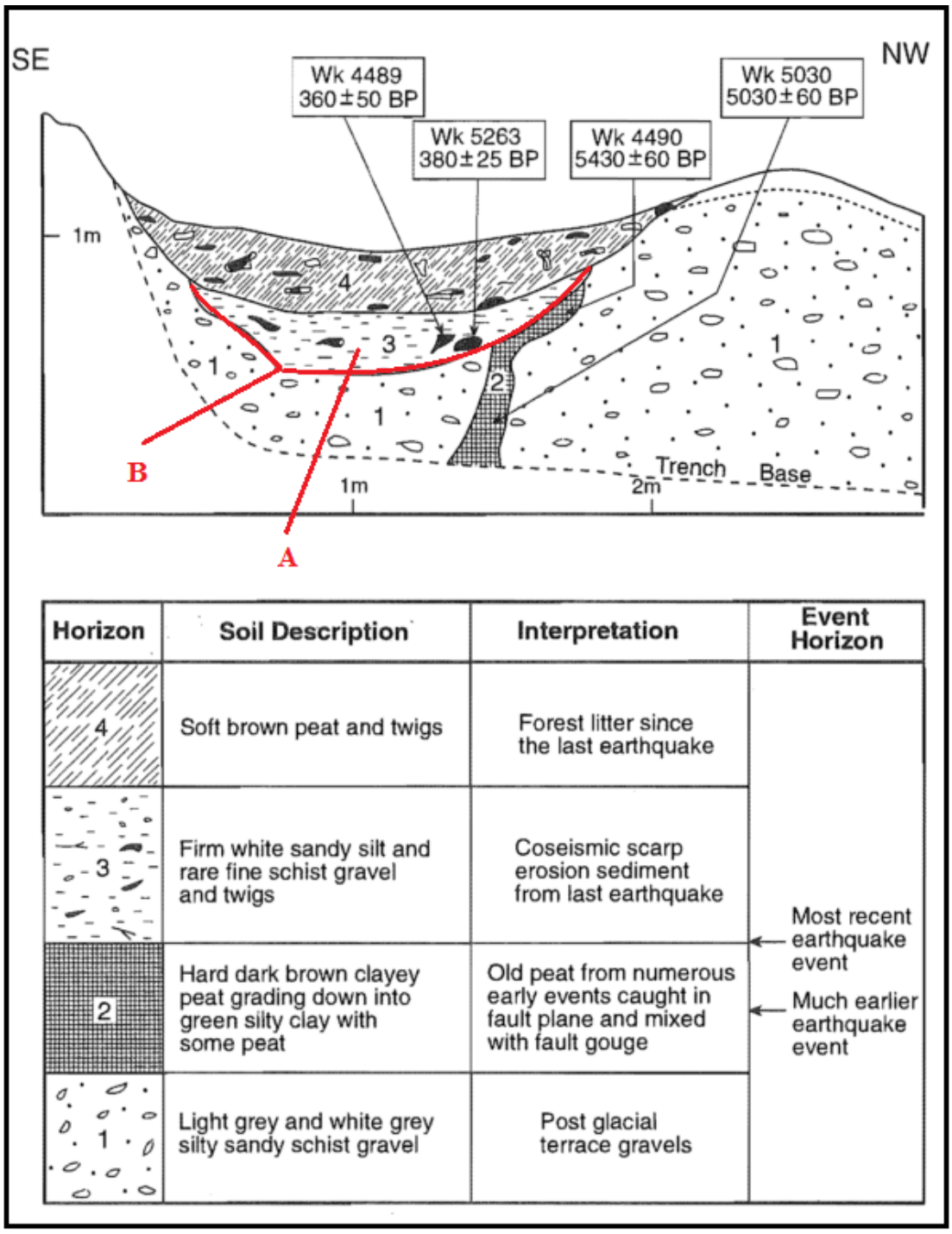

Horizon	Soil Description	Interpretation	Event Horizon
4	Soft brown peat and twigs	Forest litter since the last earthquake	
3	Firm white sandy silt and rare fine schist gravel and twigs	Coseismic scarp erosion sediment from last earthquake	← Most recent earthquake event
2	Hard dark brown clayey peat grading down into green silty clay with some peat	Old peat from numerous early events caught in fault plane and mixed with fault gouge	← Much earlier earthquake event
1	Light grey and white grey silty sandy schist gravel	Post glacial terrace gravels	

A) Only dated layer inferred as related to the scarp, although it is comprised of different sediments.

B) Base Layer of furrow comprised of terrace gravels and inferred as well vegetated pre-earthquake. Yet there exists no detritus suggesting this could have been a flow path infilled from denudation consequent from a distal earthquake.

Figure 4.2: Crane Creek trench face log. Annotations in red are related to brief descriptions at the base of the figure. Adapted from Yetton (2000).

The scarp formation itself and the furrow are more difficult to misconstrue and appear entirely representative of earthquake surface fault rupture. Their broken continuity and obstruction by landslide debris and forest cover make their dimensions difficult to estimate and the potential exists that they could be the result of a partial surface rupture before the ~1620 C.E. event. An alternative conclusion could be aggradation and/or denudation material infilling the furrow as a consequence of coseismic landsliding triggered by a distant seismogenic source. Aside from the ~5500 BP peat, the absence of any dated material below the ~1620 C.E. correlative layer does not provide conclusive evidence of either scenario. The limited depth of the trench, showing only one event horizon, and the absence of 1717 A.D. sediment input (which would imply a full-length rupture) makes it difficult to draw conclusions using available data. Both Yetton's (2000) Crane Creek event and alternative hypothetical events are therefore plausible scenarios.

With regard to the second Crane Creek Event trench, Coates Creek, the physical evidence could also be related to a non-Alpine Fault earthquake. Under the hypothetical earthquake scenario, the Coates Creek locale is also in the Grey catchment, again experiencing MMI VI shaking and landslide susceptibility values of approximately 0.3-0.7.

The ~1.2 metre trench certainly appears to have experienced previous vertical displacement on the Alpine Fault trace. However, when using the available face log, obtaining a timeframe for the uplift event does not seem possible when interpreting the trench independently and the conclusion appears predominantly based on the influence of factors external to the trench. Additionally, the amount of vertical displacement at the fault zone appears less than expected even when considering post-seismic scarp erosion/deformation. This could again be resultant of an earlier rupture, having a correspondingly longer time to erode to its current height (Figure 4.3).

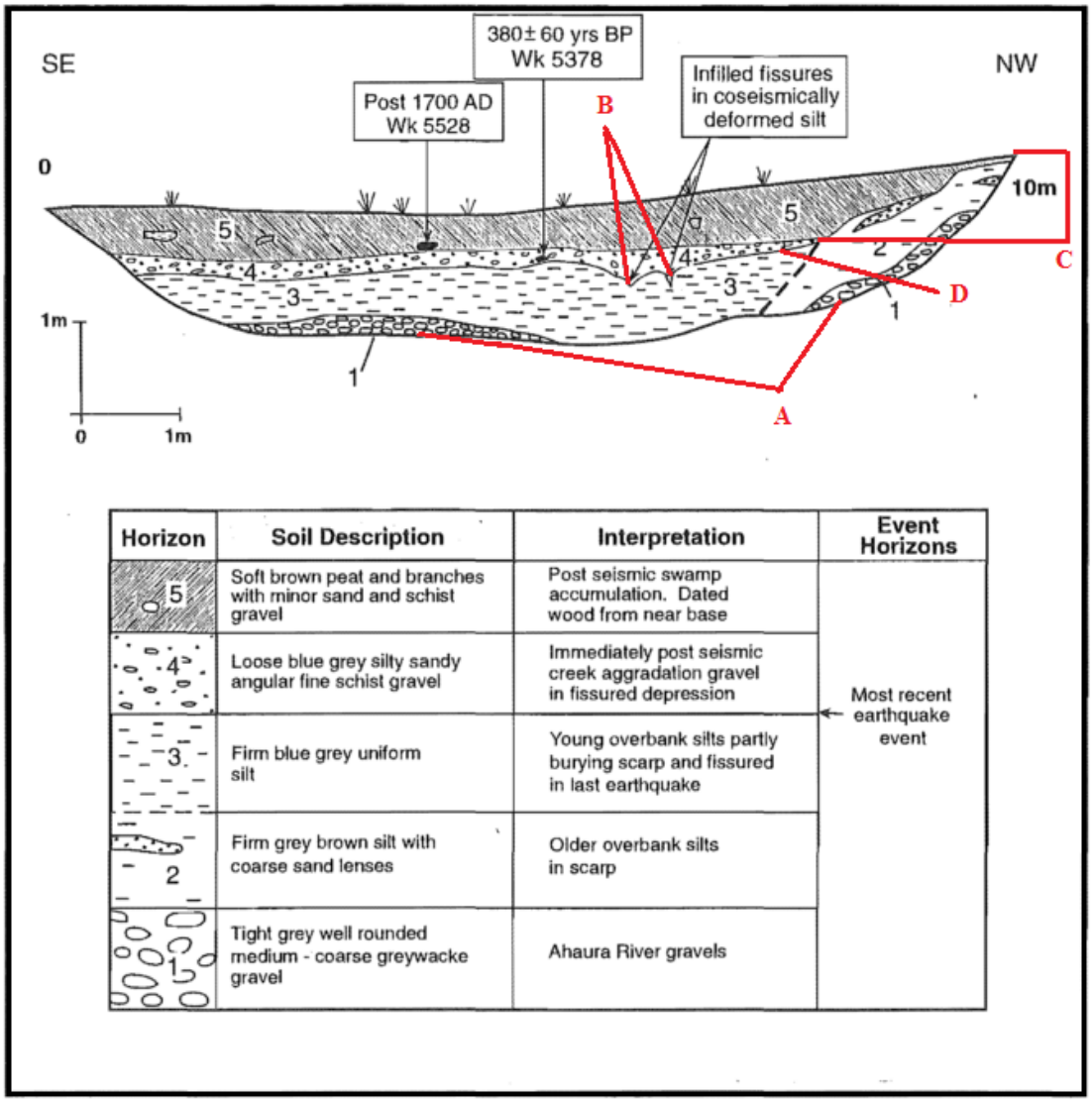

Horizon	Soil Description	Interpretation	Event Horizons
5	Soft brown peat and branches with minor sand and schist gravel	Post seismic swamp accumulation. Dated wood from near base	
4	Loose blue grey silty sandy angular fine schist gravel	Immediately post seismic creek aggradation gravel in fissured depression	Most recent earthquake event
3	Firm blue grey uniform silt	Young overbank silts partly burying scarp and fissured in last earthquake	
2	Firm grey brown silt with coarse sand lenses	Older overbank silts in scarp	
1	Tight grey well rounded medium - coarse greywacke gravel	Ahaura River gravels	

A) There is a clear vertical offset between these 2 units inferring rupture displacement at this location. Although there is no dated material within or directly adjacent to the units to suggest a time.	B) The fissures in the coseismically deformed siltcould be from any proximal seismic origin with no evidence to conclusively suggest a rupture at this location was responsible.
C) Height of scarp less than other location and could imply either more intense erosion at a location only ~2.5 Km from Crane Creek or a longer time period for which erosion to take place (i.e a 15th century earthquake).	D) No scarp colluvium present in the dated unit could infer that (C) may have been the case. Although post-seismic pertubations could be responsible.

Figure 4.3: Coates Creek trench face log. Annotations in red are related to brief descriptions at the base of the figure. Adapted from Yetton (2000).

Interpreting the layers present within the trench, the coseismically-deformed silt is not specifically a fault-proximal site effect and could be resultant of a distant earthquake or other aseismic processes. The silt horizon which contains the dated sediment is congruent with that of the first trench and is of approximately the same depth, composition and sediment type expected in a drainage system post-earthquake. It appears that the lower layer was deformed by shaking and covered by aggradation sediments and evidence of the supposedly collapsed fault scarp is not present in these layers, although it could have been remobilized. When interpreted on its own, the Coates Creek trench appears to favour an Alpine Fault earthquake surface fault rupture, although a different seismogenic source could still be responsible. Using the available data, both earthquake scenarios are plausible at this location.

The Kokatahi 2 trench is the southernmost trench indicating the Crane Creek Event. Under the hypothetical fault scenario, it experiences MMI VIII shaking and its location has landslide susceptibility values ≥ 0.7. Located in the Hokitika catchment it is represented by an LSF of 20.65 with median and upper adjacent aggradation values of 77 mm and 334 mm respectively. The local geomorphology of the trench site comprises a relatively open flood plain with large river terraces and apparent rapid reworking of fluvial sediments.

The trench includes a complex array of features and layers, with Yetton (2000) inferring two distinct event horizons. The features include multiple liquefaction injections, unconformably bedded sediment sequences and two distinct fault zones. The verticality of the liquefaction features implies they did not reach the surface. Their relative vertical positions shown by differences in sequences depths above the units on either side of the fault zones would also imply displacement at both fault zones, although during which timeframe is unknown.

Only a single unit in the trench was dated and returned an age of 220 ± 40 BP: presumably unrelated to the ~1620 C.E. earthquake. The second inferred rupture was attributed to the Crane Creek event, with an age between 1480 and 1645 A.D. suggested by Yetton (2000). Given the heavy use of inferences at this location and the ~200-400 mm depth of aggradation sediments higher than other locations, the evidence located at the Kokatahi 2 trench is favourable to the hypothetical fault scenario (Figure 4.4).

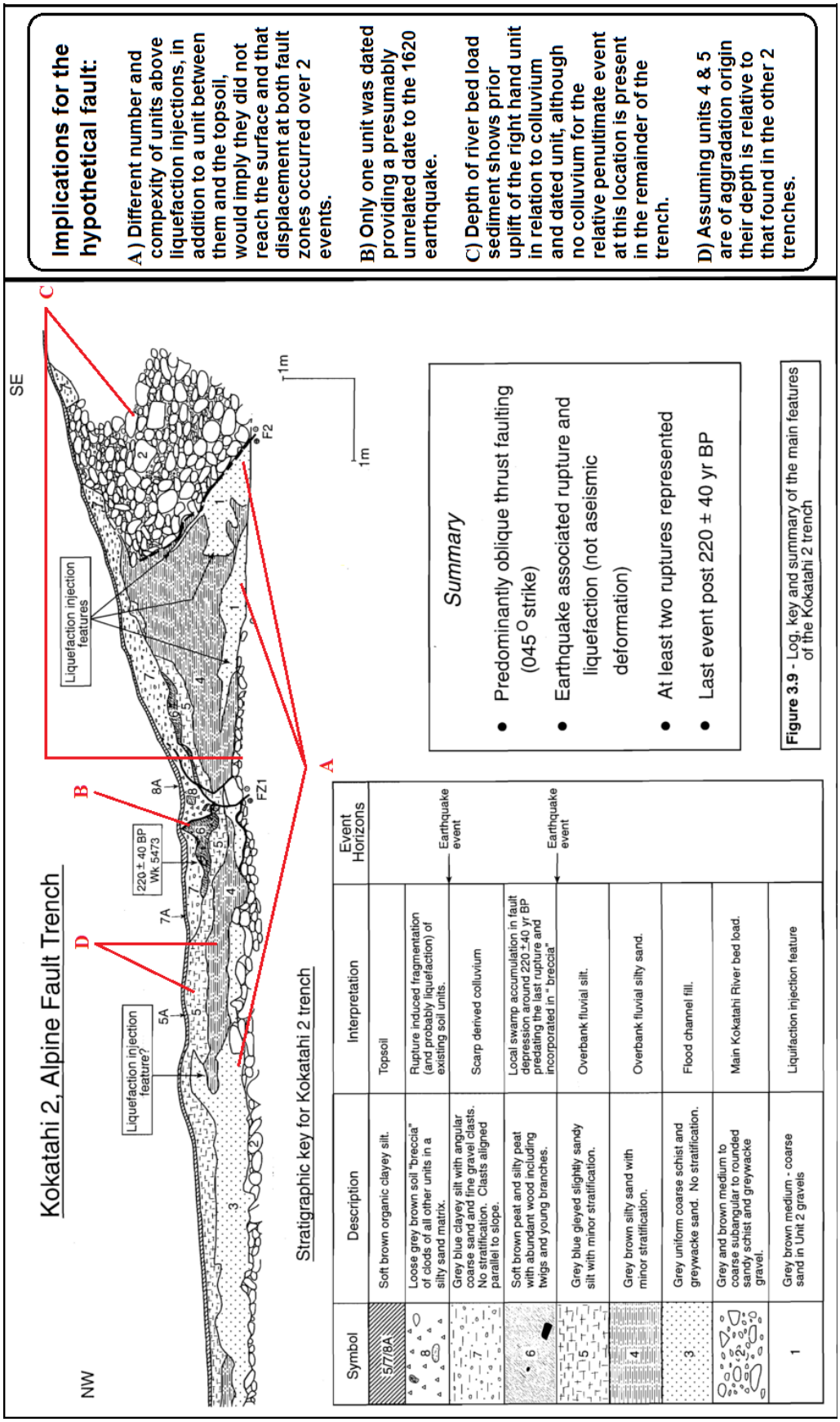

Figure 4.4: Kokatahi 2 trench face log. Annotations in red related to brief descriptions at base of figure. Adapted from Yetton (2000).

4.2.2 Southern Alpine Fault trenching – Haast, Okuru, and Turnbull River sties

As discussed in Chapter 2, Hokuri Creek represents an 8000 year palæoseismic record of the southern onshore section of Alpine Fault up to approximately 1000 years BP (Berryman et al., 2012a). For post-1000 BP data an alternative location near Haast, ~70 km north of Hokuri Creek, was trenched to complete the record for the most recent events (Berryman et al., 2012b). It is this secondary location from which a penultimate Alpine Fault earthquake of 1230 ± 50 A.D. was deduced and is apparently unrelated to a ~1620 CE event, unless as Howarth et al. (2016) stated, the ages obtained by Berryman et al. (2012) during this timeframe were poorly constrained.

In the hypothetical earthquake scenario this location produces minimal effects with MMI IV shaking, landslide susceptibility values of ~0.3 and negligible aggradation (0.005 mm). Unfortunately, the sediment sequences that were used to date the prehistoric earthquake events contain no depth values to use as a comparison with the present work. With the exception of the Alpine Fault's segmentation and its effects on recurrence intervals, and comparison with other research, it is of no further significance to this thesis' results. Berryman et al (2012a) simply state the ~1620 C.E. event was related to a rupture of the northern section of the Alpine Fault and do not consider it further.

4.3 Comparison and discussion of off-fault evidence

While more prevalent than on-fault evidence of Alpine Fault activity, off-fault evidence is inherently affected by one key limitation - any research outcomes cannot conclusively refer to the Alpine Fault as the seismic origin of the phenomenon which was researched.

4.3.1 Regional lichenometric research for palæoseismic investigation

A large body of data using lichenometry for the purpose of palæoseismology has been accumulated by W. B. Bull. Bull (2008) compiled the results into one coherent work which showed evidence of widespread landsliding throughout nine locations around the Southern Alps at 1613 A.D. ± 1.54 years. Of relevance to this thesis are

seven locations, which were used to estimate another widespread landsliding event at 1579 A.D. ± 2.08 years, temporally overlapping the ~1620 C.E. event. The evidence of two large earthquakes and the associated coseismic landsliding at these sites can be selectively compared to the hypothetical fault's modelled landslide susceptibility (Table 4.1).

Table 4.1: Lichenometry sites and estimated earthquake shaking dates from Bull (2008) and related MMI and landslide susceptibility values from this thesis' hypothetical scenario.

Lichenometry site	Age for 1620 A.D. Event	Age for 1580 A.D. Event	Hyp. EQ MMI	Hypothetical. LS susc. Range
Robert Mountain (NNE)	1614	-	4	0.0-0.4
Rainbow-Rosepatch (NNE)	1614	-	4	0.0-0.4
Zig Zag (Central)	1613	1580	7	0.7-1.0
Deaths Corner (Central)	1613	-	8	0.6-1.0
Arthurs Pass (Central)	1615	1580	7	0.6-1.0
Craigieburn (East)	1614	1579	6	0.4-0.7
Cameron (SW)	1613	1579	4	0.0-0.5
Clyde (South)	1612	1581	4	0.0-0.4
Mt. Cook (Central)	1612	1578	7	0.6-0.9
Ohau (Central)	-	1578	5	0.4-0.6

The north-eastern sites of Robert Mountain and Rainbow-Rosepatch both experience low MMI and landslide susceptibility values. Even when considering local site factors such as topographic amplification, their location in the MFZ and distal to the Alpine Fault would infer it is improbable these sites could be heavily affected by the hypothetical fault earthquake. The same can be said for the southernmost sites of Cameron and Clyde, again experiencing similar values to their northern counterparts.

Due to the position of the hypothetical fault, the lichenometry sites closest experience higher MMI shaking and landslide susceptibility values. Although suggesting that these sites align with the hypothetical scenario is plausible, the position relative to the fault detracts from the strength of conclusions regarding these sites. Nevertheless,

these higher estimates do align with selected results from this study, specifically the central and western areas, and can be additionally compared to other research.

4.3.2 Regional progradation and dune formation as evidence for historic earthquake events

With regard to the ~1620 C.E. event, episodic progradation and coastal dune formation has been employed as a proxy for coseismic landsliding at three locations; the Haast, Okuru, and Arawhata Rivers. Respective ages of 1633 A.D., 1646 A.D., and 1626 A.D. were determined (Wells & Goff, 2007). Using dune formation processes and timings, along with tree cohort colonization episodes, these dates were concluded to represent the ~1620 C.E. event.

Relating to the hypothetical fault scenario, all three rivers responsible for the dune formation produced LSFs < 1, although these river catchments have historically generated landslides of seismic origin (Korup, 2006). The Haast River covers three MMI zones ranging from VI-IV as distance from the hypothetical fault increases. The Okuru and Arawhata Rivers are fed by catchments only affected by MMI IV and are therefore much less susceptible to intense coseismic effects. The landslide susceptibility values within the catchments are consequently lower than other areas, with the vast majority of the catchment areas experiencing < 0.55. However, the upper areas of the Arawhata experiences a constant ~0.4-0.5 and the upper Haast catchment contains a small region with values of ~0.7 as noted last chapter (Figure 3.3B).

The median value for the average denudation depth in the Haast catchment is approximately 0.6 mm although the total landslide volume is a considerable 2.2 million m^3. The Okuru and Arawhata experienced 0.4 mm and 180 m^3, and 0.0014 mm and 12 m^3 respectively which are negligible. The denudation levels required for coastal progradation and dune formation are unknown and quantifying them would require extensive research. Thus comparison with the dunes without accurate measurement data is difficult. Other factors include underdeveloped knowledge of sediment transport systems and the non-uniform dune formation attributed to the ~1620 C.E. event. Using what is described by Wells and Goff (2007) as weak evidence of this event at the three sites, the southernmost Arawhata dunes were stated

as discontinuous (i.e. less evident even than the two more northern dunes described as weak). Although only using three data points cannot confidently define a definite trend, the fact that dune continuity weakens to the south aligns well with the hypothetical fault scenario, as the hypothetical fault earthquake would not cause noticeable dune formation.

4.3.3 Lacustrine palæoseismology proximal to the Alpine Fault

The research of Howarth et al. (2012, 2014, & 2016) provides a large data set of relevant factors for comparison with this thesis' results. With a focus on determining the geographic end point of past Alpine Fault ruptures, the research provides insights into the shaking distribution of previous Alpine Fault earthquakes through the measurement and aging of megaturbidite sequences in three lake beds. In an attempt to determine whether an alternate seismogenic source could have been responsible for the coseismic effects at the three study locations, Howarth et al. (2016) additionally investigated the seismic potential of other active and potentially active faults within the Southern Alps, concluding that no known faults within the region were capable of the shaking intensity required for the observed effects.

Under the hypothetical earthquake scenario, the study locations experienced various shaking intensities and landslide susceptibility value ranges. However, by using the regional estimates of this thesis on a local scale, as in the case of previous comparisons, the conclusions should be viewed with some caution.

The northernmost of Howarth et al.'s (2012, 2014, 2016) research locations, Lake Mapourika, experiences the scenario maximum of MMI VIII, whereas Lakes Paringa and Ellery experience MMI V and MMI IV respectively. When the hypothetical fault earthquake is compared to the temporally correlative event recorded in the three lakes in A.D. 1594-1549, these values do not align. Whereas the maximum value of MMI VIII is comparable, the minimum value, estimated as MMI VI, is higher. It may be significant that the mass wasting threshold at Lake Ellery could have been previously underestimated by Howarth et al. (2014). As discussed earlier, topographic amplification and other seismically relevant factors could also have affected these numbers were they included in this context, consequently the resultant MMI values could vary either way due to local conditions.

When comparison is made between the three lakes and their landslide susceptibility values, there is a considerable difference in values that is evidently based on their proximity to the hypothetical fault. Unfortunately, Lake Ellery is the only lake entirely contained within one of the catchments analysed in this thesis. Located in the Arawhata catchment and producing an LSF < 1, the hills surrounding Lake Ellery experience higher susceptibility values than the surrounding area achieving values ≤ 0.5 (Figure 4.5C). These values are still relatively low when compared to the entire modelled region but still display a relatively higher chance of landsliding with respect to the immediate area. Slope stability issues, coupled with other factors of influence, could lead to mass movement but as the susceptibility map shows where landslides are likely to occur, not where they will occur, definite conclusions cannot be drawn. Evidently mass movement did occur in this area during the ~1620 C.E. event depositing sediment layers in Lake Ellery. In this case then the hypothetical earthquake scenario does not align with present evidence.

Lake Paringa which lies approximately 70 km north of Lake Ellery experiences slightly higher susceptibility values (Figure 4.5B). The hill slopes surrounding the lake achieve values ranging from 0.5-0.6 which, when combined with MMI V shaking and other the anticipated uncertainties, make the hypothetical fault a plausible source for the results obtained by Howarth et al. (2012, 2014) at this location.

Approximately 80 km north of Lake Paringa and located on the border of the Waiho-Callery catchment from which values are inferred, Lake Mapourika is most heavily affected by the hypothetical earthquake. The Waiho-Callery catchment's LSF of 18.35, while heavily influenced by the topography of the Southern Alps, retains some relevance for comparison with Lake Mapourika. The hill slopes surrounding the lake attain maximum landslide susceptibility values with the majority of values above 0.7 with a minimum of 0.5 (Figure 4.5A). Lake Mapourika therefore shows a strong correlation in terms of shaking intensity and mass wasting potential between the hypothetical fault and Howarth et al. (2016).

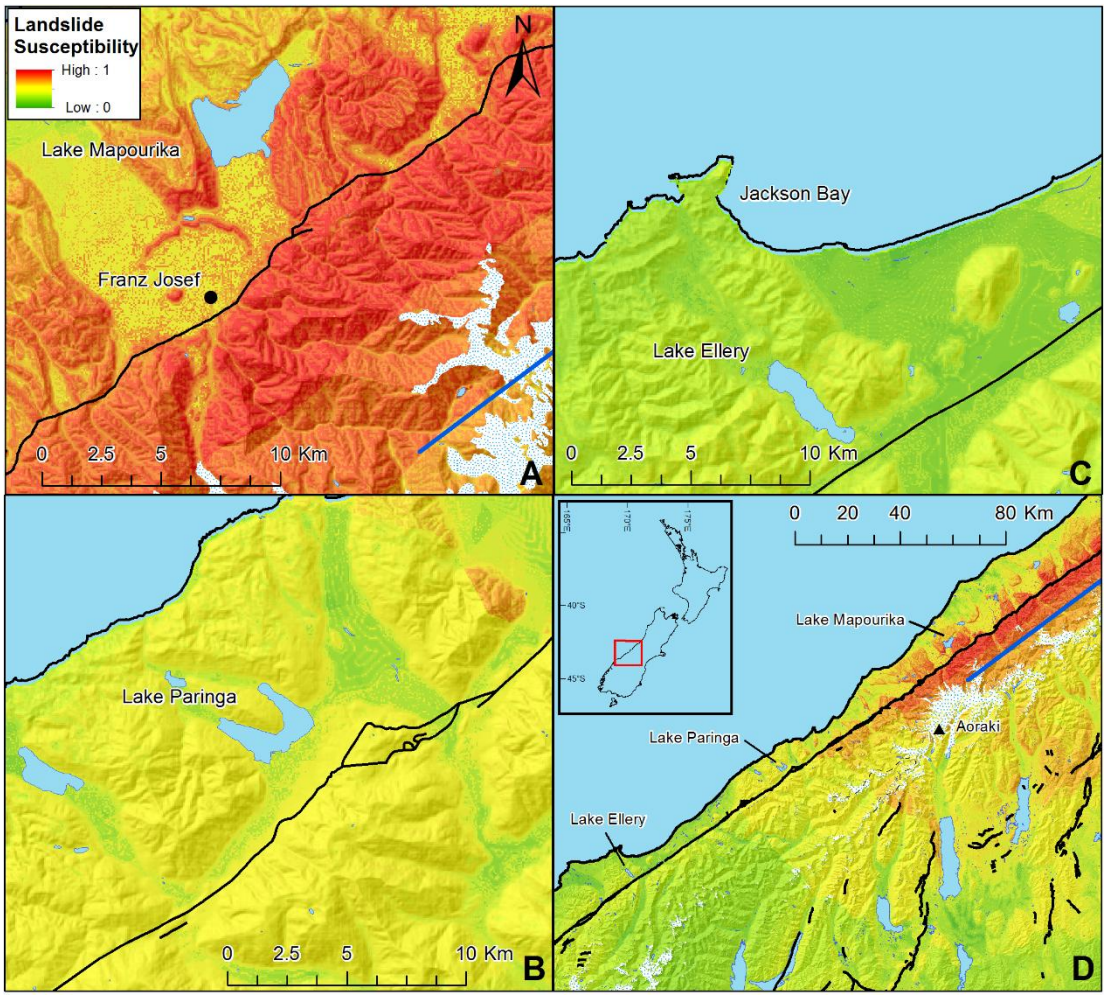

Figure 4.5A: Landslide susceptibility values of Lake Mapourika area. Figure 4.5B: Landslide susceptibility values of Lake Paringa area. Figure 4.5C: Landslide susceptibility values of Lake Ellery area. Figure 4.5D: Relative position and landslide susceptibility values of lacustrine palæoseismology locations of Howarth et al. (2012, 2014, 2016). Hypothetical fault shown in blue.

While possible, further in-depth comparison between the two datasets may not yield accurate conclusions. Average denudation depths could theoretically be compared with the terrestrial mass wasting derived megaturbidite sequence depths. Although every lake is not specifically enclosed by a catchment, nearby catchment denudation values could be used and a pseudo-quantitative assessment (i.e. using comparable units but not directly comparable values) could produce somewhat valid results. Sediment compression could be included and deposition area/volume would have to be proportioned based on lake size. If undertaken at all three lakes, values obtained would likely reflect the distance from the seismic origin increasing as sequence

depths decrease. Howarth et al. (2012, 2014, 2016) do not provide event specific depths of the comparative unit types and thus this analysis is not possible using the available information alone.

Howarth et al. (2016) concluded their A.D. ~1570 event could no longer be attributed to the Alpine Fault due to an absence of independent supportive evidence. The lakes from the three studies demonstrated a regionally synchronous event at this time which unmistakably caused widespread landsliding. No known faults within the central Southern Alps can theoretically produce earthquakes over M_W 7.2. The maximum alternate scenarios derived from these faults cannot produce intense enough shaking to affect all three lakes in unison, therefore a different hypothetical scenario, if not the Alpine Fault, should be considered.

4.3.4 Regional aggradation as an indicator of coseismic landsliding

Multiple aggradation studies exist that allow comparison with the results of this thesis. However, even when corrected for sediment yield proportions, immediate aggradation values will not completely match those found at these research locations. Comparison of recent aggradation with centuries old aggradation values exacerbates this issue. The hypothetical scenario somewhat mitigates this limitation as it represents the effects on a regional scale rather than a direct comparison of two known values.

4.3.4.1 Central West Coast alluvial fan aggradation

Temporally and physically, the aggradation episode investigated by Davies and Korup (2007) aligns with the hypothetical scenario. A trench at the Waiho fan showed a deposit of massive medium sand at ~4-5 m depth, from which ~1620 C.E. correlative dates were obtained. Findings at the Fox River also yielded fluvial gravels and massive sand deposits at ~5 m depth. However, no datable material was retrieved from this location.

When relating the aggradation and soil surfaces at different locations on the same fan, Davies and Korup (2007) further discovered soils on inactive fan heads were consistently the same age of those on the active fans. This conclusion also aligned

with an independent study, where Berryman et al. (2001) discovered soils dating from 1620 A.D. on the Whataroa fan were also consistent at varying locations.

These four locations were all affected by the hypothetical earthquake scenario. Being located in the central West Coast, where denudation and aggradation values were at their peaks, the locations were all affected by at least MM VII, with a maximum of MM VIII covering a large proportion of the catchment areas. The landslide factors ranged from ~9 to ~28 which represents a considerable 9 to 28 times aseismic background rates resulting from the hypothetical scenario. Median aggradation depths for the catchments range from 70-95 mm. Although it would appear a value of 4 metres occurred to accurately reflect the sequence depth of Davies and Korup (2007). Factors including aggradation only affecting the current active fan and not covering the entire fan, in addition to declining aggradation depths as distance from the rangefront increase, plausibly explain the differences. In this case the hypothetical fault earthquake scenario is certainly plausible, especially when considering Robinson et al.'s (2016) full Alpine Fault rupture aggradation depths discussed previously.

4.3.4.2 A northern West Coast aggradation terrace

Approximately 600 metres downstream from the trench site at Crane Creek, there exists a low aggradation terrace approximately 4 metres above the modern river. The coarse gravels forming this terrace are loose, sandy and poorly imbricated (Yetton, 2000). Although the information provided about this terrace is minimal, certain factors can be assessed to infer properties with regard to the seismic event which resulted in its formation.

Beginning with the height of the terrace, when interpreting the single available image, the proportion of aggradation sediments that comprise the terrace is unclear. Exacerbating this issue are ~400 years of geomorphic, erosional and coseismic alteration processes that have affected the channel. The formation would have increased river incision by constraining the flow path and deepening the channel at this location. Compared to the average aggradation depths of the related catchment under the hypothetical scenario, an insignificant median of 8 mm and an upper adjacent 57 mm compared to 4000 mm, displays the inability to affect this location to

the extent of the actual earthquake. Of additional consideration is the fact that aggradation has historically been known to reach ~20 metres at the Southern Alps rangefront (Davies and Korup, 2007). Thus a 4 metre high aggradation terrace 600 metres from the rangefront is well within reason.

Evidently a large amount of coseismic aggradation occurred at this location during the ~1620 C.E. timeframe. The location itself, on the southern edge of the Grey catchment, is not wholly representative of the catchment entirety and also affects what can be deduced. Consequently, without a more precise quantification of expected rangefront aggradation values, a more localized catchment average (i.e. a smaller scale) and an in-depth analysis of the terrace, further argument would simply be conjecture.

4.3.5 Regional dendrochronology as evidence for large earthquakes

As previously discussed, regional dendrochronological research can be used as a successful indicator for the widespread effects of palæoseismic activity. Relative to the hypothetical earthquake scenario, various factors of importance that influence this datatype require reiteration. Firstly, establishment rates of tree cohorts and re-establishment rates for specific growing environments have a significant but ultimately unknown impact on event dating. Secondly, the cohort disturbances measured only show an area affected by between MMI VIII and MMI X. Neither the seismic origin nor distinction between shaking intensities can be determined with certainty.

Wells et al. (1999) stated that the ~1620 C.E. event was responsible for forest damage (i.e. MMI ≥ VIII) along-strike of Alpine Fault's central and central-northern sections for at least 200 km. This distance is considerably larger than the spatial extent of the hypothetical fault earthquake, which generates only ~120 km of along-strike MMI VIII shaking. Only with the inclusion of lesser MMI zones, as low as MMI VI, is a 200 km disturbance length achieved. It is apparent the hypothetical fault results are much more constrained than the inferences originating from the physical evidence that represents the actual event.

Given the earthquake-fault length scaling relationships used in the determination of the hypothetical fault's parameters, a larger earthquake could be hypothesized to be

more comparable with Alpine Fault estimates of 7.8 M_W to 8.1 M_W. Introducing this change would consequently require an increase of the fault length, presenting further issues regarding fault positioning and other parameters incorporated into the Shakemap model.

Finally, seismic wave propagation from the hypothetical fault's northern tip demonstrated by the limiting effects of the Hura Fault could be an additional factor when considering the distribution of ≥ MMI VIII shaking and thus forest disturbance. As the Alpine Fault is the only fault in this location that is known to cross, is adjacent to, or intersects the Hura fault, determining an alternate single seismic source that affects a 200 km region with ≥ MMI VIII is difficult with current mapped fault distribution.

4.4 Review and discussion of relevant comparisons

4.4.1 Interrelationships of palæoseismic indicators and the issues devised from them

When the various data sources are compiled, multiple factors and discrepancies become apparent. These are a likely consequence of inaccuracies or inadequacies in measurement types; or the inferences drawn from them.

4.4.2 Foremost issue

Of these discrepancies, the foremost issue is the multiple ages estimated for the same event. Howarth et al. (2012, 2014, 2016) maintain an earlier date throughout multiple publications, with the most recent of these publications estimating an event between A.D. 1549-1594, which is decades earlier than other research except for a secondary lichen peak defined by Bull (2008) around this time.

Of the eight forms of palæoseismic indicators utilized in this discussion, five use wood fragment derived dating methods. Although associated standard errors were provided, their alignment with each other but not with ages derived from different sources (i.e. lake sediments and lichenometry) is curious. Bull's (2008) lichenometric research demonstrates notable lichen-size peaks aligning with both dates (1578 A.D. and 1613 A.D.). Howarth et al.'s (2016) conclusion of a single event between A.D.

1549-1594 in addition to accurate proclaimed multi-event precision, complicates matters further.

Possible explanations for the temporal disparity of events could include environmental responses to multiple large earthquakes in a small timeframe. Lake slope-stability and the ability of rivers already inundated with sediments (noting the decades-long disturbance period of Wells and Goff, 2007) could mean that although the methods used by Howarth et al. (2012, 2014, 2016) can obtain the temporal resolution required to date events over a small timeframe, the factors being tested may not themselves be capable of displaying such accuracy. Howarth et al. (2016) additionally conducted an analysis between their results and those of Berryman et al. (2012a, 2012b) with regard to the two different dating methods applied and achieved an acceptable agreement of 76.4%. The comparison showed that whereas the Hokuri Creek probability distribution functions overlap for the last two events, those derived from lake sediments did not. Howarth et al. (2016) explain that this could be a result of poorly constrained ^{14}C dates earlier in the record affecting distribution, but still conclude that the event occurred between A.D. 1549 and A.D. 1594 and was of non-Alpine Fault origin.

When the dates obtained through dendrochronology are compared with those of other palæoseismic indicators, the potential for error exists. One potential error could be the palæoclimate ~400 years BP accelerating or hindering growth-conducive environmental re-establishment times or tree cohort establishment times. If this were the case, then the establishment periods and consequently the inferred earthquake dates of Yetton (2000) and Wells and Goff (2007) could perhaps be inaccurate. This would simplify correlating the ages of fault displacement (i.e. Yetton, 2000), aggradation terraces and alluvial fan sequences (i.e. Berryman et al., 2001, as cited in Davies & Korup (2007); Davies & Korup, 2007; and Yetton, 2000), and dendrochronology (i.e. Wells et al., 1999; Wells & Goff, 2007; and Yetton, 2000) with those obtained by Bull (2008) and Howarth et al. (2016). However, the implications of the factors described above are well beyond the scope of this research and only aim to provide conjectural reasons behind the differences observed between research data.

4.4.3 Further issues

When attempting to draw conclusions inclusive of relevant available research, two further heavily related key issues affect the outcomes. These are the regional distribution of the palæoseismic indicators and the hazard intensities derived from them.

When considering regional distribution, the lineation of features becomes a key component worth consideration. Various research demonstrates the effects of a large earthquake at numerous locations but follows a linear along-strike pattern parallel to the Alpine Fault. With regard to the hypothetical fault, the lineation has a more arbitrary origin, as the scenario-derived geometry of the hypothetical fault forces this. However, with regard to other studies, lineation is not so moot as most studies follow the general SW-NE geometry of the Alpine Fault. Although this is useful in determining the extent of coseismic shaking along a parallel axis, the data are not as applicable when attempting to distinguish the lateral extents of shaking.

As most research regarding the ~1620 C.E. event has been carried out under the assumption it had an Alpine Fault origin, in addition to the western rangefront exacerbating many geomorphic effects, the conclusions drawn appear biased towards the Alpine Fault as the seismogenic source. Future investigation, using the same methods, could be useful at distal locations perpendicular to the Alpine Fault and would enable estimation of the lateral constraints of hazard distribution. Furthermore, doing so would allow better constraint of potential locations for additional hypothetical scenarios. Knowing now, to some extent, the effects of shaking distribution in the region independent of an Alpine Fault event, a more informed position could be chosen which could better reflect the physical evidence of previous research.

Howarth et al. (2016) determined that MMI IX shaking was a requirement at all three study locations to produce the observed effects, thus concluding regionally synchronicity. However, Berryman et al.'s (2012b) study at Haast showed no evidence for shaking at this time. This is curious because the Haast site is ~35 km north of Lake Ellery, so MMI IX shaking would be expected at both locations. Furthermore, as seen in the Shakemap presented in this thesis, north-south effects extending from onshore fault tips decline rapidly. So how does an earthquake, for

which most evidence points towards a northern origin, produce MMI IX shaking as far south as Lake Ellery without being present in the Haast palæoseismic record of Berryman et al. (2012b)? A possible solution could entail the shaking intensities required for the effects at the three lake sites having been overestimated or indeed a multi-earthquake scenario. The inability of the environment to repeatedly respond to multiple seismic events over a small timeframe could also be an explanation. Relating to the latter, so too could be the case where a trench may not show any indication of a specific earthquake (Akyüza et al. 2014).

Additional comparison can be made with the lichenometric results of Bull (2008), where the north-east and central-southern lichen peaks correlate with the time frames of both Howarth et al.'s (2016) mid-late 16th century event and other researchers' early 17th century event. However, as a reliable indicator lichenometry suffers the same limitations as landslide susceptibility. A model that shows potential rather than estimated locations is not the best approach to use when trying to determine distribution, as landslides can and do occur in low susceptibility regions. Nevertheless, Bull's (2008) southern date peaks at both the Ohau (1578 A.D.) and Clyde (1581 A.D., 1612 A.D.) locations align with Howarth et al. (2016). The Clyde locale aligns with both the effects of a northern rupture and the southern effects of a potential secondary rupture elsewhere demonstrated during this timeframe. Even between these two lichenometry locations disparity is present; Ohau ~110 km north of Clyde experiences the earlier event but does not experience the postulated northern rupture, whereas Clyde displays evidence of both events. Finally, the north-eastern locations of Bull (2008) align with the postulated northern rupture but show no evidence of the earlier (i.e. 1578 A.D.) event.

4.5 Discussion Summary

Even if it were in fact a singular seismic event or multiple, the location of the ~1620 C.E. event remains unclear. Multiple scenarios exist which could potentially explain the distribution of palæoseismic indicators throughout the South Island between ~1550 A.D. and ~1650 A.D. In no particular order these scenarios are that:

- An earthquake occurred on the central-northern portion of the Alpine Fault, propagating high intensity shaking as far south as Lake Ellery.

- A central-northern Alpine Fault earthquake occurred in combination with a central or southern unknown fault capable of affecting Lake Ellery and Clyde.
- A stronger earthquake occurred on the hypothetical fault modelled in this thesis, with slight repositioning and/or geometry.
- Multiple hypothetical (i.e. non-Alpine) fault earthquakes occurred within a small timeframe, in both central-northern and central-southern locations.

It is difficult to discount a multi-earthquake scenario when considering the spatial distribution of palæoseismic indicators, what is currently understood of the Alpine Fault's segmentation and the recent fault plane transfer sequence of the Kaikoura Earthquake. Ultimately, creating multiple modelled scenarios to achieve a best fit earthquake appears the most accurate method matching the evidence related to the ~ 1620 C.E. event. Combining this with calculated localized aggradation depths at known locations and assuming realism in the modelling stage, a fault and earthquake could be produced to create these effects. Therefore, analysing multiple sets of quantitative data and utilizing comparable units of measurement to generate conclusions seems an acceptable method to compare a scenario to actual, physically present evidence. Although in doing so, the "what could happen" against "what did happen" argument would inevitably gain traction. Where there is physical evidence to suggest that X occurred at Y location, it is unequivocally a factor that needs consideration. Although one could argue the effects of ~400 years of modification to manipulate the argument either way.

5 IMPLICATIONS FOR RISK MANAGEMENT AND DISASTER RESPONSE

5.1 Managing and planning for a hypothetical fault earthquake

This study presents an alternative seismic origin for the ~1620 C.E. West Coast earthquake event, and tests the hypotheses that the Alpine Fault did not rupture at this time and that the geomorphic evidence distributed about the South Island was a result of this alternative event. The evidence presented in previous chapters suggests that this hypothesis has some merit. Assuming this to be the case, an additional active, as-yet unknown seismic source would exist in the Southern Alps, west of the Main Divide, in addition to the potentially active faults identified by Cox et al. (2012). This scenario presents a hitherto unknown hazard source for the West Coast and surrounding regions for which risk management and disaster response should be considered. Given the magnitude of this scenario earthquake (i.e. > 7.6 M_W) and the unknown recurrence interval, it would be prudent to further consider a hazard source such as this and plan for the eventualities it presents.

5.2 Current state of hazard risk management and disaster response planning with regard to large seismic events in the South Island

Currently planning for large-scale earthquake scenarios in the South Island is limited. A recent contribution by Robinson (2014) explored the region's capacity to cope with a large Alpine Fault earthquake and provided effective, up-to-date information for emergency response planners. Further contributions to this area include the works of McCahon et al. (2006a, 2006b & 2006c), which again assessed the impacts of an Alpine Fault rupture scenario. These predominantly used rupture parameters from Yetton and Nobes (1998) and Yetton (1998) and were written as technical reports for governmental bodies on the West Coast. The reports clarified the anticipated severity of impacts and response/recovery options available to their respective regions and the lifelines therein. As the reports are qualitative in nature, simply estimating impacts as best as possible, they provide a reasonable starting point for preparation and can be used to identify areas where focus should be placed for effective planning.

Exercise Te Ripahapa described by Robinson et al. (2014) was a comprehensive CDEM disaster response exercise. It used a scenario earthquake on the Alpine Fault and the resultant impacts and civil defence response. Held over the course of twelve hours, the exercise was run in 'real-time' commencing 6 hours after the earthquake. Upon completion of the exercise, a conceptual Scenario Development framework was derived for future exercises. Where the Alpine Fault was employed in this exercise, other large earthquake sources could be substituted. For this purpose, Exercise Te Ripahapa is relevant when considering the seismic and coseismic effects of the hypothetical fault presented by this thesis. Although both the input parameters and output hazard properties used in the quantification of the hypothetical fault require further investigation in order to be plausible.

The relative scarcity of regional-scale disaster planning is further exacerbated by the limited financial resources available to the West Coast councils. Since the formation of the West Coast Civil Defence and Emergency Management Group in 2002, staffing of professional coordinators has been significantly limited (Raine, C., West Coast CDEM Manager and Group Controller, personal communication, 2015). With limited staff to plan for hazard scenarios and respond to disasters, in combination

with limited resources, an additional hazard source, such as the hypothetical fault, exacerbates an already unfavourable situation.

5.3 Potential national and regional societal impacts of the hypothetical fault earthquake

Locations distant from the hypothetical fault also require consideration when planning for hazards and disaster response. The spatial distribution of the geomorphic consequences that resulted from the ~1620 C.E. earthquake show that impacts occurred throughout much of the South Island. Eastern Southern Alps locations such as the Clyde valley and Ohau were affected by landsliding during this time (Bull, 2008). The Upper Waitaki hydro-electric scheme which generates and distributes large portions of New Zealand's power lies close to the Ohau site, suggesting that a recurrence of this earthquake could affect this critical infrastructure. Personnel at such sites have proactive response planning regarding seismic and coseismic hazard management, although additional hazard sources should be included in those plans (Wheeler, J., Meridian Energy Site Engineer, personal communication, 2015).

Under the hypothetical fault scenario, which has a conservatively-estimated size of M_W 7.6, when using the rupture speeds of other global earthquake examples listed by Robinson (2014), it can be estimated a full rupture of the hypothetical fault's entire 100 km length could last from 20-40 seconds. This would create a high intensity ($\geq$ 8 MMI) shaking zone along its length affecting a width of approximately 35 km. Multiple population centres will be affected by MMI $\geq$ 4 shaking intensities (Table 5.1). The implications of this will not be covered in this thesis. Suffice to say, the impacts at certain locations would be similar to those of an Alpine Fault earthquake. The gravity of this situation should therefore be considered in future hazard and disaster management and planning.

Table 5.1: Population rounded to nearest significant figure for urban areas of consideration. ([1]) Statistics New Zealand 2013 Census Data.

Urban Area	Population estimate[1]	MMI Expected
Franz Josef	330	8
Whataroa	288	8
Harihari	330	8
Fox Glacier	306	7
Arthurs Pass	30	7
Hokitika	3,000	7
Greymouth	13,000	6-7
Haast	300	5
Reefton	1,000	5
Christchurch	366,000	4-5
Westport	4,000	4-5
Queenstown	28,000	4
Dunedin	120,000	4

5.4 Potential local societal impacts of the hypothetical fault earthquake

Consequential hazards, such as those in Figure 2.7, are also in need of consideration when determining the potential effects of the hypothetical fault. The impacts of multiple likely hazards on local lifelines, such as the transport network, communications and electricity, have the potential to exacerbate the initial seismic impacts of remote or isolated locations. Anticipated hazards such as flooding, landslides and aggradation, which are estimated as severe on the West Coast, all require additional planning. Unfortunately, many locations with the above properties fall under the jurisdiction of the West Coast CDEM Group that, as well as the

aforementioned lack of funding, has alternate priorities to seismic hazard risk management. The focus is instead on coastal inundation and flood risk in coastal population centres (Raine, C., West Coast CDEM Manager and Group Controller, personal communication, 2015).

The impacts of such hazards have been historically realised multiple times as the result of seismic and aseismic events. The most recent events including flooding at Franz Josef in March 2016 and the Kaikoura Earthquake of November 2016 both demonstrate the impacts of natural hazards. At Franz Josef the stop banks in place failed to mitigate the impacts, resulting in a portion of the town being inundated by flood waters and 186 people being evacuated (Truebridge et al., 2016). Other issues such as water reticulation, sewerage and transportation also became consequent factors to manage. Flooding like this - and potentially worse events due to landslide dam failure - can be expected from any large earthquake within the region, irrespective of its source. The fatal Kaikoura Earthquake demonstrated the significant impacts of both seismic and coseismic hazards, with hundreds of people stranded in Kaikoura for days due to intense landsliding and surface fault rupture inundating or destroying transport networks. Others inland also suffered consequences, with limited supplies and aid combined with access issues. The further threat of landslide dam floods and aftershocks further complicated the situation.

Although in the case of Franz Josef, the impacts were exacerbated by previous mitigation works (i.e. the continual raising of the stop banks along the Waiho River), this example highlights the general lack of preparedness for hazard events at local scale. Furthermore, it demonstrates the region's inability to cope with hazards which, when compared to overall effects of a major earthquake, are considered minor. The local population believes this is a matter of governmental responsibility (Franz Inc. personal communication, 2015). This is not necessarily the case, as the regional government relies on the assumption that land and business owners in affected locations should have been aware of the potential hazards before purchase or operation (Raine, C., West Coast CDEM Manager and Group Controller, personal communication, 2015). The infrequency of response plan updates (every 5 years) with relevant scientific information makes this an even more dire situation.

5.5 Summary

Even with the limitations noted above, in order to build resilience and reduce disaster impacts, it would be prudent to proactively plan for multiple seismic scenarios and their consequences. Unfortunately, this is not the case at present due to a laissez-faire or business-as-usual approach to these hazards (with the exception of larger state owned enterprises, including Meridian Energy who are tasked with national level responsibilities).

The hypothetical earthquake source studied herein adds quantitative (albeit approximate) information to supplement Cox et al.'s (2012) demonstration that active faults other than the Alpine fault exist in the Southern Alps, and should therefore be an incentive for intensified planning to reduce earthquake impacts and speed response and recovery. It appears likely that an absence of funding and the focus on more obvious and more frequent but less catastrophic events will constrain this planning.

6 CONCLUSIONS AND RECOMMENDATIONS

6.1 Conclusions

On the basis of an assumed rupture of a hypothetical 100-km long fault midway between the northern part of the central Alpine Fault and the main divide of the Southern Alps generating a M_W 7.6 earthquake, the following conclusions arise:

1. Severe landsliding effects are anticipated from the hypothetical earthquake in 10 order 6 plus catchments: the Hokitika, Waiho-Callery, Whataroa, Taramakau, Rakaia, Waimakariri, Karangarua, Rangitata, Grey, and Ashburton. The smaller order 5 catchments of Waitaha, Wanganui, and Fox-Cook are also expected to be significantly affected, with major aggradation on their alluvial fans having implications for the various societal activities that currently take place at those locations.
2. Compared with the Alpine Fault rupture modelled by Robinson et al. (2016), the hypothetical scenario produced far less geographically extensive impacts. The median number of landslides estimated to occur was ~12,000 – around a quarter of the ~49,000 calculated by Robinson et al. (2016) for the Alpine Fault. However, whereas the average total volume of landsliding was estimated as 0.3 km³ for an Alpine Fault event, the hypothetical scenario produced 0.24 km³. This infers a greater number of larger individual

landslides and that the susceptibility at the focal area of seismogenesis was higher from the hypothetical event.

3. East of the Main divide, using aggradation and denudation as metrics, the effects of the hypothetical fault rupture are, as expected, less intense. The east-draining catchments have considerably larger areas, and their lower denudation and aggradation depths make determining areas of high relative susceptibility difficult. Whereas on the West Coast, topography dictates where intense effects would be expected, the more varied topography of these eastern catchments does not allow such a generalisation.
4. When considered on both temporal and spatial scales, the available palæoseismic evidence supporting an Alpine Fault event at ~1620 C.E. is inconclusive, and the inferences drawn from those data are open to reinterpretation. Therefore, the hypothetical fault rupture scenario, or a multi-fault rupture scenario around ~1620 C.E. are plausible alternative explanations for the palæoseismic data.
5. If the hypothetical fault were to be accepted as an alternative single seismic source for the ~1620 C.E. event, it would appear that an earthquake larger than 7.6 M_W would be necessary, implying that the fault responsible would need to be greater than 100 km in length.
6. The triangular-shaped wedge formed by the position of the hypothetical fault relative to the Alpine Fault (Figure 3.19) appears to have a significant effect on seismic wave propagation away from the origin. Thus the effect of the Alpine Fault's geometry should be considered in future modelling of the seismic potential of Alpine Fault-proximal faults.
7. Comparison between this thesis and Robinson et al. (2016) shows that the spatial distribution of landslide susceptibility is significantly influenced by rupture length; at least when Shakemap is employed. This is shown in the southern catchments, where Robinson et al. (2016) estimated high landslide volumes, compared to the low volumes of this thesis. Seismic waves propagate laterally from the Alpine Fault in the former scenario to affect these catchments, but do not propagate as far from the fault tips of this thesis' scenario.

8. The methods of Kritikos et al. (2015) and Robinson et al. (2016) are independent of lithology and many other limiting factors of previous regional landslide susceptibility analyses.

6.2 Recommendations for future work

- Engagement with public officials and operators within the region, as well as subsequent public education regarding the potential of hitherto unknown seismic sources within the Southern Alps should be a high priority. Understanding and consideration of the potential impacts and their spatial and temporal distributions would aid in increasing the overall resilience to these effects and reduce the severity of the disaster. Furthermore, such increased political understanding could improve the funding currently allocated to seismic hazards on the West Coast and nationally.
- The process of converting Shakemap outputs into useable data for subsequent landslide susceptibility processing could be streamlined and potentially automated for increased efficiency. This would enable a time-consuming and tedious task to be reduced for future iterations of landslide susceptibility mapping. This would be especially important if the methods were to be used for additional regional or localised analyses.
- The process whereby *k* and *RAND* are determined using uniform distributions could be tested using different statistical distributions to analyse the variability in produced intermediate values and thus overall landslide volumes. This would also affect the distribution and probability of very large landslides occurring. In their current state, the methods of Monte Carlo analysis in combination with empirical limits is mostly meaningful for total volumes, as opposed to specific individual volumes (Robinson, 2014).
- Multiple sites used in the analysis of the palæoseismic indicators contain sediments relatable to the denudation produced under the hypothetical earthquake event, but are unsuited to direct comparison due to the large variability in sediment parameters. Research into these factors and their related processes could enable more accurate estimation of the overall impacts by relating the generated sediments. In doing so, the ability to directly

compare sediment values at a location with those derived from denudation/aggradation would be possible. This could be conducted at lake sites of Howarth et al. (2016) and coastal dune sites of Wells and Goff (2007) and would provide estimates for the required sediment input volumes to create the observed physical evidence.

    - For example, the volumes produced within the Haast catchment in this thesis and in Robinson et al. (2016) provide estimates for the sediment volumes available for dune formation. Combining understanding of the longshore drift processes and suspended sediment yields with the estimated volumes of the coastal dunes and floodplain aggradation would enable testing of quantitative estimates to determine just how much sediment was produced over multiple prehistoric seismic events.

- Substituting MMI for PGV and undertaking a similar sensitivity analysis would allow the comparison of the Kritikos et al. (2015)/Robinson et al. (2016) methods with a scalable value. Given that the fuzzy operator for MMI is large, and consequently has a large impact on the produced results, a comparison would provide insight into the differences between a scalable continuous variable as opposed to the discrete MMI values currently used. This would be considerably more useful for smaller-scale or local site analyses and would translate well into subsequent engineering geology investigations regarding hazard potential.
- Additionally, for the purpose of smaller-scale analyses, a reduction in the cell size of the base DEM could also be investigated. However, this would require the sensitivity analysis undertaken by Kritikos et al. (2015) and Robinson et al. (2016) to be repeated also using smaller cell sizes and would rely on the availability of those data. Other factors, such as the frequency ratio of landslides on DEM averaged slopes at a smaller scale, would also require consideration.
- Using the information provided in Davies and Korup (2007), distributing the estimated sediment volumes over a three dimensional catchment could provide a model for Cartesian allocation of aggradation sediments. The study undertaken by Croissant et al. (in review) is one such example. Although an assumed landslide origin or origins in the upper catchment would be required,

the process could be used to simulate the minimum, physically present values of other research and model potential future events. This would enable a more realistic model of aggradation and could be applied in multiple catchments to better determine the hazard potential of this type and the magnitude of the triggering mechanism.

- As previously stated by Robinson (2014), utilising polygons for landslide area would be an improved method to establish total and individual modelled landslide volumes. This would provide likely landslide volumes based on previous empirical data and could be implemented in combination with the recommendation of alternate statistical distributions to provide a more "natural" fit of modelled landslides. It would also benefit local and smaller-scale analyses and highlight areas where special attention should be paid for the higher anticipated risks at those locations.
- As with most research of this type, additional data sources generally provide beneficial information. In this context, the methods of Howarth et al. (2012) could usefully be applied at northern and eastern lakes with respect to the Alpine Fault, such as Lake Ahaura and Lake Heron. Although the varied lithology of the sediments could create difficulties for direct comparison, conducting such research would provide an effective gauge for the distribution of intense shaking throughout the Southern Alps.
    - Further palæo-aggradation research locations, specifically for suitable dating material and sequence depths would also aid this goal.
- Refining the hypothetical scenario to better suit the available physical evidence would provide further insight into the effects of the ~1620 C.E. event at locations where there is no known evidence or research has not been previously conducted. The newly determined sensitivity of the produced Shakemap to various inputs would also allow further manipulation of the scenario to the point where an accurate model could be produced for shaking and consequently the impacts of the time.
- Further research into the delineation of the A.D. 1549-1594 range of dates and ~1620 C.E. events should be a priority to determine if this event was a single earthquake or multiple.

7 REFERENCES

Abercrombie, R. E., Webb, T. H., Robinson, R., McGinty, P. J., Mori, J. J., & Beavan, R. J. (2000). The enigma of the Arthur's Pass, New Zealand, earthquake: 1. Reconciling a variety of data for an unusual earthquake sequence. *Journal of Geophysical Research: Solid Earth*, *105*(B7), 16119-16137.

Adams, J. (1980). Paleoseismicity of the Alpine fault seismic gap, New Zealand. *Geology*, *8*(2), 72-76.

Akyüza, H. S., Karabacakb, V., & Zabcıa, C. (2014). Paleoseismic Trenching.

Beavan, J., Tregoning, P., Bevis, M., Kato, T., & Meertens, C. (2002). Motion and rigidity of the Pacific Plate and implications for plate boundary deformation. *Journal of Geophysical Research: Solid Earth*, *107*(B10).

Berryman, K. R., Cochran, U. A., Clark, K. J., Biasi, G. P., Langridge, R. M., & Villamor, P. (2012a). Major earthquakes occur regularly on an isolated plate boundary fault. *Science*, *336*(6089), 1690-1693.

Berryman, K., Cooper, A., Norris, R., Villamor, P., Sutherland, R., Wright, T., Schermer, E., Langridge, R. and Biasi, G. (2012b). Late Holocene rupture history of the Alpine fault in south Westland, New Zealand. *Bulletin of the Seismological Society of America*, *102*(2), 620-638.

Berryman, K., Alloway, B., Almond, P., Barrell, D., Duncan, R., McSaveney, M., Read, S. & Tonkin, P. (2001). Alpine fault rupture and landscape evolution in Westland, New Zealand. *Trans. Jap. Geomorph. U*, *22*(4).

Berryman, K., & Beanland, S. (1991). Variation in fault behaviour in different tectonic provinces of New Zealand. *Journal of structural geology*, *13*(2), 177-189.

Boese, C. M., Jacobs, K. M., Smith, E. G. C., Stern, T. A., & Townend, J. (2014). Background and delayed-triggered swarms in the central Southern Alps, South Island, New Zealand. *Geochemistry, Geophysics, Geosystems*, *15*(4), 945-964.

Boese, C. M., Townend, J., Smith, E., & Stern, T. (2012). Microseismicity and stress in the vicinity of the Alpine Fault, central Southern Alps, New Zealand. *Journal of Geophysical Research: Solid Earth*, *117*(B2).

Brunetti, M. T., Guzzetti, F., & Rossi, M. (2009). Probability distributions of landslide volumes. *Nonlinear Processes in Geophysics*, *16*(2), 179-188.

Buech, F., Davies, T. R., & Pettinga, J. R. (2010). The little red hill seismic experimental study: topographic effects on ground motion at a bedrock-dominated mountain edifice. *Bulletin of the Seismological Society of America*, *100*(5A), 2219-2229.

Bull, W. B. (2008). Tectonic geomorphology of mountains: a new approach to paleoseismology. John Wiley & Sons.

Bull, W. B. (1996). Prehistorical earthquakes on the Alpine fault, New Zealand. Journal of Geophysical Research: *Solid Earth*, *101*(B3), 6037-6050.

Clough, R. W., & Chopra, A. K. (1965). *Earthquake stress analysis in earth dams*. Department of Civil Engineering, University of California.

Cox, S. C., Stirling, M. W., Herman, F., Gerstenberger, M., & Ristau, J. (2012). Potentially active faults in the rapidly eroding landscape adjacent to the Alpine Fault, central Southern Alps, New Zealand. *Tectonics*, *31*(2).

Cox, S. C., & Sutherland, R. (2007). Regional geological framework of South Island, New Zealand, and its significance for understanding the active plate boundary. *A Continental Plate Boundary: Tectonics at South Island, New Zealand*, 19-46.

Cox, S. C., & Barrell, D. J. A. (2007). *Geology of the Aoraki area*. Institute of Geological & Nuclear Sciences.

Cox, S. C., & Findlay, R. H. (1995). The Main Divide fault zone and its role in formation of the Southern Alps, New Zealand. *New Zealand Journal of Geology and Geophysics, 38*(4), 489-499.

Croissant, T., Lague, D., Davy, P., Davies, T.R. & Steer, P. (In review, 2016). Morphodynamic modeling of hydro-sedimentary hazards induced by large sediment supplies in alluvial fans: Application to the 1999 Mount Adams landslide, New Zealand.

Darby, D. J., & Beanland, S. (1992). Possible source models for the 1855 Wairarapa earthquake, New Zealand. *Journal of Geophysical Research: Solid Earth, 97*(B9), 12375-12389.

Davey, F. J., Eberhart-Phillips, D., Kohler, M. D., Bannister, S., Caldwell, G., Henrys, S., Scherwath, M., Stern, T. & Van Avendonk, H. (2007). Geophysical structure of the Southern Alps Orogen, South Island, New Zealand. *A Continental Plate Boundary: Tectonics at South Island, New Zealand*, 47-72.

Davies, T. R., & Korup, O. (2007). Persistent alluvial fanhead trenching resulting from large, infrequent sediment inputs. *Earth Surface Processes and Landforms, 32*(5), 725-742.

Davies, T. R. H., McSaveney, M. J., & Doscher, C. (2005). Final Report on Research Project No. 03/499 Monitoring and effects of landslide-induced aggradation in the Poerua Valley, Westland. *Earthquake Commission, Wellington, New Zealand*.

DeMets, C., Gordon, R. G., & Argus, D. F. (2010). Geologically current plate motions. *Geophysical Journal International, 181*(1), 1-80.

DeMets, C., Gordon, R. G., Argus, D. F., & Stein, S. (1994). Effect of recent revisions to the geomagnetic reversal time scale on estimates of current plate motions. *Geophysical research letters, 21*(20), 2191-2194.

De Pascale, G. P., Quigley, M. C., & Davies, T. R. (2014). Lidar reveals uniform Alpine fault offsets and bimodal plate boundary rupture behavior, New Zealand. *Geology, 42*(5), 411-414.

De Pascale, G. P., Quigley, M. C., & Davies, T. R. (2014). Lidar reveals uniform Alpine fault offsets and bimodal plate boundary rupture behavior, New Zealand: REPLY. *Geology, 42*(10), e352-e352.

De Pascale, G. P., & Langridge, R. M. (2012). New on-fault evidence for a great earthquake in AD 1717, central Alpine fault, New Zealand. *Geology, 40*(9), 791-794.

Field, E. H., Jordan, T. H., & Cornell, C. A. (2003). OpenSHA: A developing community-modeling environment for seismic hazard analysis. *Seismological Research Letters, 74*(4), 406-419.

Fuller, M. L. (1912). *The new Madrid earthquake* (Vol. 494). US Government Printing Office.

Gutenberg, B. U., & Richter, C. F. (1954). *Seismicity of the earth and related phenomena*. Princeton (NJ).

Gu Gongxu (1983). Catalog of Chinese earthquakes.

Hancox, G. T., Langridge, R. M., Perrin, N. D., Vandergoes, M., Archibald, G. (2013). Recent mapping and radiocarbon dating of three giant landslides in northern Fiordland, New Zealand, GNS Science Report 2012/45. 52p.

Hancox, G. T., Dellow, G. D., & Perrin, N. D. (1997). Earthquake-induced landsliding in New Zealand and implications for MM intensity and seismic hazard assessment. Institute of Geological & Nuclear Sciences.

Haneberg, W. C. (2000). Deterministic and probabilistic approaches to geologic hazard assessment. *Environmental & Engineering Geoscience, 6*(3), 209-226.

Herman, F., Cox, S. C., & Kamp, P. J. (2009). Low-temperature thermochronology and thermokinematic modeling of deformation, exhumation, and development of topography in the central Southern Alps, New Zealand. *Tectonics, 28*(5).

Hicks, G; Campbell, H. eds (1998): *Awesome Forces*. Te Papa Press, Museum of New Zealand Te Papa Tongarewa, Wellington.

Howarth, J. D., Fitzsimons, S. J., Norris, R. J., Langridge, R., & Vandergoes, M. J. (2016). A 2000 yr rupture history for the Alpine fault derived from Lake Ellery, South Island, New Zealand. *Geological Society of America Bulletin, 128*(3-4), 627-643.

Howarth, J. D., Fitzsimons, S. J., Norris, R. J., & Jacobsen, G. E. (2014). Lake sediments record high intensity shaking that provides insight into the location and rupture length of large earthquakes on the Alpine Fault, New Zealand. *Earth and Planetary Science Letters, 403*, 340-351.

Howarth, J. D., Fitzsimons, S. J., Norris, R. J., & Jacobsen, G. E. (2012). Lake sediments record cycles of sediment flux driven by large earthquakes on the Alpine fault, New Zealand. *Geology, 40*(12), 1091-1094.

Hsü, K. J. (1975). Catastrophic debris streams (sturzstroms) generated by rockfalls. *Geological Society of America Bulletin, 86*(1), 129-140.

ISDR. (2009). *Global Assessment Report on Disaster Risk Reduction*. United Nations, Geneva, Switzerland.

Kamp, P. J., Green, P. F., & White, S. H. (1989). Fission track analysis reveals character of collisional tectonics in New Zealand. *Tectonics, 8*(2), 169-195.

Kerr, J., Nathan, S., Van Dissen, R., Webb, P., Brunsdon, D., & King, A. (2003). Planning for development of land on or close to active faults. *Wellington, Ministry for the Environment*.

Koons, P. O., Norris, R. J., Craw, D., & Cooper, A. F. (2003). Influence of exhumation on the structural evolution of transpressional plate boundaries: An example from the Southern Alps, New Zealand. *Geology, 31*(1), 3-6.

Koons, P.O. & Henderson, C.M. (1995). Geodetic analysis of model oblique collision and comparison to the Southern Alp. *New Zealand Journal of Geology and Geophysics, 38*, 545–542.

Koons, P.O. (1990). The two sided wedge in orogeny; erosion and collision from the sand box to the Southern Alps, New Zealand. *Geology, 18*, 679–682.

Koons, P. O. (1989). The topographic evolution of collisional mountain belts; a numerical look at the Southern Alps, New Zealand. *American journal of Science, 289*(9), 1041-1069.

Koons, P.O. (1987). Some thermal and mechanical consequences of rapid uplift; an example from the Southern Alps, New Zealand. *Earth and Planetary Science Letters, 86*, 307–319.

Korup, O. (2006). Effects of large deep-seated landslides on hillslope morphology, western Southern Alps, New Zealand. *Journal of Geophysical Research: Earth Surface, 111*(F1).

Korup, O. (2005). Distribution of landslides in southwest New Zealand. *Landslides, 2*(1), 43-51.

Korup, O., McSaveney, M. J., & Davies, T. R. (2004). Sediment generation and delivery from large historic landslides in the Southern Alps, New Zealand. *Geomorphology, 61*(1), 189-207.

Kritikos, T., Robinson, T. R., & Davies, T. R. (2015). Regional coseismic landslide hazard assessment without historical landslide inventories: A new approach. Journal of Geophysical Research: *Earth Surface*, *120*(4), 711-729.

Langridge, R. M., Ries, W. F., Litchfield, N. J., Villamor, P., Van Dissen, R. J., Barrell, D. J. A., Rattenbury, M.S., Heron, D.W., Haubrock, S., Townsend, D.B. and Lee, J.M. (2016). The New Zealand Active Faults Database. *New Zealand Journal of Geology and Geophysics*, *59*(1), 86-96.

Langridge, R. M., Ries, W. F., Farrier, T., Barth, N. C., Khajavi, N., & De Pascale, G. P. (2014). Developing sub 5-m LiDAR DEMs for forested sections of the Alpine and Hope faults, South Island, New Zealand: Implications for structural interpretations. *Journal of Structural Geology, 64*, 53-66.

Langridge, R. M., Villamor, P., Basili, R., Almond, P., Martinez-Diaz, J. J., & Canora, C. (2010). Revised slip rates for the Alpine fault at Inchbonnie: Implications for plate boundary kinematics of South Island, New Zealand. *Lithosphere, 2*(3), 139-152.

Lawson, A. C., & Reid, H. F. (1908). The California Earthquake of April 18, 1906: Report of the State Earthquake Investigation Commission, (No. 87). Carnegie institution of Washington.

Leitner, B., Eberhart-Phillips, D., Anderson, H., & Nabelek, J. L. (2001). A focused look at the Alpine fault, New Zealand: Seismicity, focal mechanisms, and stress observations. Journal of Geophysical Research: Solid Earth, 106(B2), 2193-2220.

Litchfield, N. J., Van Dissen, R., Sutherland, R., Barnes, P. M., Cox, S. C., Norris, R.J., Beavan, R.J., Langridge, R., Villamor, P., Berryman, K., Stirling, M., Nicol, A.,

Nodder, S., Lamarche, G., Barrell, D.J.A., Pettinga, J.R., Little, T., Pondard, N., Mountjoy, J.J. & Clark, K. (2014). A model of active faulting in New Zealand. *New Zealand Journal of Geology and Geophysics, 57*(1), 32-56.

Little, T. A., Cox, S., Vry, J. K., & Batt, G. (2005). Variations in exhumation level and uplift rate along the obliqu-slip Alpine fault, central Southern Alps, New Zealand. *Geological Society of America Bulletin*, *117*(5-6), 707-723.

Little, T. A., Savage, M. K., & Tikoff, B. (2002). Relationship between crustal finite strain and seismic anisotropy in the mantle, Pacific–Australia plate boundary zone, South Island, New Zealand. *Geophysical Journal International, 151*(1), 106-116.

Little, T. A., Holcombe, R. J., & Ilg, B. R. (2002). Kinematics of oblique collision and ramping inferred from microstructures and strain in middle crustal rocks, central Southern Alps, New Zealand. *Journal of Structural Geology*, *24*(1), 219-239.

Louderback, G. D. (1947). Central California earthquakes of the 1830's. *Bulletin of the Seismological Society of America, 37*(1), 33-74.

McCahon, I., Dewhirst, R., and Elms, D. (2006a). Alpine Fault Earthquake Scenario. Technical report, Buller District Council.

McCahon, I., Dewhirst, R., Mackenzie, J., and Elms, D. (2006b). Alpine Fault Earthquake Scenario. Technical report, Grey District Council.

McCahon, I., Elms, D., and Dewhirst, R. (2006c). Alpine Fault Earthquake Scenario. Technical report, West Coast Engineering Lifelines Group.

McSaveney, E. (2014). *'Historic earthquakes - The 1929 Arthur's Pass and Murchison earthquakes'*, Te Ara - the Encyclopedia of New Zealand. Retrieved October 21, 2016, from: http://www.TeAra.govt.nz/en/historic-earthquakes/page-5

Morton, J. (2016). *Kaikoura quake: 100,000 landslides*. Retrieved Nov. 17, 2016, from: http://www.nzherald.co.nz/nz/news/article.cfm?c_id=1&objectid=11747915

Nathan, S., Rattenbury, M. S., & Suggate, R. P. (2002). *Geology of the Greymouth area*. Institute of Geological and Nuclear Sciences.

Newmark, N. M. (1965), Effects of earthquakes on dams and embankments, *Geotechnique, 15*, 139–159.

Nicol, A., Van Dissen, R. J., Stirling, M. W., & Gerstenberger, M. C. (2016). Completeness of the Paleoseismic Active-Fault Record in New Zealand. Seismological Research Letters.

Norris, R. J., & Toy, V. G. (2014). Continental transforms: A view from the Alpine Fault. *Journal of Structural Geology, 64*, 3-31.

Norris, R. J., & Cooper, A. F. (2007). The Alpine Fault, New Zealand: surface geology and field relationships. *A Continental Plate Boundary: Tectonics at South Island, New Zealand*, 157-175.

Norris, R. J., & Cooper, A. F. (2001). Late Quaternary slip rates and slip partitioning on the Alpine Fault, New Zealand. *Journal of Structural Geology, 23*(2), 507-520.

Norris, R. J., & Cooper, A. F. (1997). Erosional control on the structural evolution of a transpressional thrust complex on the Alpine Fault, New Zealand. *Journal of Structural Geology*, *19*(10), 1323-1342.

O'Keefe, B. C. (2008). Microseismicity of the central Alpine Fault region, New Zealand.

Rattenbury, M. S., & Jongens, R. (2010). *Geology of the Haast area*. Institute of Geological and Nuclear Sciences.

Reyners, M. (1988). Reservoir-induced seismicity at lake Pukaki, New Zealand. Geophysical Journal International, 93(1), 127-135.

Rhoades, D. A., & Van Dissen, R. J. (2003). Estimates of the time-varying hazard of rupture of the Alpine fault, New Zealand, allowing for uncertainties. *New Zealand Journal of Geology and Geophysics, 46*(4), 479-488.

Robinson, T. R., Davies, T. R. H., Wilson, T. M., & Orchiston, C. (2016). Coseismic landsliding estimates for an Alpine Fault earthquake and the consequences for erosion of the Southern Alps, New Zealand. *Geomorphology*, *263*, 71-86.

Robinson, T.R. (2014). Effective disaster scenarios for emergency response planning — A case study of an Alpine Fault earthquake, South Island, New Zealand. Department of Geological Sciences. University of Canterbury.

Robinson, T. R., Wilson, T. M., Davies, T. R., Orchiston, C., & Thompson, J. R. (2014). Design and development of realistic exercise scenarios: a case study of the 2013 Civil Defence exercise Te Ripahapa.

Robinson, T. R., & Davies, T. R. H. (2013). Review article: Potential geomorphic consequences of a future great (M w= 8.0+) Alpine Fault earthquake, South Island, New Zealand. *Natural Hazards and Earth System Sciences, 13*(9), 2279-2299.

Robinson, R., & McGinty, P. J. (2000). The enigma of the Arthur's Pass, New Zealand, earthquake: 2. The aftershock distribution and its relation to regional and induced stress fields. *Journal of Geophysical Research: Solid Earth, 105*(B7), 16139-16150.

Schwartz, D. P., & Coppersmith, K. J. (1986). *Seismic hazards: new trends in analysis using geologic data* (No. DOE/ER/12018--T10).

Schwartz, D. P., & Coppersmith, K. J. (1984). Fault behavior and characteristic earthquakes: Examples from the Wasatch and San Andreas fault zones. *Journal of Geophysical Research: Solid Earth, 89*(B7), 5681-5698.

Shreider, Y. A. (Ed.). (2014). The Monte Carlo method: the method of statistical trials (Vol. 87). Elsevier.

Sibson, R. H. (1989). Earthquake faulting as a structural process. *Journal of Structural Geology, 11*(1-2), 1-14.

Statistics New Zealand (2013). *New Zealand Census 2013*. Wellington: Statistics New Zealand.

Stern, T., Okaya, D., Kleffmann, S., Scherwath, M., Henrys, S., & Davey, F. (2007). Geophysical exploration and dynamics of the Alpine fault zone. *A Continental Plate Boundary: Tectonics at South Island, New Zealand*, 207-233.

Stirling, M., Goded, T., Berryman, K., & Litchfield, N. (2013). Selection of earthquake scaling relationships for seismic-hazard analysis. *Bulletin of the Seismological Society of America*.

Stirling, M., McVerry, G., Gerstenberger, M., Litchfield, N., Van Dissen, R., Berryman, K., Barnes, P., Wallace, L., Villamor, P., Langridge, R. & Lamarche, G. (2012). National seismic hazard model for New Zealand: 2010 update. *Bulletin of the Seismological Society of America, 102*(4), 1514-1542.

Stirling, M. W., Mc Verry, G. H., & Berryman, K. R. (2002). A new seismic hazard model for New Zealand. *Bulletin of the Seismological Society of America*, *92*(5), 1878-1903.

Sutherland, R., Eberhart-Phillips, D., Harris, R. A., Stern, T., Beavan, J., Ellis, S., Henrys, S., Cox, S., Norris, R.J., Berryman, K.R., Townend, J., Bannister, S., Pettinga, J., Leitner, B., Wallace, L., Little, T.A., Cooper, A.F., Yetton, M., Stirling, M. (2007). Do great earthquakes occur on the Alpine fault in central South Island, New Zealand?. *A continental plate boundary: tectonics at South Island, New Zealand*, 235-251.

Sutherland, R., Berryman, K., & Norris, R. (2006). Quaternary slip rate and geomorphology of the Alpine fault: Implications for kinematics and seismic hazard in southwest New Zealand. *Geological Society of America Bulletin, 118*(3-4), 464-474.

Summerfield, M. A. (2014). *Global geomorphology*. Routledge.

Stewart, J. P., Blake, T. F., and Hollingsworth, R. A. (2003). A screen analysis procedure for seismic slope stability. *Earthquake Spectra, 19*:697–712.

Truebridge, N., Carrol, J. & Ensor, B. (2016). *Drone footage shows extent of flooding after West Coast overnight deluge*. Retrieved October 26, 2016, from: http://www.stuff.co.nz/national/78223436/tourists-evacuated-state-of-emergency-after-west-coast-river-breaks-banks

United States Geological Survey. (2004) *Landslide Types and Processes*. Retrieved October 26, 2016, from: http://pubs.usgs.gov/fs/2004/3072/fs-2004-3072.html

Upton, P., Koons, P. O., Craw, D., Henderson, C. M., & Enlow, R. (2009). Along-strike differences in the Southern Alps of New Zealand: Consequences of inherited variation in rheology. *Tectonics, 28*(2).

Van Avendonk, H. J., Holbrook, W. S., Okaya, D., Austin, J. K., Davey, F., & Stern, T. (2004). Continental crust under compression: A seismic refraction study of South Island Geophysical Transect I, South Island, New Zealand. *Journal of Geophysical Research: Solid Earth, 109*(B6).

Varnes, D. J. (1978). *Slope movement types and processes*. Transportation Research Board Special Report, (176).

Wald, D. J., & Allen, T. I. (2007). Topographic slope as a proxy for seismic site conditions and amplification. *Bulletin of the Seismological Society of America, 97*(5), 1379-1395.

Wald, D. J., Earle, P. S. & Quitoriano V. (2004). Topographic Slope as a Proxy for Seismic Site Correction and Amplification, *EOS. Trans. AGU, 85*(47), F1424.

Wallace, L. M., Beavan, J., McCaffrey, R., Berryman, K., & Denys, P. (2007). Balancing the plate motion budget in the South Island, New Zealand using GPS, geological and seismological data. *Geophysical Journal International, 168*(1), 332-352.

Wells, A., & Goff, J. (2007). Coastal dunes in Westland, New Zealand, provide a record of paleoseismic activity on the Alpine fault. *Geology, 35*(8), 731-734.

Wells, A., & Goff, J. (2006). Coastal dune ridge systems as chronological markers of palaeoseismic activity: a 650-yr record from southwest New Zealand. *The Holocene, 16*(4), 543-550.

Wells, A., & Yetton, M. D. (2004). *Earthquake tree-ring impacts in the middle and upper Buller River catchment*. New Zealand Earthquake Commission Research Report, 3, 492.

Wells, A., Yetton, M. D., Duncan, R. P., & Stewart, G. H. (1999). Prehistoric dates of the most recent Alpine fault earthquakes, New Zealand. *Geology*, *27*(11), 995-998.

Wells, D. L., & Coppersmith, K. J. (1994). New empirical relationships among magnitude, rupture length, rupture width, rupture area, and surface displacement. *Bulletin of the seismological Society of America, 84*(4), 974-1002.

Whitehouse, I. E., & Griffiths, G. A. (1983). Frequency and hazard of large rock avalanches in the central Southern Alps, New Zealand. *Geology, 11*(6), 331-334.

Wright, T. (2016). *Anatomy of the Kaikoura quakes*. Retrieved Nov. 17, 2016, from: http://www.newshub.co.nz/nznews/anatomy-of-the-kaikoura-quakes-2016111617?ref=newshubFB

Yetton, M. D. (2000). The probability and consequences of the next Alpine Fault earthquake, South Island, New Zealand. Department of Geological Sciences. University of Canterbury.

Yetton, M. D. (1998). Progress in understanding the paleoseismicity of the central and northern Alpine Fault, Westland, New Zealand. *New Zealand Journal of Geology and Geophysics, 41*(4), 475-483.

Yetton, M. D., & Nobes, D. C. (1998). Recent vertical offset and near-surface structure of the Alpine Fault in Westland, New Zealand, from ground penetrating radar profiling. *New Zealand Journal of Geology and Geophysics, 41*(4), 485-492.

Zadeh, L. A. (1965). Fuzzy sets. *Information and control, 8*(3), 338-353.

Zielke, O., & Arrowsmith, J. R. (2008). Depth variation of coseismic stress drop explains bimodal earthquake magnitude-frequency distribution. *Geophysical Research Letters, 35*(24).

8 APPENDICES

APPENDIX A

Area km²	0-1	1-2	2-3	3-4	4-5	5-6	6-7	7-8	8-9	9-10
Waitaha	0	0	1.80050494	15.2364284	18.7130008	21.490014	57.567665	93.954004	83.562412	17.713899
Hokitika	0	958.119089	22154.9543	79734.3103	102360.398	88163.333	243417	263812.32	201278.63	37955.767
Waiho-Callery	0	223.2	1250.0866	11225.9926	28773.9712	9544.1142	34256.042	77329.977	49777.871	9881.1931
Wanganui	0	0.00359702	7.38343438	21.9938862	59.7181746	38.1463	155.50361	116.48784	63.075081	11.025993
Whataroa	0	329.369549	8862.39474	19952.442	44775.3183	47869.383	194566.48	147047.34	56196.626	12290.787
Taramakau	0	203.336701	10959.119	62007.304	93236.4116	132993.18	332369.03	241439.9	124488.52	2188.3486
Fox-Cook	0	0	0.41843382	14.2236164	36.62878	34.515405	78.573948	70.643651	24.686272	0
Rakaia	10985.672	36656.5744	151388.085	223706.73	360144.819	924771.05	793062.42	171228.11	51100.563	7237.6383
Waimakariri	193666.53	300688.613	484241.624	238172.053	651640.576	758521.26	798751.59	126276.56	44952.945	3.6
Karangarua	0	7.34144371	1505.42807	17680.5075	115336.651	157270.01	75702.459	1667.3286	51.089983	0
Rangitata	71646.972	87125.693	90695.4643	176339.724	441420.696	656639.73	253167.33	64.721612	0	0
Grey	442.8	32739.4635	415543.277	848391.789	1540182.15	692039.55	306610.78	44792.998	8626.4426	0
Ashburton	102058.66	124064.14	199752.282	200180.073	419341.464	326765.88	219834.66	3.6	0	0
Ashley	0	8372.46389	198655.639	97742.9509	605264.637	239722.75	0	0	0	0
Hurunui	28.8	51981.6394	505582.864	859515.612	851229.293	359733.51	22151.871	7.2	0	0
Waitaki	60479.959	438158.197	3088214.78	3762255.89	2029963.84	1405096.8	335763.06	4415.8853	0	0
Opihi	5186.4471	129506.528	459060.357	670731.356	855472.773	238938.09	10864.53	18	0	0
Haast	367.2	24351.8994	288611.774	393510.8	470362.35	112566.83	10909.486	0	0	0
Waiau (Cant.)	36	131183.449	549367.135	2209495.54	282849.544	155074.16	0	0	0	0
Selwyn	309390.18	460903.817	555735.213	146103.897	303623.396	62216.14	1453.3516	0	0	0
Clarence	0	10161.6002	229546.194	3056713.52	338.4	0	0	0	0	0
Hollyford	428.95814	30341.9348	121939.637	911339.396	457.2	0	0	0	0	0
Awatere	0	31655.3569	357476.03	1184927.83	36	0	0	0	0	0
Buller	859.39219	131817.061	2757901.59	3218494.28	194189.191	37150.5	0	0	0	0
Waimea	0	18665.7487	281626.341	470558.1	0	0	0	0	0	0
Okuru	1225.5929	16979.0412	264506.242	170242.757	9647.03412	1523.1175	0	0	0	0
Wairau	2682	265680.326	1216296.75	2095371.87	172.8	0	0	0	0	0
Arawhata	2498.7002	59825.6312	367016.416	408642.041	0	0	0	0	0	0
Clutha	35195.867	3632110.49	9180174.31	6731275.92	152321.339	6970.1542	0	0	0	0
Taieri	2848.6042	852530.826	2859950.97	1940004.25	0	0	0	0	0	0
Waiatoto	1169.4397	41448.4961	286463.092	150851.359	310.218621	17.262055	0	0	0	0
Mokihinui	454.10102	27519.3903	591877.427	130701.452	0	0	0	0	0	0
Motueka	7541.3008	156708.598	1432444.38	460971.895	0	0	0	0	0	0
Aorere	26611.55	333342.067	4687.2	0	0	0	0	0	0	0
Karamea	3322.6876	506566.49	700241.473	0	0	0	0	0	0	0
Pelorus	8620.4197	547988.172	320093.247	14350.0897	0	0	0	0	0	0
Waiau (South.)	318444.89	4958466	2336939.29	21809.4403	0	0	0	0	0	0
Mataura	549079.82	3645230.68	1112395.99	47350.5522	0	0	0	0	0	0
Oreti	1124436.9	1733670.53	646812.282	5945.73962	0	0	0	0	0	0

Figure A1: Area in km² of landslide susceptibility hazard bins per catchment.

APPENDIX B

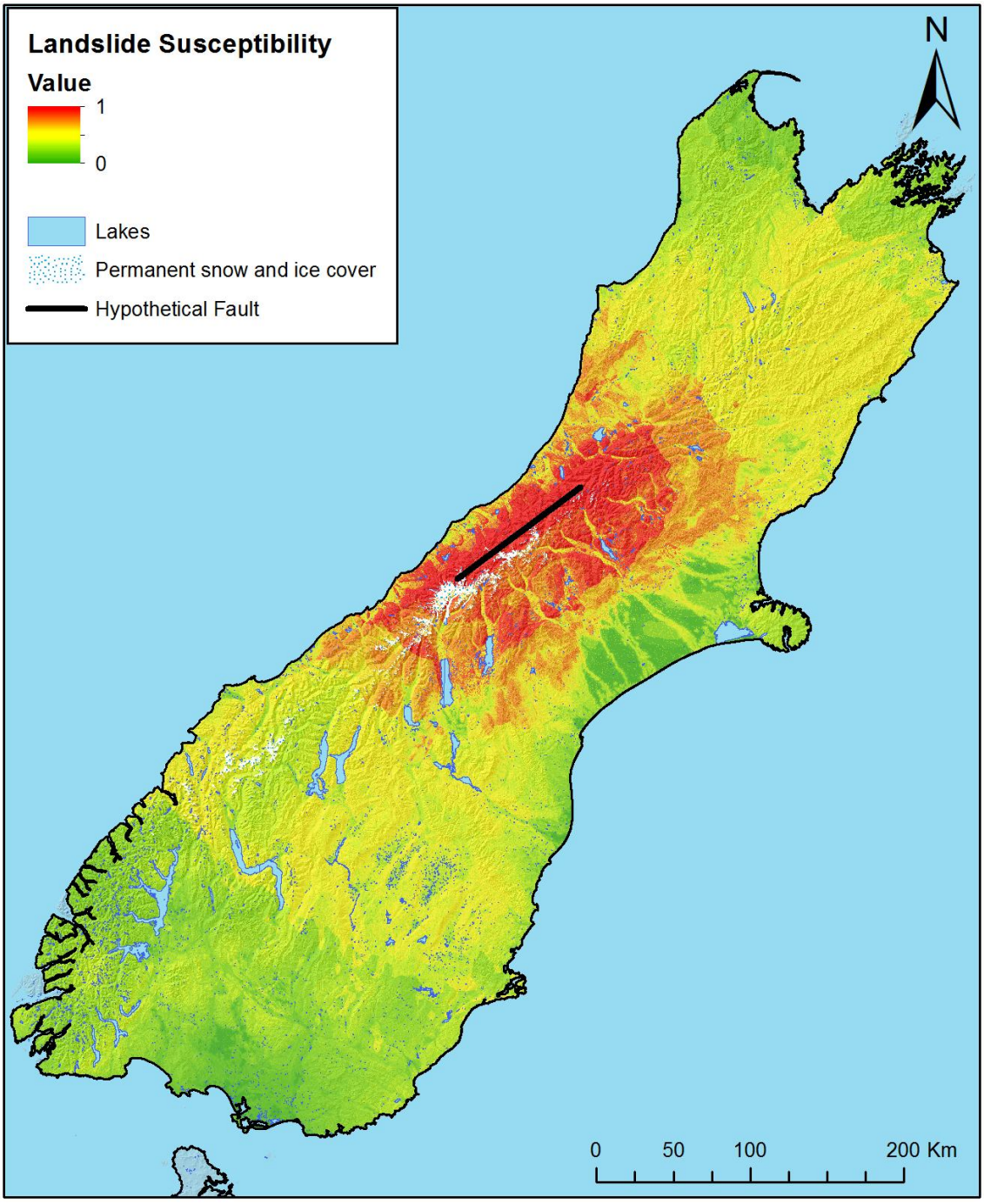

Figure B2: Landslide susceptibility displayed using standard deviation set to 2.5 in ArcGIS, defining areas of high susceptibility in higher contrast.